

Aspherical, Nanostructured
Microparticles
For Pulmonary Gene Delivery To Alveolar
Macrophages

DISSERTATION

zur Erlangung des Grades
des Doktors der Naturwissenschaften
der Naturwissenschaftlich-Technischen Fakultät
der Universität des Saarlandes

von

Michael Möhwald

Saarbrücken
2017

Tag des Kolloquiums: 07.03.2018
Dekan: Prof. Dr. Guido Kickelbick
Berichterstatter: Prof. Dr. Marc Schneider
Prof. Dr. Claus-Michael Lehr
Vorsitz: Prof. Dr. Andriy Luzhetskyy
Akad. Mitarbeiter: Dr. Stefan Boettcher

Die vorliegende Arbeit wurde im Zeitraum April 2014 – März 2015 an der Philipps-Universität Marburg und von April 2015 – März 2017 an der Universität des Saarlandes angefertigt.

It was their farewell message as they signed off. Stay Hungry. Stay Foolish. And I always wished that for myself. And now, as you graduate to begin anew, I wish that for you:

Stay Hungry. Stay Foolish.

Steve Jobs, 2005

Meinen Eltern
Dorothea und Jürgen

Table of Content

Summary	- 1 -
Kurzzusammenfassung	- 2 -
Chapter I - General Introduction	- 3 -
I.1 Principles of Pulmonary Delivery	- 4 -
I.2 Aspherical Particles in Pulmonary Drug Delivery	- 8 -
I.3 Layer-by-Layer Coating Technique	- 13 -
I.4 Macrophage Engineering	- 17 -
I.5 Aim of the Work	- 19 -
I.6 References	- 21 -
Chapter II - Template-assisted Production of Aspherical, Nanostructured Microparticles Using DNA	- 24 -
II.1 Introduction: Microrod Fabrication	- 25 -
II.2 Monitoring of the Engineering Steps	- 29 -
II.2.1 Infiltration of Nanomaterial into the Templates	- 29 -
II.2.1.1 Material and Methods	- 29 -
II.2.1.2 Results and Discussion	- 31 -
II.2.2 Layer-by-Layer Coating Using DNA	- 34 -
II.2.2.1 Material and Methods	- 34 -
II.2.2.2 Results and Discussion	- 37 -
II.2.3 Yield Evaluation and Calculations	- 43 -
II.3 Preliminary Cargo Release Studies in Simulated Lung Fluids	- 44 -
II.3.1 Material and Methods	- 44 -
II.3.2 Results and Discussion	- 44 -
II.4 References	- 48 -
Chapter III - Microrods Featuring Biodegradability	- 49 -
III.1 Introduction: Stimuli-Responsive Drug Delivery Strategies	- 50 -
III.2 Microrod Stabilization by Amino-Functionalized Sugar Polymers and DNA	- 52 -
III.2.1 Material and Methods	- 52 -
III.2.2 Results and Discussion	- 53 -
III.3 Enzyme-Induced Release of DNA from Microrod Systems	- 57 -
III.3.1 Material and Methods	- 57 -

III.3.2 Results and Discussion.....	- 58 -
III.4 References	- 65 -
Chapter IV - Technological Characterization of Microrods.....	- 66 -
IV.1 Quantification of Microrod System Components	- 67 -
IV.1.1 Introduction to Layer-by-Layer Quantification	- 67 -
IV.1.2 Material and Methods	- 69 -
IV.1.3 Results and Discussion.....	- 71 -
IV.2 Aerodynamic Properties of Microrods.....	- 74 -
IV.2.1 Introduction to the Next Generation Impactor	- 74 -
IV.2.2 Materials and Methods.....	- 77 -
IV.2.3 Results and Discussion.....	- 79 -
IV.3 References	- 83 -
Chapter V - Transfection Studies on Murine Alveolar Macrophages	- 84 -
V.1 Introduction: Macrophage Transfection.....	- 85 -
V.2 Materials and Methods	- 87 -
V.3 Results and Discussion	- 94 -
V.4 References	- 101 -
Chapter VI - Transfection Studies in BALB/c Mice	- 102 -
VI.1 Introduction: Mouse Lung Models	- 103 -
VI.2 Material and Methods	- 105 -
VI.3 Results and Discussion.....	- 109 -
VI.4 References	- 114 -
Summary and Outlook	- 115 -
Abbreviations	- 119 -
Acknowledgements	- 120 -
Curriculum Vitae.....	- 122 -

Summary

The introduction of shape as a design parameter for particulate carrier systems shows promising potential to improve drug and gene delivery. In order to optimize current therapeutic strategies, various new particle geometries were proposed to adapt to specific hurdles of application routes and to modify interactions within biological environments. For the transport of active agents into the respiratory tract, elongated, aspherical particles were shown to reach the alveolar region and additionally offering the modification of the clearance rate by alveolar macrophages.

In the presented work a template-assisted particle engineering technique was used to fabricate elongated, cylindrical microparticles of defined diameter and length. Therefore, nanoparticles were interconnected with each other within shape defining pores of a template membrane building up a micron structure. Designed as a gene delivery system, plasmid DNA and a lysosomal buffering agent were applied as a functional polymer coating, which at the same time provided the stabilization of the system. The resulting microparticles were shown to be qualified for pulmonary administration featuring aerodynamic properties to reach the deep lung. In addition, particle geometry was adjusted to provide high uptake rates into alveolar macrophages as the target cells while showing no cytotoxicity. A successful implementation of the transported gene into the phagocytes could be shown in cell culture studies on MH-S cells (murine alveolar macrophages). The transfection provided by the carrier system was also successfully translated into a mouse lung model (BALB/c) qualifying the presented microparticles for the targeted gene delivery to alveolar macrophages.

Kurzzusammenfassung

Die Formgebung von partikulären Trägersystemen birgt großes Potential für die Verbesserung der Pharmako- und Gentherapie. Um den spezifischen Ansprüchen verschiedener Applikationen gerecht zu werden, wurde bereits eine Vielzahl unterschiedlicher Formen eingeführt, insbesondere mit der Absicht den Transport der Wirkstoffe zu verbessern und Interaktionen mit dem Organismus zu modifizieren. Speziell für den effizienten Transport von Therapeutika in die Lunge konnten asphärische Partikel als vorteilhaft identifiziert werden. Zusätzlich konnte für diese Partikelart gezeigt werden, dass die Aufnahme durch Makrophagen gezielt verbessert oder auch verlangsamt werden kann. In der vorliegenden Arbeit wurde eine Template-gestützte Methode für die Herstellung von asphärischen, zylindrisch geformten Mikropartikeln angewendet. Die Methode erlaubte dabei die exakte Einstellung des Durchmessers und der Länge der Partikel. Dafür wurden kleinere Nanopartikel innerhalb einer formgebenden Matrize miteinander verbunden, indem eine Beschichtung mit Polymeren erfolgte. Die hierfür verwendeten Substanzen waren eine Plasmid-DNA und ein Stickstoffpolymer mit hoher Pufferkapazität, um die Partikel als Gentransportsystem einzusetzen. Die erhaltenen Mikropartikel wurden erfolgreich auf ihre Lungengängigkeit geprüft und ermöglichen eine hohe Aufnahme in Alveolarmakrophagen. Toxische Effekte konnten für die Partikel nicht beobachtet werden. In Zellkultur-Experimenten an Alveolarmakrophagen der Maus konnte gezeigt werden, dass die Partikel eine Einschleusung des transportierten Gens in den Kern der Zellen bewerkstelligen können. Zusätzlich konnte auch im lebenden Tier (BALB/c Mäuse) eine Expression des Gens gezeigt werden, was die präsentierten Mikropartikel zu einem geeigneten Kandidaten für die Gentherapie in der Lunge macht.

Chapter I

General Introduction

I.1 Principles of Pulmonary Delivery

In pharmacotherapy the lung is a very prominent compartment of the human body. Offering a non-invasive route of administration, pulmonary drug delivery in theory can be used for both local and systemic treatment. For the latter, the high surface area of up to 150 m² in combination with a distinct vascularization indicates the lung to be a suitable target for delivery approaches.^[1] Additionally, the air-blood barrier is a very thin epithelial layer featuring a minimum thickness of only 0.1 μm.^[2] This consequentially facilitates air exchange in the alveoli, but also the introduction of drugs into the blood stream. However, up to now there is no successful market product available using this particular application route.^[3]

In contrast to that, the local delivery of therapeutic agents into the respiratory tract is the recommended strategy for treating inflammatory disorders such as chronic obstructive pulmonary disease (COPD), asthma or pulmonary fibrosis.^[4] Therefore, active pharmaceutical ingredients (APIs) such as glucocorticoids or β₂-sympathomimetic drugs are aerosolized for inhalation to mitigate the common symptoms of patients. For aerosolization, three different principles can be distinguished. Metered dose inhalers (MDI) use propellants that are liquefied under pressure.^[5] The drug is suspended or dissolved in the propellant, which evaporates upon activation of the inhaler. A single metered dose is released as API-containing droplets to reach the respiratory tract following the inhalation stream. By using vaporizers aqueous drug solutions can be applied, which are nebulized into a fine mist. Here, the droplets are generated *e.g.* by oscillations provided by a piezo crystal, which are transferred to the drug solution.^[6] As a third option for aerosolization, dry powder inhalers (DPI) can be used. Therefore, solid drug substance particles, that can be associated to a carrier to prevent the formation of larger agglomerates, are inhaled.^[7] In order to reach an effective deposition of the droplets or solid particles within the pulmonary system, specific parameters have to be considered for the formulation. The size of the droplets or particles is of major impact

determining the site of action for the active agent. As presented in **Figure 1**, for large particles exceeding the size of 5 microns, high impaction rates in the upper airways can be expected.^[8] Here, they can cause the common local side effects during treatment. The optimum size is reported to be in the range from 1 to 5 μm leading to sedimentation and diffusion into the deeper compartments of the lung.^[8, 9] Regarding very fine aerosols featuring sizes below 0.5 μm the majority of the formulation is expected to be exhaled after application.^[10-12]

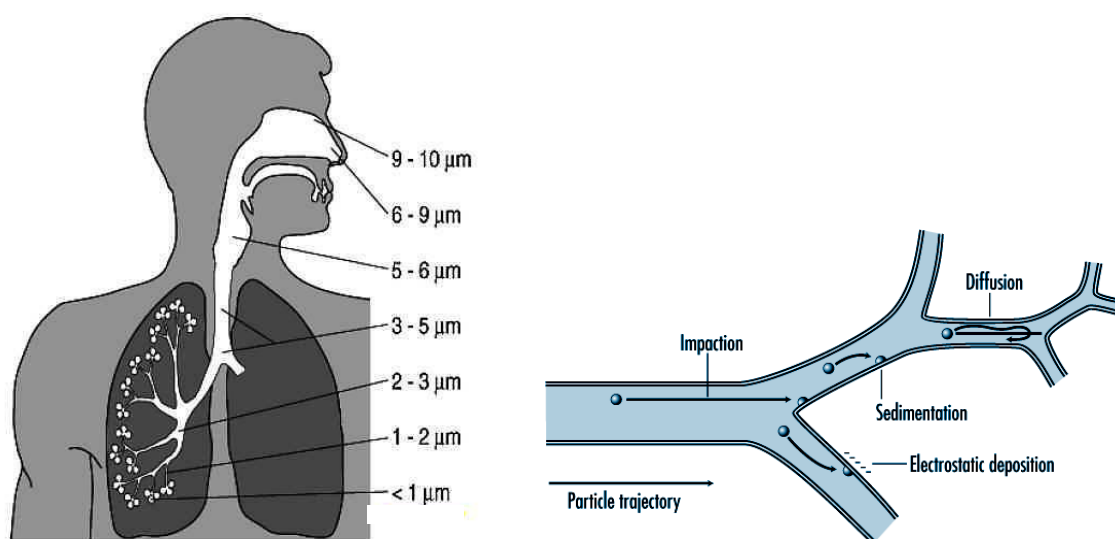


Figure 1: Aerosol deposition within the respiratory tract in dependence on particle size.^[8] Whereas larger particles show impaction in the upper airways, particles in the size range of 1-5 microns reach the deep lung.^[9]

However, as presented in **Figure 2**, a second maximum for the deposition can be observed for particles in the low nanometer scale.^[13] In this study an efficiency of up to 50 % was found for the alveolar region regarding nanoparticles in the range of 10 nm. An additional aspect, which highly influences particle deposition patterns, is particle density.^[14] The group of Robert Langer at MIT published a study on large porous particles made of insulin and testosterone.^[14] They produced particle diameters of up to 20 μm , which usually show high impaction in the upper lung. But at the same time the density of the particles was reduced enabling high deposition and therefore bioavailability of the delivered drugs. They impressively emphasized

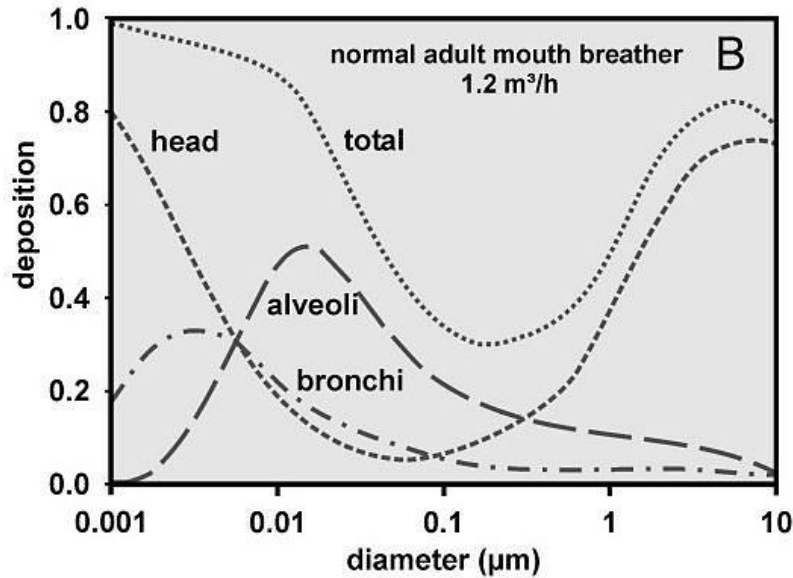


Figure 2: Particle deposition efficiency in dependence on region and particle size.^[13]

density as a crucial parameter for the aerodynamic behavior of airborne particles. Both size and density are expressed in the aerodynamic diameter $d(aer)$ (**Equation 1**), which is a prominent parameter for aerosol characterization. It provides information about the accessibility of an aerosolized particle formulation for the pulmonary system as an important quality attribute. Described in both the US and European pharmacopeias, $d(aer)$ can be assessed by cascade impactor testing.^[15]

$$d(aer) = d(geo)\sqrt{\rho}$$

Equation 1: The aerodynamic diameter $d(aer)$ expressed as a function of the geometric diameter $d(geo)$ of the particle and its density ρ .

In **Figure 3**, as an example the most commonly used Andersen impactor is depicted. After aerosolization the formulation follows the undertow of the vacuum and enters the impactor. A

first selection of particle sizes can be conducted by a preseparator, which prevents particles larger than 10 μm from entering the setup as correspondingly they would not enter the deep lung. In the next step heterogeneous particle populations of the formulation will be sized by inertia. This means whenever a particle is not able to follow the undertow anymore, it impacts in the respective stage allowing a separation of defined particle $d(\text{aer})$ ranges. For the Andersen impactor the aerosol stream passes 8 particle collection stages. At stage 0 particles of 9.0 microns and larger impact whereas stage 7 forces 0.4 to 0.7 μm particles to deposit onto the collection plates. Mentioned as apparatus E in the European pharmacopeia, a new impactor design is listed based on a horizontal cascade setup.^[15] Commercialized as New Generation Impactor (NGI) the device was developed by the pharmaceutical industry for facilitated high-throughput testing. Featuring high accuracy and reproducibility, the new

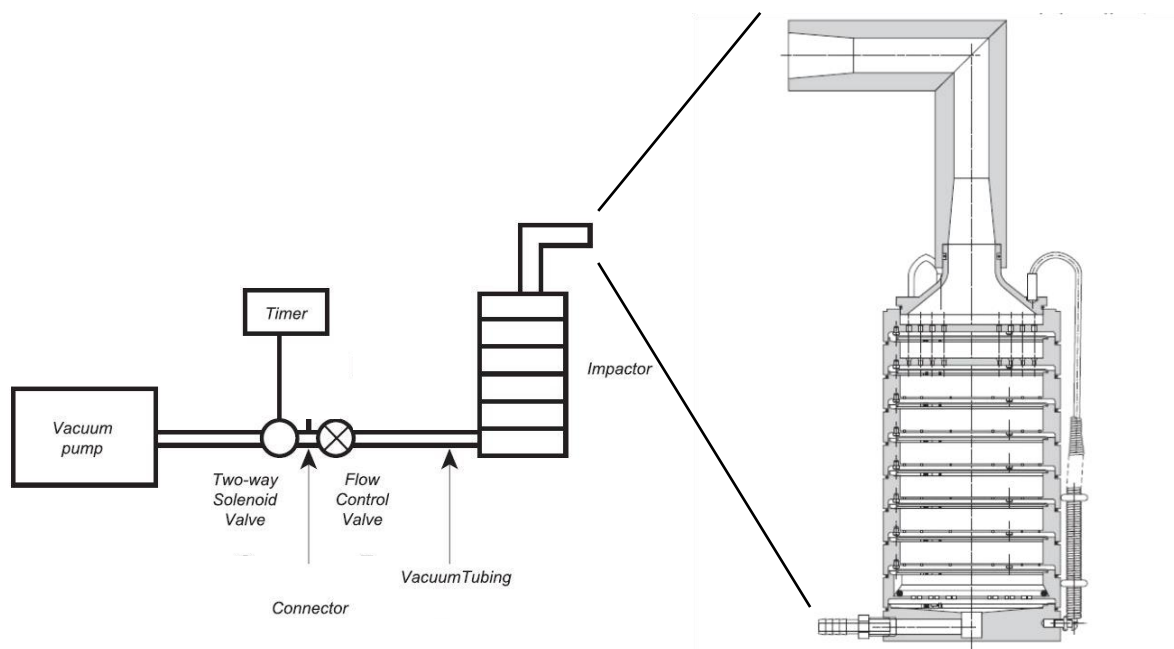


Figure 3: Schematic overview of an Andersen cascade impactor including a vacuum setup for aerosolization.^[12]

design meets all pharmacopeia specifications. For the presented work, the NGI was used for the determination of the aerodynamic properties of the fabricated delivery system. Hence, a detailed description with a focus on the metrics which can be calculated from an NGI run is presented in chapter IV. Besides size and density a third particle design parameter, even though still under-represented in recent publications, is shape. On the one hand shape modifications can be exploited for improved delivery results, but on the other hand shape is a relevant parameter for biological interactions after reaching the desired target compartment. For pulmonary delivery only few studies are available, however, results indicated a beneficial behavior of elongated, fiber-like particles, which is outlined in the following section. Here, examples of non-spherical shapes in drug delivery are presented focusing on advancements for pulmonary carrier systems.

I.2 Aspherical Particles in Pulmonary Drug Delivery

In recent years, shape as a design parameter for particulate drug delivery systems gained increasing attention. The encapsulation of active agents into polymeric carrier systems adds beneficial features regarding API protection, release profiles or facilitated application.^[16] In this regard, a lot of emphasis was put on chemistry and surface modifications to create biocompatible systems enabling a targeted delivery and controlled release of the transported cargo. In addition to that, shape was identified as an important and relevant parameter *e.g.* to modify interactions within biological environments or to improve delivery for specific administration routes.^[17] As presented in **Figure 4**, many novel shapes were introduced, which clearly differ from the regular spherical systems. Therefore, scientists used a wide range of different fabrication techniques. Xu and colleagues published a work on the production of rod-like shaped particles (**Figure 4 D**).^[18] They applied a microfluidic device

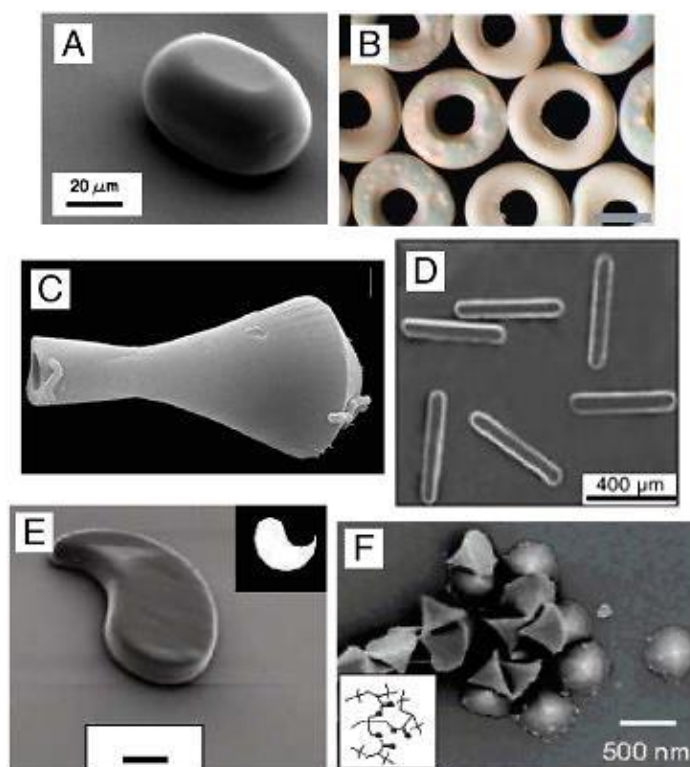


Figure 4: Overview of various aspherical shapes of particle systems. Different methods were applied for the fabrication of plug-shaped (A), torroidal (B), vase- or rod-shaped (C, D) particles. Even perfectly curved or conical shapes could be presented (E, F).^[17]

providing full control on the shape of the resulting particles. However, their experimental setup was limited to the production of rod sizes from 20 to 100 μm , which is not convenient for many administration routes such as pulmonary application. However, for suitable sizes the elongated structure of rod- or fiber-like carrier systems has been evaluated for the transport into the respiratory tract. Su et al. published a study on fibers and spherical particles comparing their efficiency to reach the peripheral lung.^[19] They could demonstrate fibers to have a higher probability to deposit in the desired pulmonary region, whereas spheres featuring the same aerodynamic diameter are held back in the oral and nasal region. This was supported by a mathematical approach carried out by Sturm and colleagues.^[20] They again stated improved chances of fibers for deep lung deposition. In this context, aspect ratio (AR),

the quotient of length to diameter of the particle system, is a crucial parameter. By adjusting AR, particle deposition patterns can be estimated, which indicates the possibility of a site specific transport into the lung.^[19] In addition to potentially improved pulmonary delivery aspects, rod-like shaped particles provide the possibility to alter cellular interactions. Upon aerosolization and deposition within the respiratory tract, spherical microparticles can be efficiently engulfed by phagocytes, *e.g.* alveolar macrophages, and cleared from the target site. This leads to the removal of the active agents and therefore a reduced therapeutic outcome. In this regard, Champion and Mitragotri demonstrated the invagination of carrier systems by phagocytes to be drastically dependent on their shape.^[21] High aspect ratios can be utilized to delay uptake into macrophages.^[22] This can prolong the residence time of APIs resulting in higher bioavailability and as a result superior therapeutic performance of the carrier. Besides decreased phagocyte interactions for uptake retardation, rod-like particles can also be designed to act as an agent for cell surface functionalization. The group of Michael Rubner at MIT presented a study on the fabrication of polymer rods, which act as a “cellular backpack” for macrophages.^[23] In order to leverage the native functions of the cells, they again exploited the rod-like shape to create phagocytosis-resistant particles. By picking suitable polymers such as chitosan, they were able to immobilize the particles on the cell membrane (**Figure 5**). As a carrier system for diagnostic and therapeutic agents, the rods are reported to be qualified for targeted delivery without hampering proliferation or viability of the cells. For the fabrication of the particles, they applied a template-assisted approach depicted in **Figure 6**. A polycarbonate membrane was coated by different polymers, which cover the whole surface of the membrane including the inner surface of the pores. By plasma etching, they had to selectively remove the polymer film from the surface, whereas the coating within the pores was maintained. After sufficient polymer deposition the template was dissolved in an organic solvent to harvest the particles. A similar engineering technique for the production of rod-like shaped particles was introduced by our group.^[24] Here, Kohler and

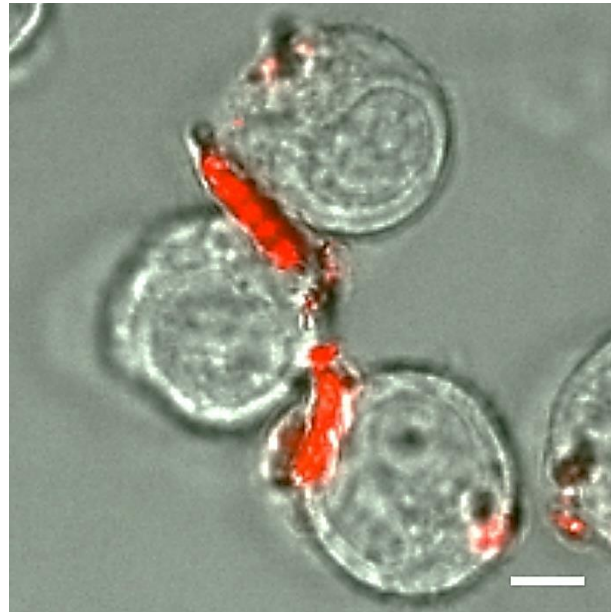


Figure 5: Rod-like shaped polymer particles (red) acting as cellular backpack on mouse macrophages; scale bar 10 μm .^[23]

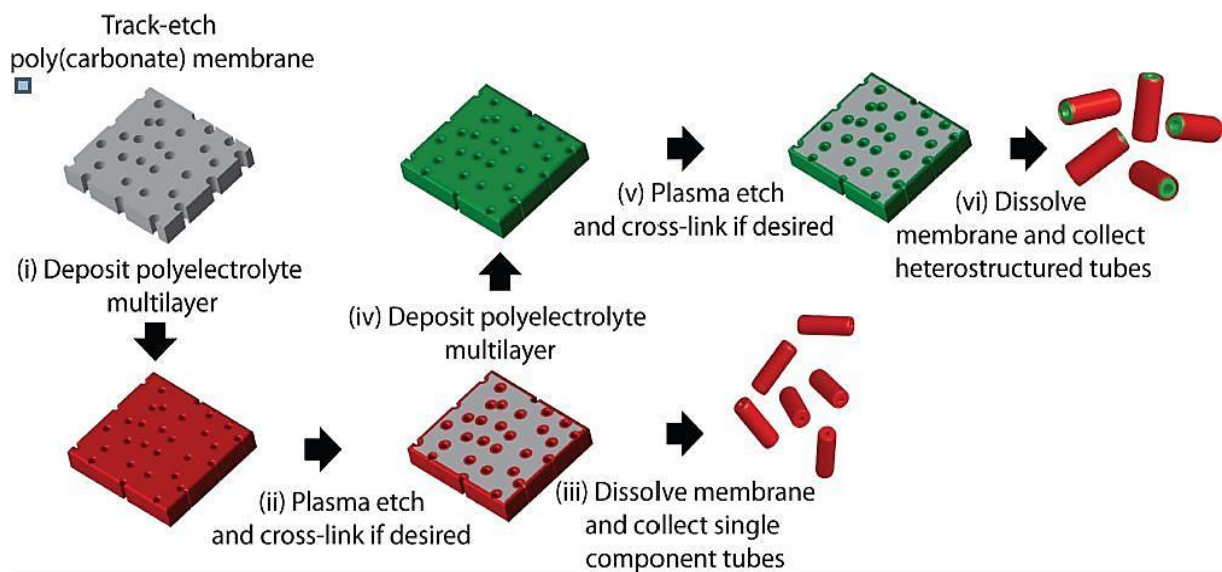


Figure 6: Template-assisted production of hollow, rod-like shaped microparticles. The template membrane gets coated with different polymers, which are released by membrane dissolution.^[23]

colleagues created rod- or fiber-like shapes by the interconnection of nanoparticles. Based on a bottom-up engineering approach, nanomaterial built up micron structures within the pores of

a template membrane. According to the geometry of the pores, the resulting particles featured an elongated, cylindrical shape. Using this method, it was possible to connect single nanoparticles to a chain applying a polymer coating (**Figure 7**). By changing the pore diameter of the template, AR can be easily adjusted for the particles. In contrast to uptake retardation, specific ARs are reportedly engulfed to a higher extent than comparable spheres.^[21] This indicates the possibility of targeted delivery to phagocytes and shows rod-like shaped particles to be a versatile tool box to modify interactions at the micro-bio interface.

In general, shape is a promising new design parameter within particle engineering, which should always be considered to optimize delivery efficiencies. For the presented thesis, the method by Kohler et al. was applied for the fabrication of particles achieving a macrophage targeting followed by high uptake rates. The further development and the transition into a delivery system for DNA will be carried out in detail in chapter II.

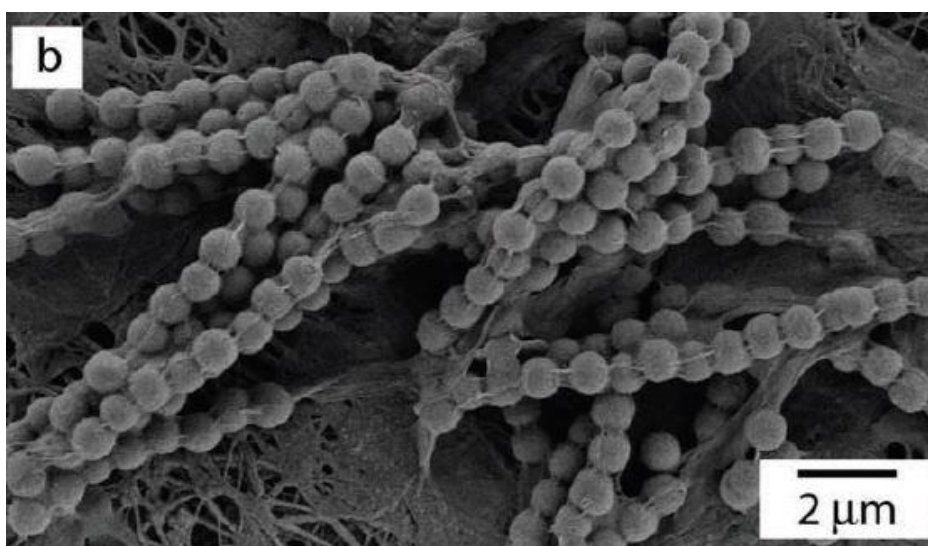


Figure 7: Template-assisted connection of single nanoparticles into a chain structure.^[24]

I.3 Layer-by-Layer Coating Technique

The Layer-by-Layer (LbL) coating technique was for the first time described by Gero Decher in 1991 on planar surfaces.^[25] Based on the assembly of mainly polymeric materials, electrostatic, but also hydrophobic forces and H-bonds can be exploited to provide the deposition of thin films onto almost any kind of substrate.^[26, 27] The basic coating procedure is shown in **Figure 8** utilizing opposite charges of two polyelectrolytes for attachment.^[25] As the substrate shows positive surface charges, polyanions can be used to start the coating procedure. The initial surface charges get overcompensated by the polymeric material allowing the deposition of polycations in a second step. In between the coating steps, additional washing steps are used to get rid of excess polymer. Since the introduction of the technique, the number of applied excipients was constantly increased to challenge its potential within the fields of material or biomedical sciences. The method provides the deposition of

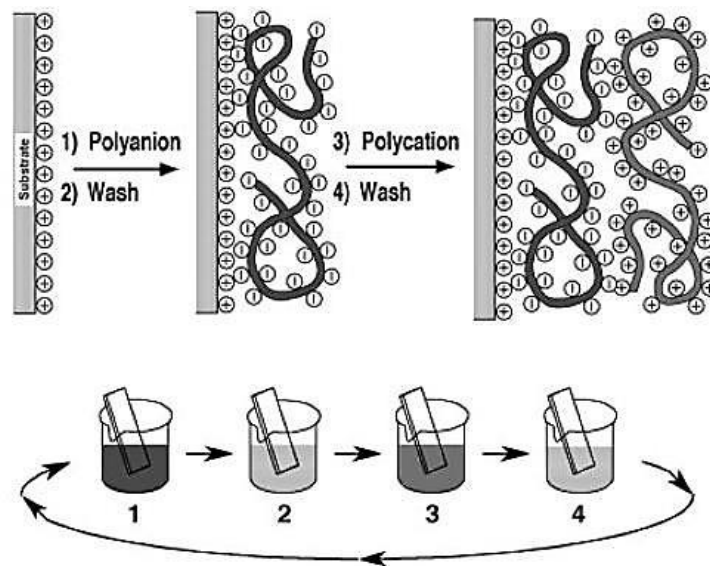


Figure 8: Schematic illustration of LbL polymer deposition of polyelectrolytes onto a planar substrate.^[22]

nanometer-thin polymer layers offering the freedom to incorporate a broad range of functional components to create new materials according to the desired application

purpose.^[28] In **Figure 9**, the transmission electron microscopy (TEM) visualization of an LbL meshwork cross-section is shown, illustrating the subsequent coating of different polymers.^[29] The composition of the layers can be changed by the operator as desired to control the position and total amount of the applied compounds. Regarding biomedical applications, LbL coating procedures can provide the deposition of active agents into polymeric matrices for modified release profiles and targeting purposes while preserving their therapeutic activity.^[30-32] Both synthetic and natural polymers, such as therapeutic proteins or nucleic acids, can be applied. The fabricated films are applicable to medical devices like stents and tissue engineering implants or colloidal drug delivery systems.^[33-36] Reibetanz et al. published a

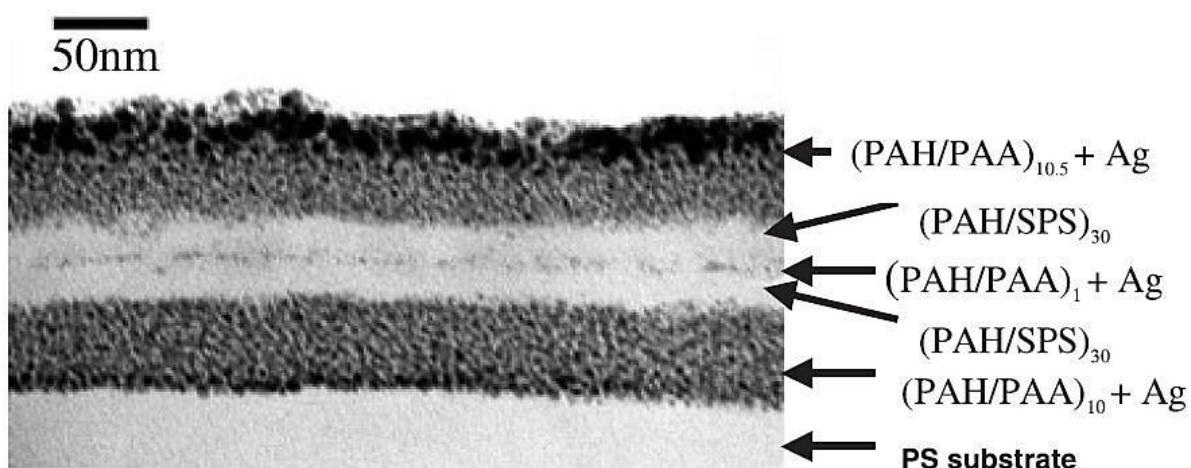


Figure 9: TEM image of an LbL meshwork built up by polyallylamine hydrochloride (PAH), polyacrylic acid (PAA), sulfonated polystyrene (SPS) and silver nanoparticles (Ag). The layers are coated onto a polystyrene (PS) substrate.^[29]

work on the LbL assembly of plasmid DNA encoding for green fluorescent protein (GFP) in combination with protamine.^[37] As a substrate, they applied colloidal silica particles of 3 μm in size. After preparation, the multi-layered particles were applied to HEK 293T cells as presented in **Figure 10**. Due to the red fluorescence label of protamine, they could confirm the uptake of the particles into the cytosol of the cells. In addition, the cells expressed GFP

indicating a successful delivery of the plasmid DNA into the nuclear core of the target cells. Here, the LbL meshwork was on the one hand able to provide protection of the incorporated active agent from degrading cellular enzymes. On the other hand the intracellular release was sufficient for transgene expression qualifying the presented LbL-based system for the introduction of genes into HEK 293T cells. In order to optimize the efficiency of LbL-promoted gene delivery, different strategies were introduced *e.g.* focusing stimuli-responsive behavior. Blacklock et al. published a work on the fabrication of multilayered films using DNA and a cationic peptide featuring disulfide bonds.^[38] Whereas the peptide is stable under non-reducing conditions, the bonds are cleaved within a suitable reductive environment.

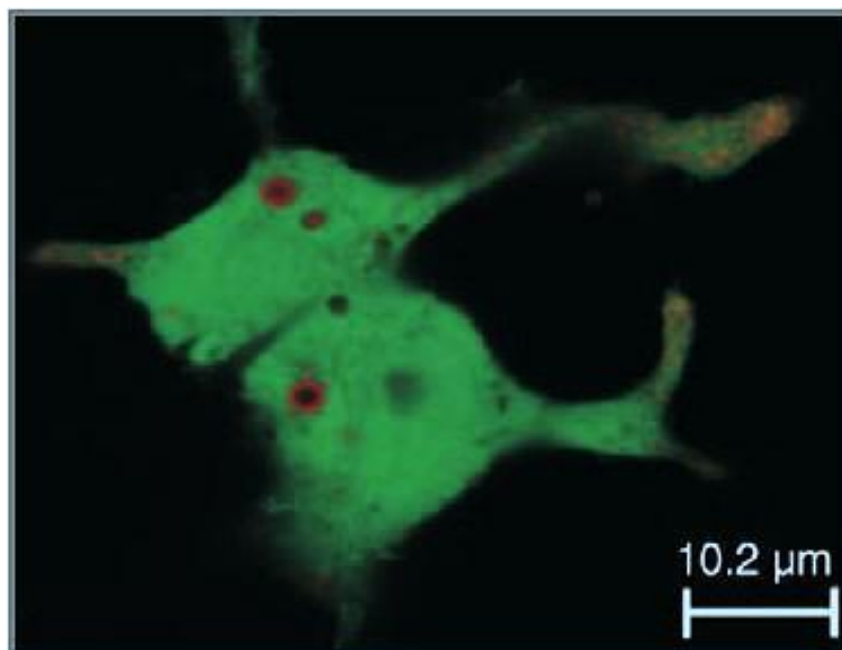


Figure 10: Fluorescence micrograph of LbL coated and labeled silica microparticles (red) into HEK 293T cells. Cells appear in green due to expressed GFP.^[37]

As a consequence, the LbL meshwork gets destabilized for a triggered cargo release (**Figure 11 A**). Another strategy is based on materials, which can be cleaved within an enzymatic environment (**11 B**).^[39] Utilizing degrading enzymes for triggered release is in particular a promising approach for intracellular cargo delivery taking into account the enzymatic arsenal

present in endo- and phagolysosomes of the target cells.^[41] In summary, the introduction of LbL coating techniques into drug and gene delivery adds a versatile tool to the controlled delivery of therapeutic agents. The method is very robust to excipient changes offering the possibility of customized film designs, which can be optimized to the needs of specific applications. The technique especially benefits from progress in polymer chemistry and material sciences indicating LbL coating techniques to be a promising platform technology for advanced surface functionalization.

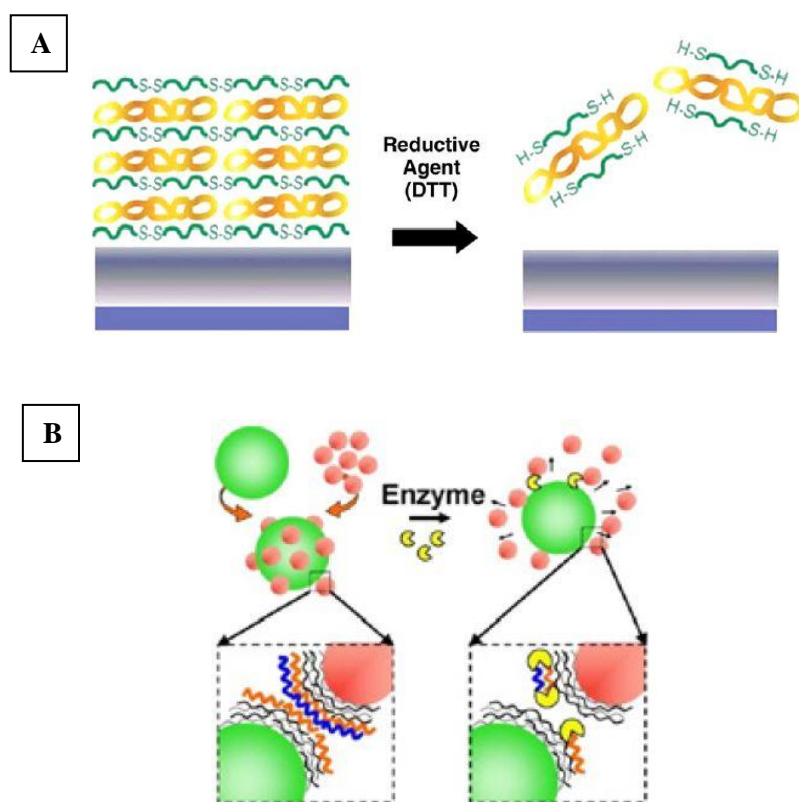


Figure 11: Stimuli-responsive LbL designs for triggered cargo release due to polymer reduction (A) or enzymatic degradation (B).^[35, 36]

I.4 Macrophage Engineering

Macrophages are part of the innate immune system and play a pivotal role in a large number of immunological cascades. In their role as scavenger cells, they stand sentinel to pathogen exposure in all tissues and at important body barriers as presented in **Figure 12**.^[41] In this regard, they present initially processed pathogens to T-lymphocytes and act as cytokine secreting cells.^[42, 43] Thereby, macrophages mediate, but also regulate immune-based inflammatory conditions. Due to their important role in immunological responses, an altered activity or dysfunction of macrophages can have crucial impact on the development and exacerbation of various diseases. Macrophage participation is frequently discussed for many pathological conditions including cancer and chronic inflammatory disorders.^[44] Recently

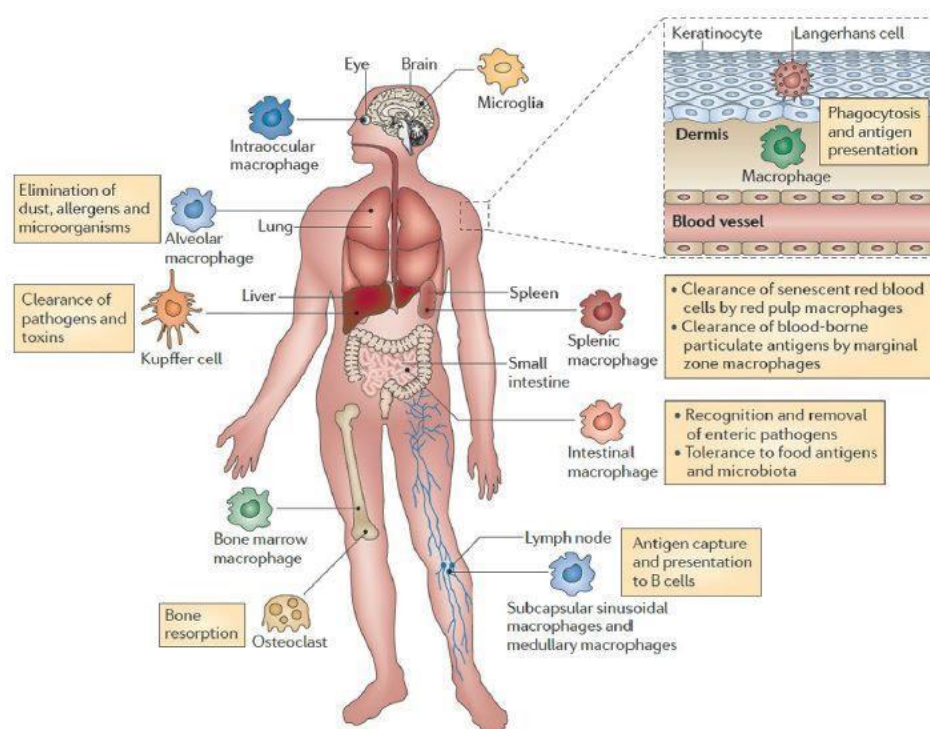


Figure 12: Overview of macrophage presence throughout the human body. All important biological barriers such as the intestines, the blood-brain barrier or the lung are settled with macrophages.^[37]

focused by many working groups, the involvement of macrophages in malignant diseases is a very prominent research topic. Tumor-associated macrophages (TAMs) play a major role in the development of carcinoma potentially promoting cellular remodeling and proliferation, neovascularization and metastasis.^[45] Therefore, TAMs highly express and secrete growth factors as well as cytokines defining a microenvironment that is directly involved in tumor progression.^[46] Regarding lung carcinoma, high density of infiltrating macrophages has been correlated with poor clinical outcomes.^[47] This is due to alveolar macrophages secreting *e.g.* vascular epidermal growth factor (VEGF), which is expected to contribute to increased tumor angiogenesis.^[43] In addition to malignant diseases, macrophage participation is also discussed for many different inflammatory disorders. Keeping the focus onto the lung, pulmonary fibrosis and chronic obstructive pulmonary disease (COPD) are expected to be promoted and worsened by overly active pro-inflammatory macrophages.^[48] Within these conditions, they secrete cytokines such as TNF- α at high levels, which is a key player in chronic inflammation.^[49]

Both malignant and chronic inflammatory diseases are up to the present day only insufficiently treatable demanding novel therapeutic strategies. Therefore, gene therapy can be a powerful tool promoting access to the relevant genes by highly specific transfection systems. In order to modify mediator secretion on DNA level, many techniques were developed for the genetic engineering of target cells. Both vectors or non-viral, polymer-based delivery systems for the introduction of pDNA, siRNA or mRNA were introduced.^[50-52] In the context of inflammatory disorders of the respiratory system, Kelly and colleagues presented a microparticulate delivery system, which they showed to be effective in introducing siRNA into alveolar macrophages.^[53] Optimizing the carrier to be biodegradable and qualified for pulmonary administration, the delivered cargo selectively knocked down TNF- α expression in a cell culture model. The study is one example among many others,

which contributes to the progression and further development of gene therapy towards the translation into clinical applications. Very recently, CRISPR/Cas9 tools again provided the spirit of optimism within the scientific community, showing promising potential and receiving the approval for human clinical trials in June, 2016.^[54] In this regard, novel transfection tools concurrently increase the demand for equally advanced delivery systems to overcome the specific hurdles of cellular targets and specific application routes defining the scope of the presented thesis.

I.5 Aim of the Work

The presented work is characterized by its strong interdisciplinarity combining aspects of pharmaceutical technology, biopharmacy, gene delivery and cell biology. A novel particulate carrier system of aspherical shape is in the focus merging delivery into the respiratory system with the introduction of a model gene into a target cell line.

In this regard, a novel particle engineering method, initially developed by our group, was adapted and extended to the requirements of a gene delivery approach. Prior studies explored the possibility to fabricate fiber-like or rod-like shaped particles of defined sizes by using regular filter membranes. Within the pores of the membranes, nanomaterial can be interconnected leading to cylindrical microparticles. The first particles gained from this technique did not feature pharmaceutically relevant excipients, such as functional polymers or active agents. A general development of the engineering technique and smart excipient choices were prioritized in order to stabilize the shape of the carrier. In addition, the interaction of the particles with macrophages was evaluated, visualizing the engulfment by phagocytosis in much detail.

Building on these preliminary studies, the objective of the presented work was the transition of the particles into a pulmonary gene delivery system. A targeted delivery of DNA into alveolar macrophages was in particular focused, proving the system to be qualified for the genetic engineering of phagocytes, a cell species, which is generally considered as hard-to-transfect. Therefore, a comprehensive physicochemical characterization had to be performed including aerodynamic properties after aerosolization. The introduction of a model gene into macrophages within biological environments was investigated, both under *in vitro* and *in vivo* conditions. The work is divided into five scientific chapters displaying the systematic steps of the development process:

Chapter II – Template-assisted Production of Aspherical, Nanostructured Microrods Using DNA

Chapter III – Microrods Featuring Biodegradability

Chapter IV – Technological Evaluation of Microrods

Chapter V – Transfection Studies on Murine Alveolar Macrophages

Chapter VI – Transfection Studies in BALB/c Mice

I.6 References

- [1] P. S. Hasleton, *J. Anat.* **1972**, *112*, 391–400
- [2] J. P. T. Ward, J. Ward, R. M. Leach, *The Respiratory at a Glance*, 3rd Edition, Wiley-Blackwell **2011**
- [3] L. Heinemann, *J. Diabetes Sci. Technol.* **2008**, *2*, 518–529
- [4] C. Vogelmeier, R. Buhl, C. P. Cri_e, A. Gillissen, P. Kardos, D. Köhler, H. Magnussen, H. Morr, D. Nowak, D. Pfeiffer-Kascha, W. Petro, K. Rabe, K. Schultz, H. Sitter, H. Teschler, T. Welte, R. Wettengel, H. Worth, *COPD-Leitlinie - Deutsche Atemwegsliga*
- [5] S. P. Newman, *Respir. Care* **2005**, *50*, 1177–1188
- [6] S. Ehrmann, A. Lyazidi, B. Louis, D. Isabey, D. Le Pennec, L. Brochard, G. Apiou-Sbirlea, *Respir. Care* **2014**, *10*, 1508–1516
- [7] P. J. Atkins, *Respir. Care* **2005**, *50*, 1304–1312
- [8] T. G. D. Capstick, I. J. Clifton, *Expert Rev. Resp. Med.* **2012**, *6*, 91–103
- [9] ILO Encyclopaedia of Occupational Health & Safety, *The Human Respiratory Tract – Structure and Function*, **2011**
- [10] C. Davies, D. Muir, *Nature* **1966**, *211*, 90–9
- [11] K. K. Jain, Drug delivery systems. Springer; 2008. Drug delivery systems-an overview; pp. 1–50
- [12] T. V. Thulasiramaraju, K. B. Tejeswar, B. M. Nikilesh, *Asian J. Res. Pharm. Sci. Biotechnol.* **2013**, 16–34
- [13] M. Geiser, W. G. Kreyling, *Part. Fibre Toxicol.* **2010**, *20*, 2
- [14] D. A. Edwards, J. Hanes, G. Caponetti, J. Hrkach, A. Ben-Jebria, M.L. Eskew, J. Mintzes, D. Deaver, N. Lotan, R. Langer, *Science* **1997**, *276*, 1868–1871
- [15] Preparations for Inhalation: Aerodynamic Assessment of Fine Particles, European Pharmacopoeia 8th Edition, Supplement 8.7, 2016
- [16] R. Langer, *Science* **1990**, *249*, 1527–1533
- [17] J. A. Champion, Y. K. Katare, S. Mitragotri, *J. Control. Release* **2007**, *121*, 3–9
- [18] S. Xu, Z. Nie, M. Seo, P. Lewis, E. Kumacheva, H. A. Stone, P. Garstecki, D. B. Weibel, I. Gitlin, G. M. Whitesides, *Angew. Chem. Int. Ed.* **2005**, *44* 724–728
- [19] W.-C. Su, Y. S. Cheng, *J. Aero. Sci.* **2006**, *37*, 1429 – 1441
- [20] R. Sturm, W. Hofmann, *J. Hazard. Mater.* **2009**, *170*, 210–218
- [21] J. A. Champion, S. Mitragotri, *PNAS* **2005**, *103*, 4930–4934
- [22] J. Möller, T. Luehmann, H. Hall, V. Vogel, *Nano Lett.* **2012**, *12*, 2901–2905
- [23] N. Doshi, A. J. Swiston, J. B. Gilbert, M. L. Alcaraz, R. E. Cohen, M. F. Rubner, S. Mitragotri, *Adv. Mater.* **2011**, *23*, 105–109
- [24] D. Kohler, M. Schneider, M. Kruger, C.M. Lehr, H. Mohwald, D.Y. Wang, *Adv. Mater.* **2011**, *23*, 1376–1379

- [25] G. Decher, J.-D. Hong, *Makromol. Chem. Macromol. Symp.* **1991**, *46*, 321–327
- [26] N. Kotov, *Nanostruct. Mat.* **1999**, *12*, 789-796
- [27] Y. Fu, S. Bai, S. Cui, D. Qiu, Z. Wang, X. Zhang, *Macromolecules* **2002**, *35*, 9451-9458
- [28] J. D. Hong, K. Lowack, J. Schmitt, G. Decher, *Progr. Colloid Polym. Sci.* **1993**, *93*, 98–102
1993, *93*, 98–102. *Symp.* **1991**, *46*, 321–327.
- [29] R.T. Clay, R.E. Cohen, *Supramol. Sci.* **1995**, *2*, 183
- [30] O.S. Sakr, S. Berndt, G. Carpentier, M. Cuendet, O. Jordan, G. Borchart, *J. Control. Release* **2016**, *244*, 199-207
- [31] S.T. Gunawan, K. Kempe, T. Bonnard, J. Cui, K. Alt, L. S. Law, X. Wang, E. Westein, G. K. Such, K. Peter, C. E. Hagemeyer, F. Caruso, *Adv. Mater.* **2015**, *27*, 5153-5157
- [32] C. Bishop, A. L. Liu, D. S. Lee, R. J. Murdock, J.J. Green, *Biomed Mater Res A* **2015**, *104*, 707-713
- [33] J. Min, K. Y. Choi, E. C. Dreaden, R. F. Padera, R. D. Braatz, M. Spector, P. T. Hammond, *ACS Nano* **2016**, *10*, 4441-4450
- [34] G. England, M. C. Miller, A. Kuttan, J. O. Trent, H. B. Frieboes, *Eur. J. Pharm. Biopharm.* **2015**, *92*, 120-129
- [35] J. Huang, Q. Shu, L. Wang, H. Wu, A. Y. Wang, H. Mao, *Biomaterials* **2015**, *39*, 105-113 28
- [36] D. V. Voronin, D. Grigoriev, H. Möhwald, D. G. Shchukin, D. A. Gorin, *ACS Appl. Mater. Interfaces* **2015**, *51*, 28353-28360
- [37] U. Reibetanz, C. Claus, E. Typlt, J. Hofmann, E. Donath, *Macromol. Biosci.* **2006**, *6*, 153–160
- [38] J. Blacklock, H. Handa, D. Soundara Manickam, G. Mao, A. Mukhopadhyay, D. Oupicky, *Biomaterials* **2007**, *28*, 117–124
- [39] I. Marchenko, A. Yashchenok, T. Borodina, T. Bukreeva, M. Konrad, H. Möhwald, A. Skirtach, *J. Control. Release* **2012**, *162*, 599–605
- [40] E. R. Unanue, *Am. J. Pathol.* **1976**, *83*, 396–417
- [41] S. Gordon, *Fundamental Immunology*, Vol. 4 (Ed: W. Paul), Lippincott Raven, Philadelphia, PA, USA **1999**, Ch. 15
- [42] F. Geissmann, M. G. Manz, S. Jung, M. H. Sieweke, M. Merad, K. Ley, *Science* **2010**, *327*, 656–661
- [43] P. J. Murray, T. A. Wynn, *Nat. Rev. Immunol.* **2011**, *11*, 723–737
- [44] E. M. Conway, L. A. Pikor, S. H. Y. Kung, M. J. Hamilton, St. Lam, W. L. Lam, K. L. Bennewith, *Am. J. Respir. Crit. Care Med.* **2016**, *193*, 116–130
- [45] J. A. Joyce, J. W. Pollard, *Nat. Rev. Cancer* **2009**, *9*, 239-252
- [46] J. B. Wyckoff, Y. Wang, E. Y. Lin, J. F. Li, S. Goswami, E. R. Stanley, J. E. Segall, J. W. Pollard, J. Condeelis, *Cancer Res.* **2007**, *67*, 2649-2656
- [47] A. G. Paul, *Eukaryon*, Vol. 1, Lake Forest College, **2005**. Jan 4-5, *NF-kB: A novel therapeutic target for cancer.*
- [48] J. B. Morjaria, M. Malerba, R. Polosa, *Drug Discovery Today* **2010**, *15*, 396–405.

- [49] J. R. Murdoch, C. M. Lloyd, *Mutat. Res.* **2010**, *690*, 24–39
- [50] A. Singpiel, J. Schneider, R. Maus, J. Bohling, F. Behler-Janbek, R. Stripecke, T. Welte, U. Maus, , *Eur. Respir. J.* **2015**, *46*, 2748
- [51] D. He, K. Müller, A. Krhac Levacic, P. Kos, U. Lächelt, E. Wagner, *Bioconjugate Chem.* **2016**, *27*, 647–659
- [52] A. J. Mahiny, A. Dewerth, L. E. Mays, M. Alkhaled, B. Mothes, E. Malaeksefat, B. Loretz, J. Rottenberger, D. M. Brosch, P. Reautschnig, P. Surapolchai, F. Zeyer, A. Schams, M. Carevic, M. Bakele, M. Griese, M. Schwab, B. Nürnberg, S. Beer-Hammer, R. Handgretinger, D. Hartl, C.-M. Lehr, M. S. D. Kormann, *Nat. Biotechnol.* **2015**, *33*, 584–586
- [53] C. Kelly, A. B. Yadav, C. Lawlor, K. Nolan, J. O'Dwyer, C. M. Greene, N. G. McElvaney, N. Sivadas, J. M. Ramsey, S.-A. Cryan, *Mol. Pharmaceutics* **2014**, *11*, 4270–4279
- [54] S. Reardon, *Nat. News* **2016**, doi:10.1038/nature.2016.20137

Chapter II

Template-assisted Production of Aspherical, Nanostructured Microparticles Using DNA

II.1 Introduction: Microrod Fabrication

For the production of aspherical, nanostructured microparticles a template-assisted method was applied. Based on a bottom-up engineering approach, which was previously introduced by our group, nanoparticles got infiltrated into the shape-defining pores of a template membrane.^[1] Followed by the interconnection of the nanomaterial by a polymer coating, the aspherical structure was stabilized leading to microparticles representing the cylindrical shape of the given template pores.

Starting the microparticle production with the infiltration of the nanomaterial into the membrane, the template (blue membrane, **Figure 1 A**) was applied to a regular filter holder system. Placing a second membrane (orange) underneath, which is referred to as blocking membrane and featuring pore sizes far below the nanomaterial size, can guarantee particle retention. The nanomaterial was applied by a syringe as an aqueous suspension, which led to a piling within the template pores. The water could pass the setup freely providing a continuous flow of the suspension through the filter holder system. As presented in **Figure 1 B** the method allows an immediate qualitative feedback about the infiltration result. Whereas a turbid nanosuspension is applied to the filter holder system, the suspension water leaves the setting as clear filtrate. In a second consecutive step the nanomaterial gets cross-linked by thin polymer layers. Therefore the template membranes were treated with two different polyelectrolyte (PE) solutions within an LbL procedure. The alternating exposure to positively (PE+) and negatively (PE-) charged coating agents (**Figure 2**) led to the deposition of thin films on the particles' surface. As polyanion plasmid DNA was used according to the intended gene delivery approach. Providing negative charges from the phosphate-sugar backbone, the plasmid can be combined with positively charged polycations to build up the coating arranged in double-layers (PE+/PE-).

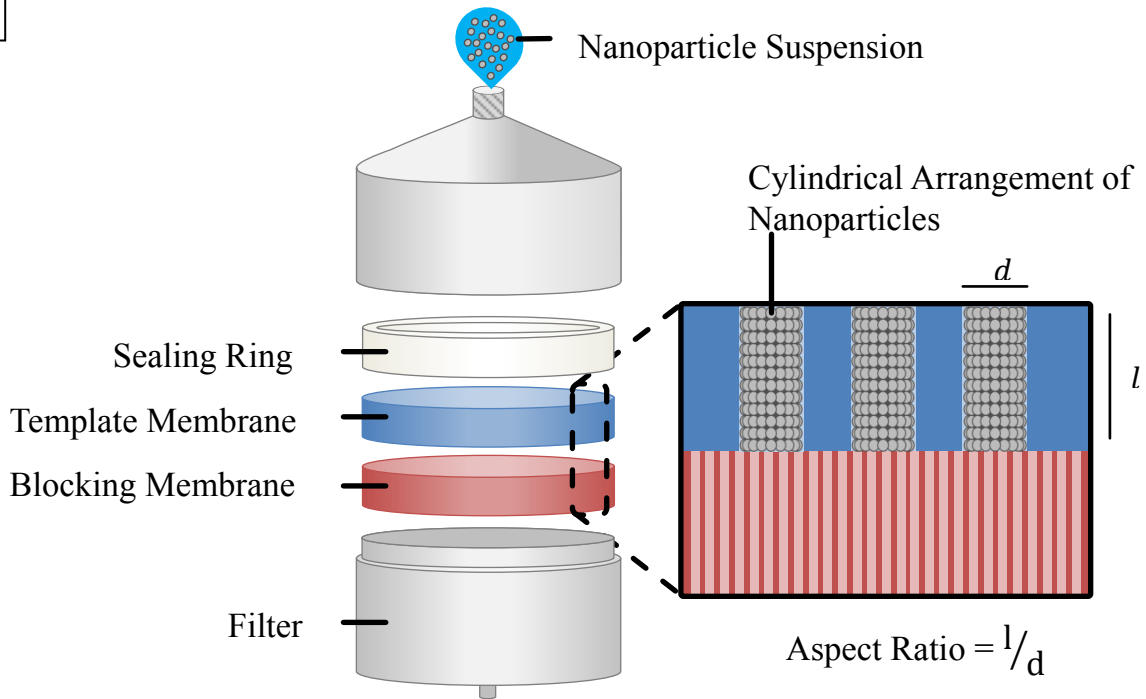
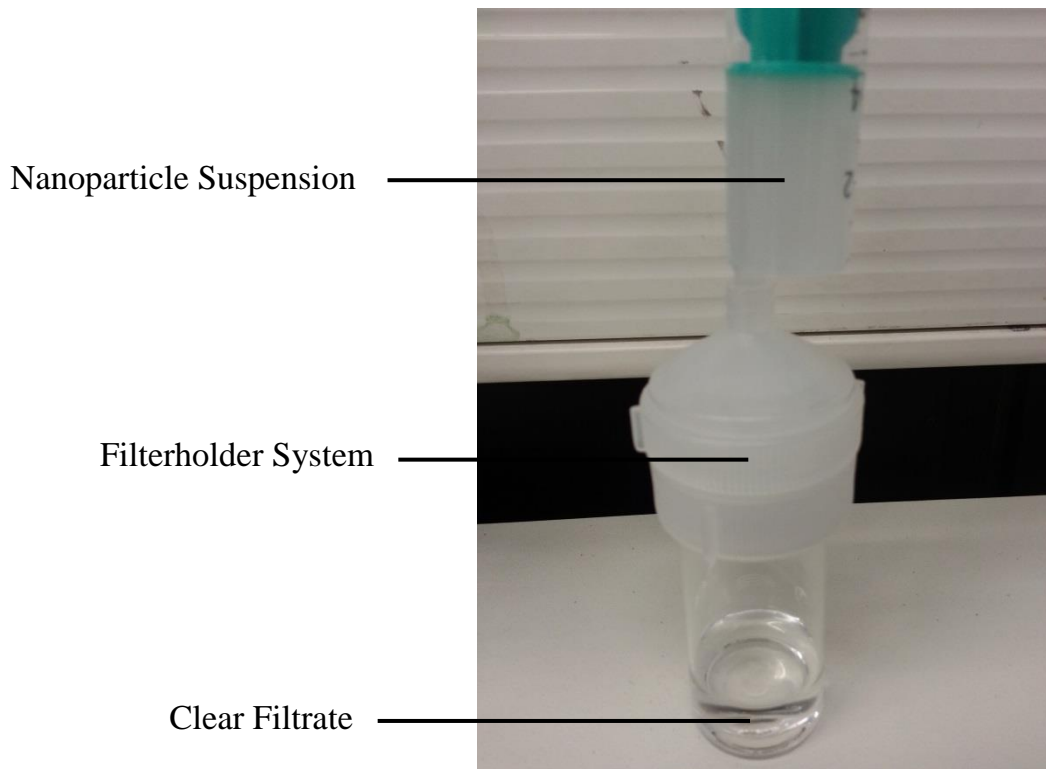
A**B**

Figure 1: **A.** Filter holder system hosting the template (blue) and blocking membrane (orange) for particle retention. The nanomaterial is applied to the system as an aqueous suspension. Whereas the dispersion medium water can pass the setting freely, the particles pile up within the template pores as they are not able pass the blocking membrane. Particle length (l) and diameter (d) are defined by the geometry of the template pores; **B.** Syringe-based infiltration of a turbid nanosuspension into the filter holder system leading to particle retention in the template pores and a clear filtrate.

For every successful gene delivery regimen a lysosomal buffering agent is needed besides the genetic material.^[2-4] The structural characteristics all these excipients share are amino groups, which can be protonated under physiological conditions and therefore showing a high buffering capacity in biological environments.^[5] The positively charged amines can be used as the counterpart to the negative plasmid DNA charges to fabricate a functional coating and at the same time providing structural integrity for the resulting microparticles. For the presented systems, which are exclusively assembled by electrostatic interactions, charge densities of the involved polymers determine the stability of the carrier.^[6] Therefore polymer and additional electrolyte concentrations, coating time and pH values are critical parameters influencing the deposition behavior of the polymers.^[7, 8] First of all pH values have a strong impact to reach high ratios of charged functional groups and are easily modified. By adding additional electrolytes to the LbL solutions, polymer deposition can be forced due to the displacement from hydration envelopes within defined concentration ranges.^[9-11] Especially for template-engineering techniques the salting-out effect has to be adjusted precisely to avoid excessive

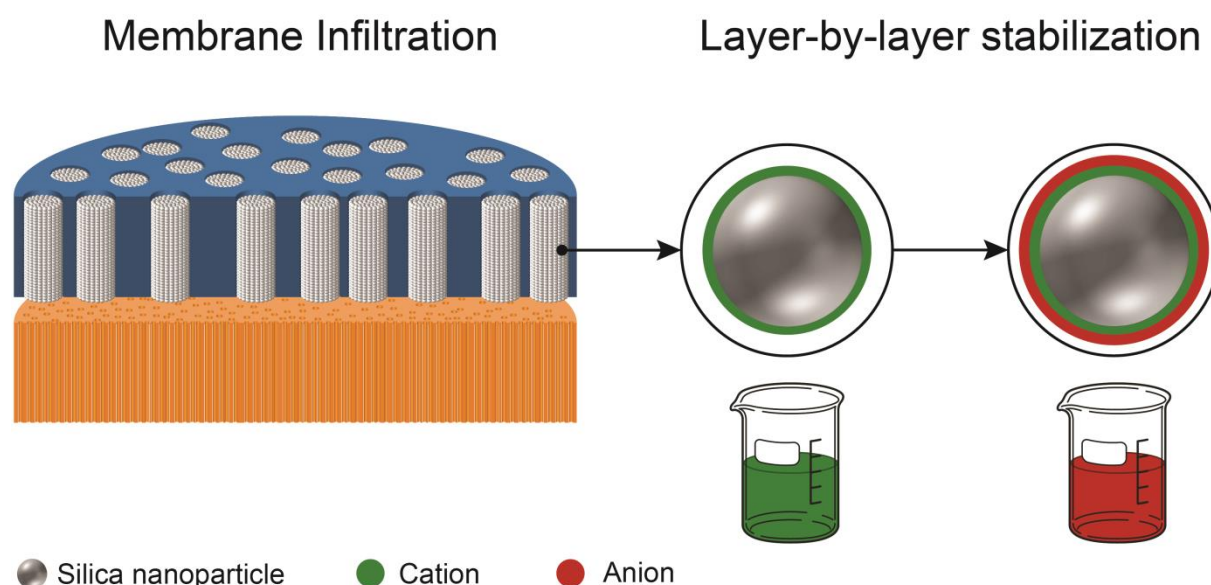


Figure 2: After the infiltration of the nanomaterial into the template pores, the particles get interconnected by a polymer coating. In a Layer-by-layer procedure the templates are applied to solutions of cationic and anionic coating agents leading to a cross-linking film and therefore to the stabilization of the cylindrical micron structure.

coating of the template itself corrupting the release of the particles, which is representing the last step of the engineering method. On that front, an example is presented in Figure **11 A** in this chapter visualizing polymer layers on the template surface as impediment for particle release.

Applied as a sacrificial template, the membrane gets dissolved in an organic solvent to harvest the nanostructured microparticles. For this approach, it is vital to use a suitable combination of materials and chemicals providing the efficient removal of membrane material while not dissolving the functional coating of the carrier system. Using polycarbonate (PC) as membrane material combined several advantages for the production method. Showing a sufficient degree of flexibility and being tear-proof, the templates can be easily handled during the infiltration and coating step. In addition, the range of organic solvents showing high solubility for PC such as tetrahydrofuran (THF) or dichloromethane (DCM) does not interfere with the LbL coating. After the dissolution of the template, particles can be collected by centrifugation and the removal of the polycarbonate in the supernatant. In order to reach high yields of microparticles showing the expected uniformity in geometry, the production steps were monitored in order to facilitate a rational optimization process. Especially the infiltration efficiency of the nanomaterial is regarded as crucial, since insufficiently filled pores will consequentially lead to micron structures differing from the template pore shape. Therefore, a protocol had to be established providing both the information about the amount of nanomaterial needed for one template and about a standard filling procedure making sure the pores are filled homogeneously. The LbL conditions were adjusted for the stabilization of the nanomaterial using DNA with respect to the parameters previously mentioned. In addition to that, the alternating nature of the coating procedure could be visualized proving both the incorporation of the cargo and the LbL coating progress. Finally, a protocol for the release and purification was established separating the microparticles from free nanomaterial and

template debris. In the following chapter sections the decisive engineering steps are presented leading to a robust and reproducible protocol for the fabrication of aspherical, nanostructured microparticles.

II.2 Monitoring of the Engineering Steps

II.2.1 Infiltration of Nanomaterial into the Templates

II.2.1.1 Material and Methods

II.2.1.1.1 Material

As template and blocking membrane track-etched Whatman Nuclepore polycarbonate filter membranes (25 mm; pore diameter 3 μm , pore length 10 μm) were used. Placed into Swinnex 25 mm filter holder systems, the nanosuspension can be applied by a syringe. All components of the setting were obtained from Sigma-Aldrich (Taufkirchen, Germany). For infiltration spherical silica nanoparticles of 200 nm in size were purchased as aqueous suspension (50 mg/mL) from Kisker Biotech (Steinfurt, Germany).

II.2.1.1.2 Methods

Template Preparation

For the following studies, a model nanoparticle made of silica (SNP) was used combining a wide range of advantages. Commercially available from numerous manufacturers to inexpensive conditions, SNPs are offered at a large size range including surface modifications. Especially the availability of different fluorescence labels makes them a straight forward candidate concerning tracking and visualization within biopharmaceutical and *in vitro/ in vivo* experiments. Furthermore, SNPs show high efficiency for the presented infiltration technique in comparison to organic polymers such as PLGA, which was also observed by our group.^[12] SNPs are provided exclusively in amorphous state showing density

values of 2.2 g/cm³ (PLGA 1.34 g/cm³) potentially leading to a superior sedimentation behavior within the template pores. In addition to that, most inorganic nanomaterials show high and constant stiffness compared to organic polymers.^[13-15] Especially sugar-based systems show significant swelling and shrinking when applied to aqueous media and in consecutive drying procedures respectively.^[16, 17] This implies size changes of the nanoparticles during microparticle preparation consequentially leading to variations in length and diameter of the desired micron structure. Lastly, indicated by the chemical structure in **Figure 3**, SNPs offer negative surface charges due to terminal oxygen groups providing the electrostatic environment needed for the LbL stabilization. For the evaluation of the amount

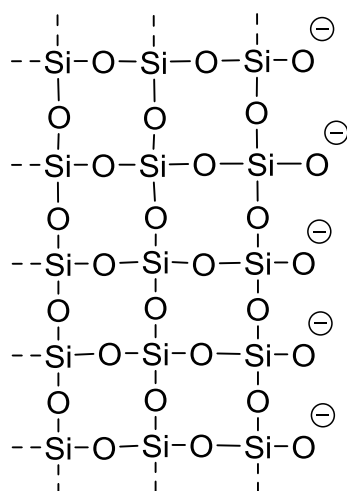


Figure 3: Chemical structure of silica (SiO₂) providing negative surface charges due to anionic oxygen groups.

of SNPs needed, the stock suspension was diluted with MilliQ water to a final concentration of 1.0 mg/mL. Using aliquots of 500 μL, the diluted nanosuspension got infiltrated into the template membranes in multiple steps. After every step, a part of the membrane was cut out, dried and prepared for visualization. To determine the rate of sufficiently filled pores, 5

random parts of the sample were focused by an electron microscope. For $n = 100$ pores, the number of SNP filled pores were counted.

Electron Microscopy Visualization

The membrane cutouts were applied to a carbon disk and sputtered with platinum or gold to a layer thickness of 10 nm prior to scanning. An accelerating voltage of 5 or 6 kV with a focal distance of 7.5 mm was used. The visualization was performed by a JEOL JSM-7500F scanning electron microscope (SEM).

II.2.1.2 Results and Discussion

In **Figure 4** the SEM visualization of a membrane cutout is shown focusing a single pore of 3 μm in diameter. The picture is taken from the top side of the membrane highlighting infiltrated SNPs in a loose packing. Clearly visible, the pore was sufficiently filled and therefore regarded as being representative for a positive result during the evaluation of the

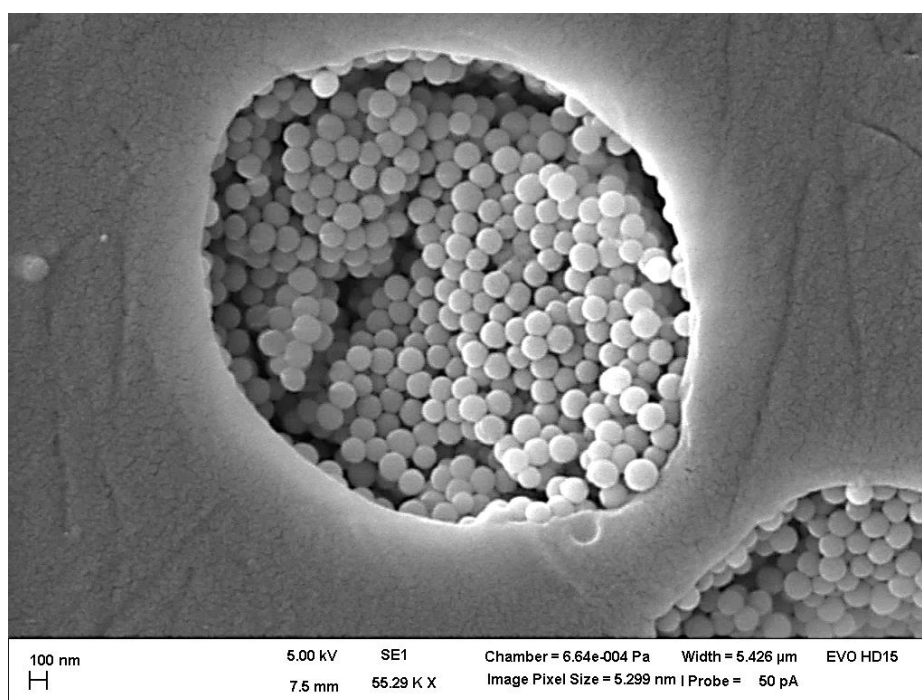


Figure 4: Electron microscopy (SEM) visualization of SNPs after the infiltration into the template membrane. The close-up shows particles of 200 nm in size piling up within the pore of 3 μm in diameter.

filling efficiency. Starting off with the first 500 μL aliquot of the SNP suspension only 44 % of the counted pores were filled sufficiently (**Figure 5 A**). By adding two consecutive infiltration steps, the applied SNP amount was increased to 1.5 mg reaching 83 % of filled pores (**Figure 5 C**). The increase by an additional fourth and fifth step to 85 % and 86 % respectively was not regarded as beneficial taking into account the time expenditure of a single infiltration.

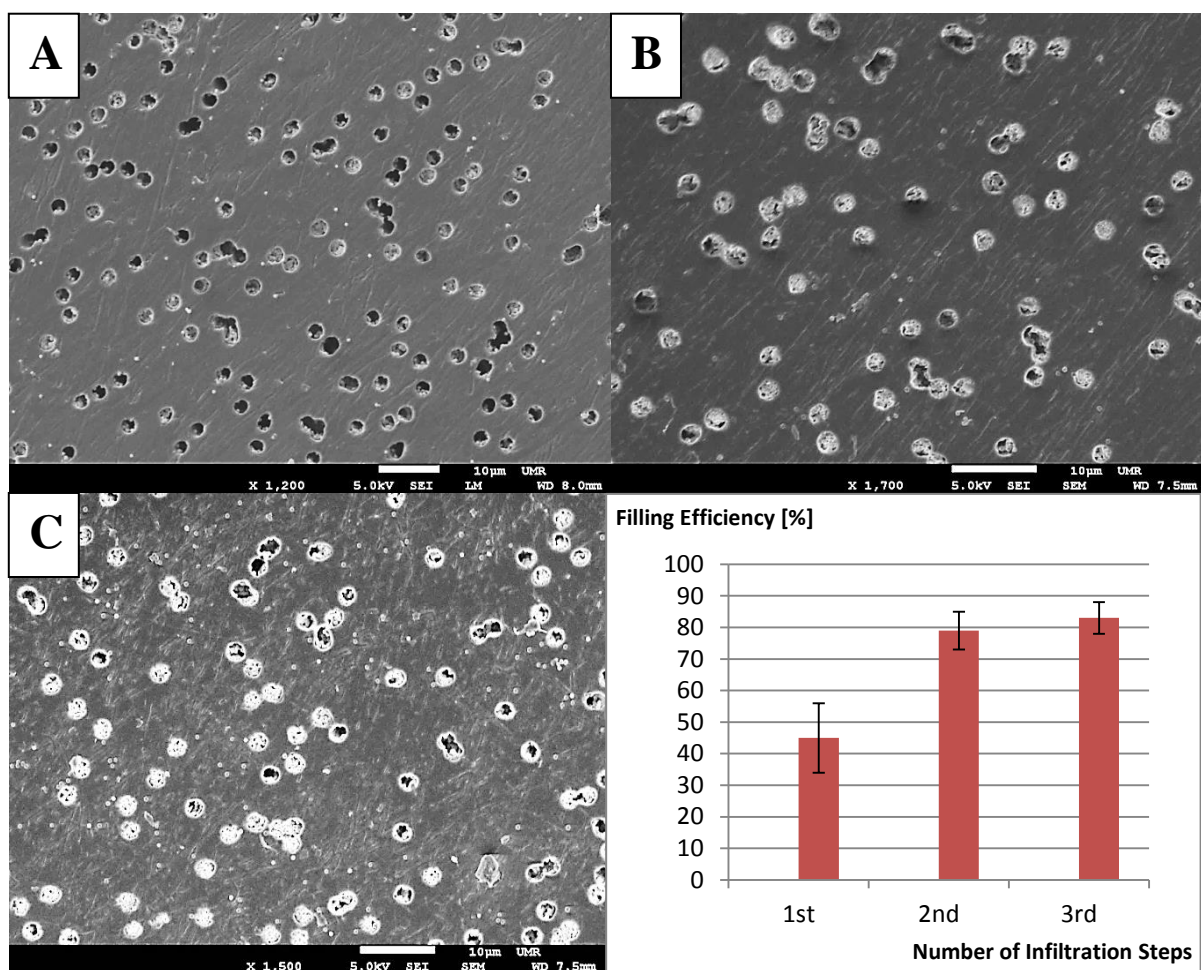
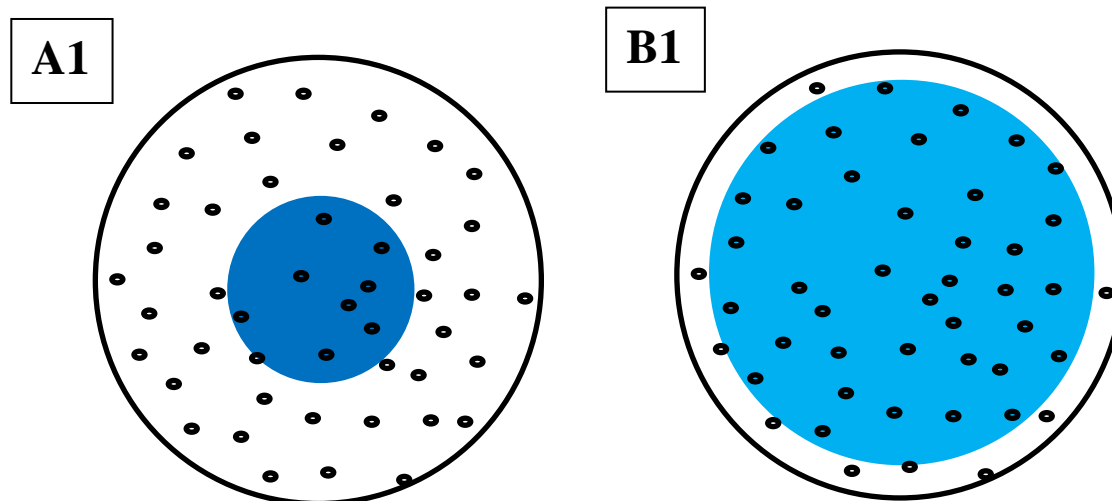


Figure 5: SNP infiltration progress as a triple infiltration step visualized by SEM microscopy. Whereas the percentage of filled pores was below 50% for a single filling step (**A**), the efficiency could be increased above 80% after a second (**B**) and third (**C**) infiltration summarized in the corresponding plot.

It seems logical to expect a higher percentage of properly filled pores by providing higher amounts of nanomaterial, but SNPs also showed the tendency to mainly deposit in the center of the membrane sparing out the pores at the edges. This was due to the filter holder inlet, which is placed above the center of the membrane compelling the suspension droplets from the syringe into the same area. Initially intended to stepwise determine the right amount of SNPs for one template, the multiple filling steps additionally turned out to shift the excessive nanomaterial from the inner to the peripheral pores. Since the complete template surface was cleansed prior to coating, the loss of nanomaterial could therefore be minimized leading to higher yields of microrods. To evaluate this spreading effect, the amount of 1.5 mg SNPs was kept constant for the comparison of a single and triple filling step. Illustrated in **Figure 6**, central pores of the template were focused after the infiltration. The excessive nanomaterial could be efficiently flushed from the center confirming the multiple infiltration steps to be beneficial for homogenously filled templates. To conclude from the first monitoring step, a sufficient amount of 1.5 mg of SNP per membrane was determined in addition identifying multiple infiltration steps to be beneficial for a homogenous distribution. For all the following experiments, the infiltration of the mentioned amount in triplets was maintained.



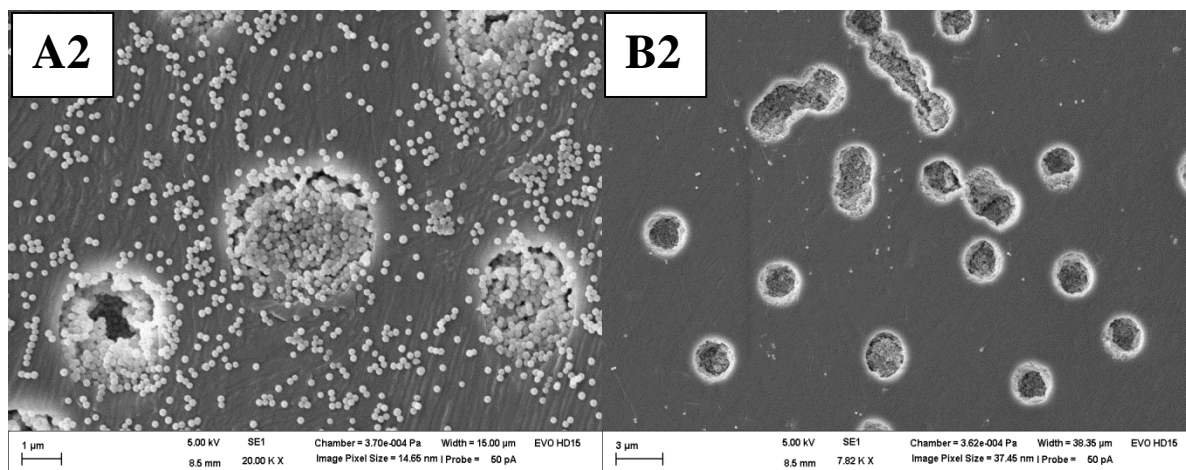


Figure 6: Comparison of the deposition behavior of SNPs in a single (A1+2) and triple (B1+2) infiltration step by SEM visualization. Whereas a single infiltration step leads to excess nanomaterial in the center of the membrane, a triple infiltration allows a homogenous distribution by flushing SNP to peripheral pores.

II.2.2 Layer-by-Layer Coating Using DNA

II.2.2.1 Material and Methods

II.2.2.1.1 Material

For the production of nanostructured microrods the protocol for the infiltration from the prior section was applied using SNPs of 200 nm and templates featuring 3 μm pores. For the LbL coating the plasmid DNA pCMV-luc encoding for the reporter gene firefly luciferase was obtained from PlasmidFactory (Bielefeld, Germany). For the opposite charges branched polyethylenimine (bPEI, M_w 25 kDa) was purchased from Sigma Aldrich (Taufkirchen, Germany). For agarose gels, agarose NEEO as well as sodium chloride, bromophenol blue-glycerine mixture, TAE buffer (tris-(hydroxymethyl)-aminomethane (TRIS), sodium acetate, ethylenediaminetetraacetic acid (EDTA)) and the intercalating agent ethidium bromide (EtBr) were kind gifts from the Helmholtz Institute for Pharmaceutical Research Saarland (HIPS). The visualization was performed by a benchtop Transilluminator UVP (Cambridge, UK). The organic solvent THF for the template dissolution was obtained from VWR (Darmstadt, Germany).

II.2.2.1.2 Methods

LbL Coating Procedure

After the infiltration of SNPs into the pores, the template membranes were applied to aqueous solutions of pCMV-luc and bPEI. The procedure was performed in glass vials for 12 min each for both polyelectrolytes. During coating the membranes floated freely in the solution without additional stirring. A rinsing step in MilliQ water was performed after every coating step to get rid of excess polymer especially on the template's surface. Since the initial charge provided by silica was negative, the LbL cycle (**Figure 7**) was always started with a first layer of bPEI. The pH of a 2 % (m/V) bPEI solution was adjusted to 7.0 with the addition of 0.1 M sodium chloride. The overcompensation of negative charges by bPEI to positive values allows the deposition of the plasmid DNA onto the particles' surface in the second coating step. Therefore, 1 mg pCMV-luc was dispersed in 10 mL of purified water also with an additional 0.1 M sodium chloride. The resulting coating of one LbL cycle is constituted as one double-layer (PE+/PE-). The cycle can be repeated as often as desired, until the nanoparticles get interconnected with each other stabilizing the micron structure within the template pores.

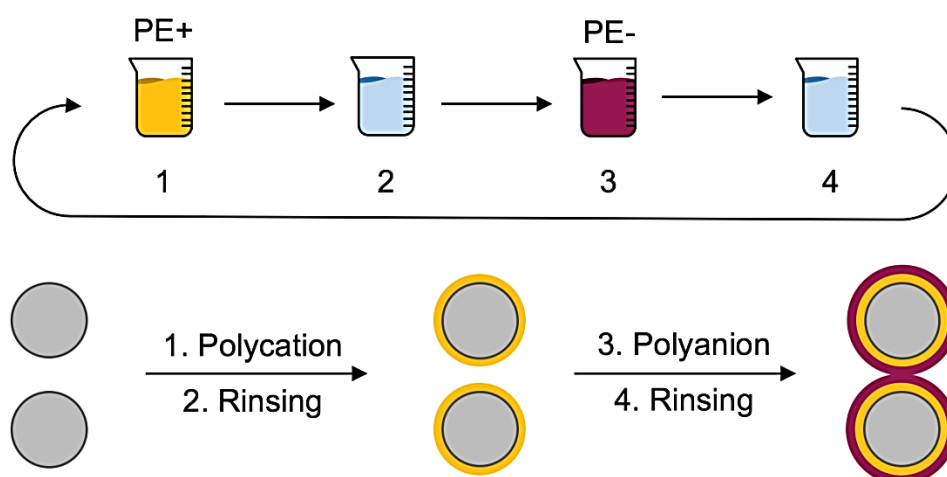


Figure 7: The LbL coating procedure is performed in cycles starting with the initial deposition of PE+ onto the negatively charged SNPs. In a second step PE- can be deposited due to the electrostatic attraction leading to one double-layer of PE coating. Adding rinsing steps after polymer deposition, the procedure can be performed in cycles until the coating material interconnects the individual nanoparticles.

Microrod Release from the Template and Purification

After the deposition of the needed amount of double-layers, the templates got dried at room temperature. Transferred to Eppendorf tubes, the templates were exposed to 1.0 mL THF, which dissolved the membrane material immediately. To remove the PC and free nanomaterial from the sample, centrifugation at 6500 g for 7 minutes was applied. Afterwards the supernatant got disposed and another 1.0 mL THF was used to redisperse the particle pellet. The purification protocol was repeated 5 times to remove all remaining PC debris from the microrods.

Agarose Gels for DNA Visualization

For gel preparation, 0.8 g agarose NEEO were dissolved in 80 mL TAE buffer by heating at 60 °C for 2 minutes. After cooling down to room temperature, 5 µL ethidium bromide (EtBr) solution (10 mg/mL) were added and the mixture was applied to the tray to solidify. The gel formation was completed after 30 min and the tray was applied to the electrophoresis chamber. Fully covered in TAE buffer, 50 µL of microrod suspension was mixed with 10 µL bromophenol blue-glycerine mixture as loading agent and applied to the pockets. At 80 V the electrophoresis was performed for 60 minutes with a consecutive fluorescence evaluation at Excitation 360 nm, Emission 590 nm.

Electron Microscopy Visualization

For visualization the regular SEM settings from last section were used. In addition to that, eSEM settings were used increasing the atmospheric pressure to 200 Pa allowing the sample to be visualized in dispersed state in MilliQ water.

II.2.2.1 Results and Discussion

Evaluating the wide range of commercially available polycations, the ideal candidate to combine with the plasmid DNA had to be characterized by tolerating high charge densities for both engineering and application purposes. On the one hand, high charge densities are important for a sufficient polymer coating. Providing an environment of high electrostatic attraction promotes polyelectrolyte deposition and is therefore vital for the fabrication of films reaching the structural integrity for the resulting microparticulates. Furthermore, in the presented system the stabilizing agents are at the same time the active ingredient and transfection agent respectively. Higher polymer content due to high electrostatic forces can in addition contribute to a desired increase in cargo loading. On the other hand, macrophages as the cells of interest are able to generate harsh enzymatic and acidic conditions within phagolysosomes upon particle uptake. Therefore, the efficient protection and escape of DNA/RNA-based cargos from the disruptive environment has to be provided. While high buffering capacities are expected to contribute to overcome the lysosomal barrier, the protection is related to the DNA/RNA condensation capabilities. Transfection agents such as bPEI (**Figure 8**) show both a high buffering capacity spanning the physiological pH range and high condensation efficiencies for polyanions, which can both be ascribed to the ability of exhibiting high surface charge densities. Since the introduction of PEI in 1995 by Boussif et al., it is up to the present day the most investigated and commonly used agent providing high transfection efficiencies.^[18] It was therefore the first candidate to apply to the microrod engineering approach in order to design a novel gene delivery system. For the monitoring of the progress of the LbL coating, a method was applied to prove the deposition of both of the excipients in a qualitative manner. Making use of the DNA intercalating properties of ethidium bromide, a fluorescence dye frequently used in molecular biology for the detection

of nucleic acids, a strong fluorescence emission can be visualized whenever the plasmid DNA is the outermost layer of the coating. With an additional layer of bPEI coated onto the pDNA,

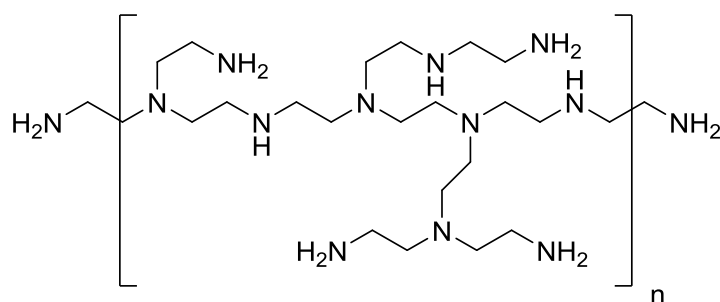


Figure 8: Chemical structure of bPEI providing positive charges due to amino groups, which can be protonated within aqueous environments.

intercalation is prevented and therefore no fluorescence signal can be detected. In **Figure 9**, the consecutive coating of 3 double-layers is presented. Due to their micron size the rods remain in the pockets of the gel showing no mobility. Starting the visualization in frame 1, no fluorescence can be detected from bPEI (PE⁺), whereas a signal from the EtBr staining is clearly visible when pCMV-luc (PE⁻) is applied as the outermost layer (frame 2). For the subsequent LbL layers the same results could be obtained allowing the following conclusions. Ethidium bromide-promoted fluorescence signals from pDNA layers showed the successful incorporation of the cargo into the microparticles. The strongly suppressed fluorescence signal by an additional layer of bPEI supported the assumption for the genetic material to be shielded to a certain degree from a potentially degrading environment, such as phagolysosomes. And lastly, EtBr-loaded agarose gels were introduced as an in-process control proving the coating procedure to be robust and suitable for the fabrication of multiple double-layers for microrod stabilization.

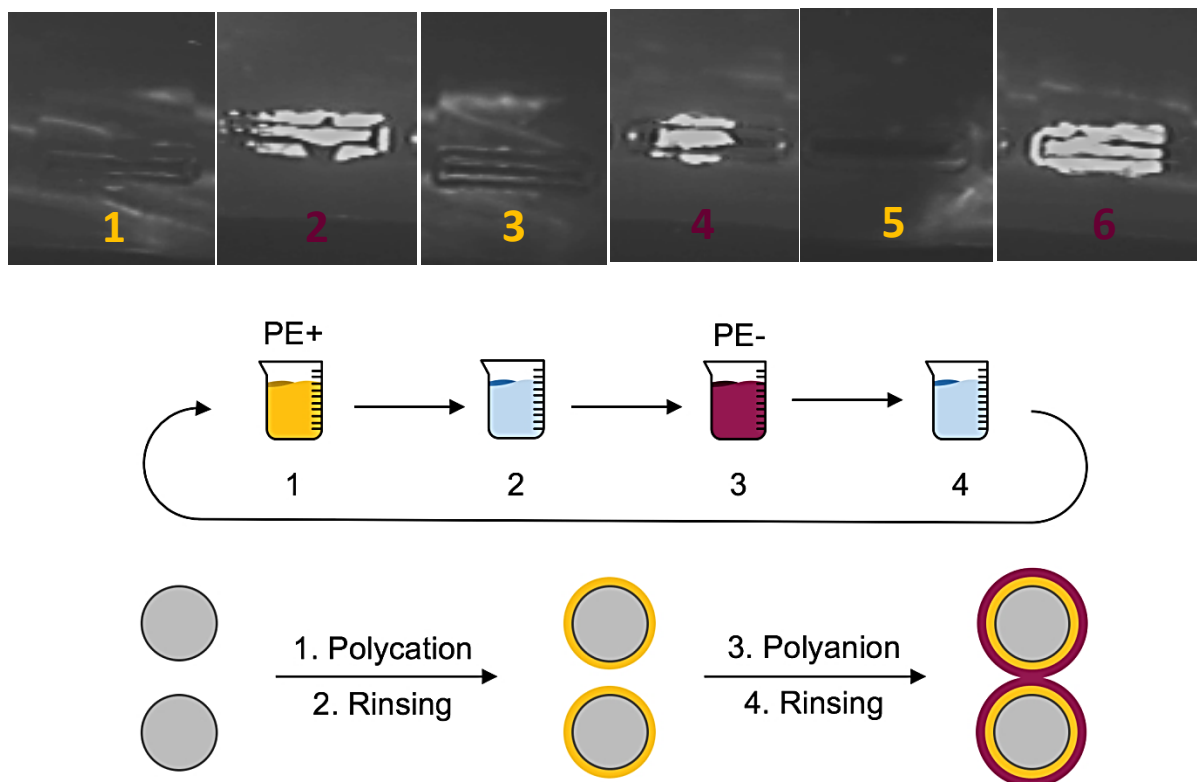


Figure 9: Visualization of the subsequent deposition of three double-layers bPEI//pCMV-luc onto the microrod system. Frames 1-6 show particle-loaded agarose gel pockets and strong signals upon UV excitation, whenever pCMV-luc is the outermost layer (frames 2, 4, 6). With an additional layer of bPEI the signal is shut down avoiding EtBr intercalation (frames 1, 3, 5).

An important aspect about the LbL coating, which had to be adjusted carefully, was the concentration of additional electrolytes in the PE solutions. The first protocol for the presented method was established by Kohler et al. using the model PEs polyallylamine and polystyrene sulfonate with the addition of 0.5 M sodium chloride.^[1] In a first experiment, the salt concentration was maintained and applied to the bPEI-pCMV-SNP system. The initial concentration was supported by Ren et al. who presented a study on the deposition efficiency of DNA into LbL layers depending on the sodium chloride concentration in the coating solution.^[19] They found an optimum of again 0.5 M for maximum DNA incorporation (**Figure 10**).

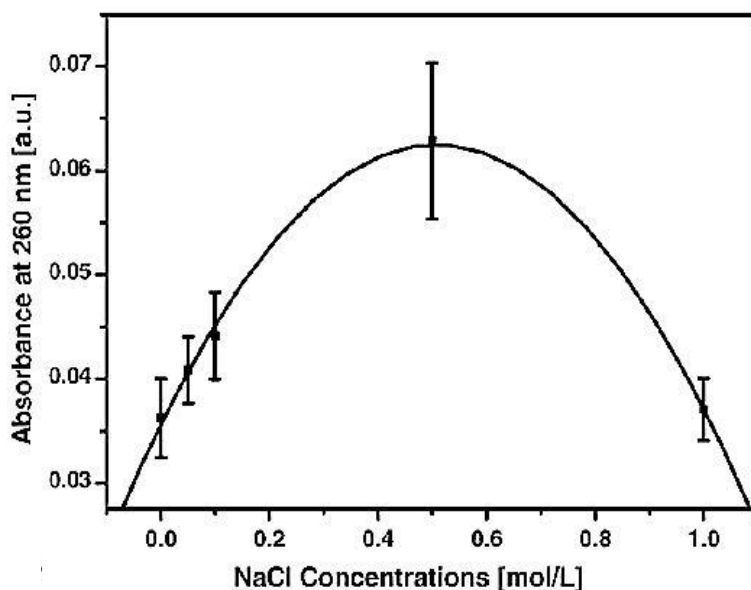


Figure 10: Graph by Ren et al. on the dependence of DNA incorporation into LbL layers on the sodium chloride concentration. DNA amount of the resulting layers was measured by UV spectroscopy at 260 nm. An optimum was found for 0.5 mol/L.^[19]

For the presented microrod system, the displacement of hydration envelopes turned out to be too harsh leading to an excessive PE deposition on the template surface. Even though the membranes were cleansed thoroughly between the different coating steps, the polymeric film was consistent isolating PC from the organic solvent. As a consequence, the template could not be dissolved, but was prepared for SEM visualization. In **Figure 11 A**, the template is shown covered by polymer layers, which are also immobilizing the microrods on its surface. Preventing the recovery of the particles completely, the sodium chloride concentration had to be reduced down to 0.1 M for unhindered release. The particles, gained after the purification, are characterized by high uniformity throughout the whole batch (**Figure 11 B**). They remained well dispersed in THF and did not show any tendencies for agglomeration when transferred to aqueous media, which was important for consecutive cell culture or animal studies. Looking closer at the microrods (**Figure 12**), it was indicated that they highly correspond to the template pore shape. At the surface, the polymer coating can be observed in filament-like structures interconnecting the nanomaterial.

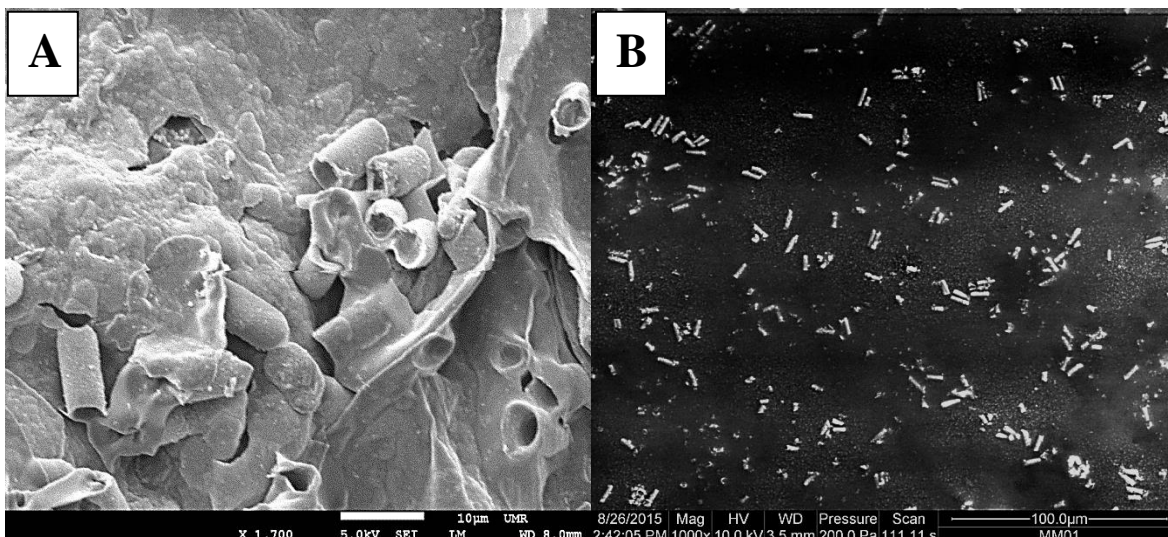
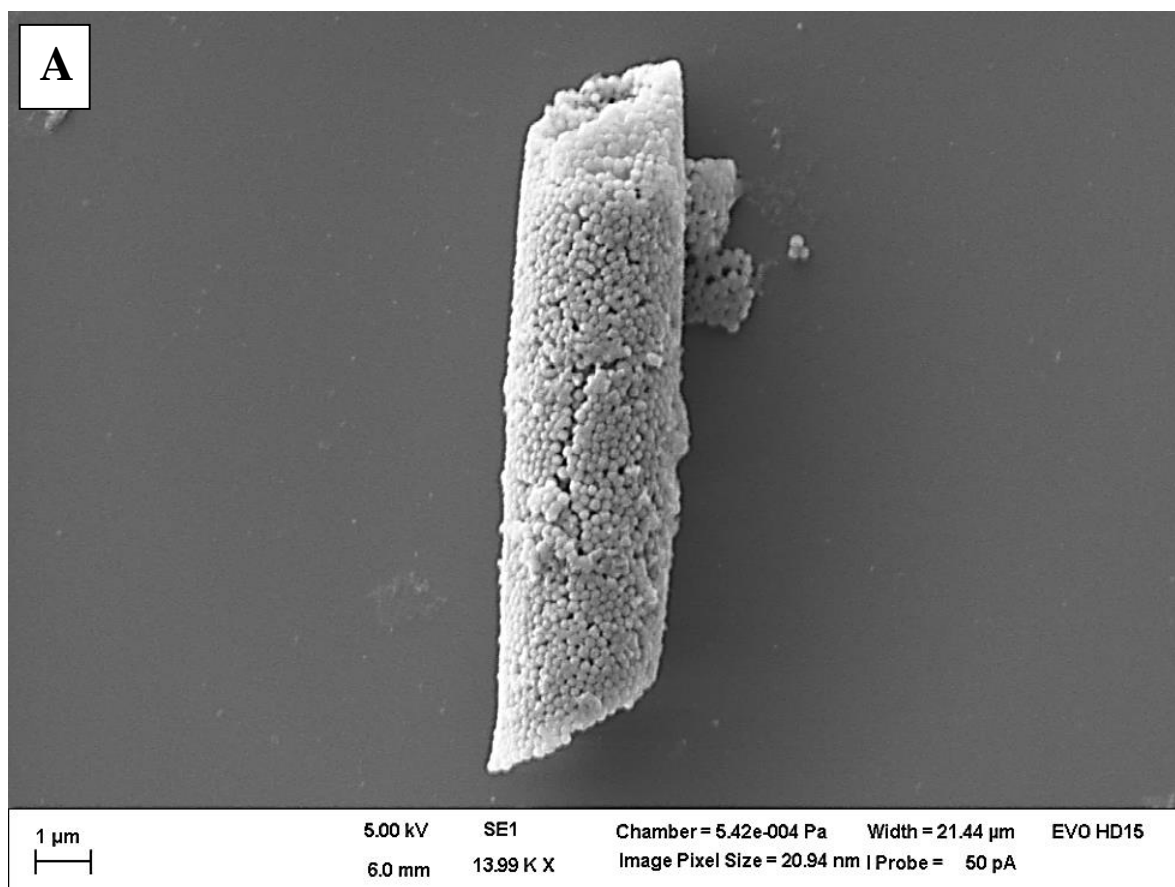


Figure 11: Electron microscopy visualization of microrods in immobilized (A) and released (B) state; A: Polymer layers on the surface of the template inhibited particle release; B: Reduction of sodium chloride concentration led to a full dissolution of the template in THF and therefore released microrods.



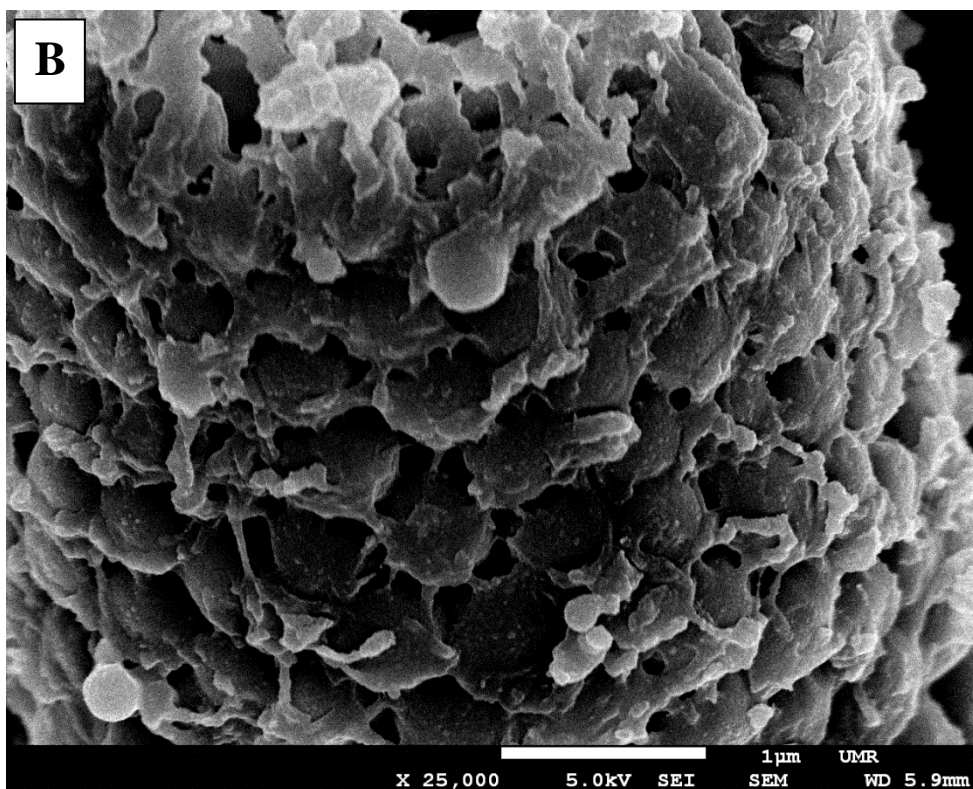


Figure 12: SEM close-up visualization of a bPEI-pCMV-stabilized microrod. **A.** the microrod shows high correspondence to the template pore shape. **B.** The polymer coating can be observed in fine filament-like structures interconnecting SNPs.

In summary, the established engineering protocol led to the stabilization of SNPs into the micron structure given by the template pores. The cylindrical geometry of 10 μm in length and 3 μm in diameter could be maintained to build up the desired rod formation. Therefore, the plasmid DNA cargo and the buffering agent bPEI were successfully introduced into the system adding functionality for the introduction of genes into target cells. For the conduction of cell culture experiments, rod amounts in the milligram scale were needed. Evaluating the amount of particles gained from one template, the rods were weighed after drying. A mass of 2.5 mg per template were found to be the average yield for the presented system. Scaling up the amount by preparing up to 15 templates in parallel, the sufficient amounts for cell culture studies could be easily reached.

II.2.3 Yield Evaluation and Calculations

To determine the efficiency of the engineering method, experimental data was correlated with the corresponding calculations. Due to their micron size, rods can be applied to a regular hemocytometer. Intended for the counting of red blood cells, an aliquot of the sample is infiltrated into a chamber featuring a grid. By visual determination using a microscope, the number of particles on the grid can be counted leading to an approximation for the whole sample. A suspension of defined concentration was used leading to a rod count of 3×10^6 rods per milligram. Including the average yield of 2.5 mg per membrane led to an overall count of 7.5×10^6 microrods per template membrane. For the used membranes of 25 mm (1) in diameter, an average pore count of 0.02 per μm^2 (2) was found leading to a total pore count of 10.95×10^6 (3) pores for one template membrane. The number reflects the maximum possible yield of microrods assuming a perfect infiltration and stabilization result. It was compared to the result gained from the experiments (4) leading to an overall efficiency of 75.4 % (5) of the engineering method.

$$(1) A_{\text{Template}} = \pi r^2 = \pi \times (12.5 \text{ mm})^2 = 491 \text{ mm}^2 = 4.91 \times 10^8 \mu\text{m}^2$$

$$(2) N_1 [\text{Pores}/\mu\text{m}^2] = 0.02$$

$$(3) N_2 [\text{Pores}/\text{Template, calculated}] = 4.91 \times 10^8 \mu\text{m}^2 \times 0.02 \text{ 1}/\mu\text{m}^2 = 10.95 \times 10^6$$

$$(4) N_3 [\text{Rods}/\text{Template, experimental}] = 7.5 \times 10^6$$

$$(5) \text{Efficiency } [\%] = \frac{7.5 \times 10^6}{10.95 \times 10^6} * 100 = 75.4$$

II.3 Preliminary Cargo Release Studies in Simulated Lung Fluids

II.3.1 Material and Methods

II.3.1.1 Material

For the simulated lung fluids magnesium chloride, sodium chloride, potassium chloride, disodium hydrogen phosphate, sodium sulfate, calcium chloride dihydrate, sodium acetate, sodium hydrogen carbonate, sodium citrate dihydrate and sodium hydroxide were obtained from VWR (Darmstadt, Germany). Citric acid, sodium tartrate dehydrate, sodium lactate and sodium pyruvate were purchased from Sigma Aldrich (Taufkirchen, Germany). For agarose gel electrophoresis the same excipients were used according to II.2.2.1.1. In addition a DNA ladder was used, which was a kind gift from Nicole Kuntschke, HIPS Saarbrücken.

II.3.1.2 Methods

Release Media

For the production of two relevant simulated lung fluids the following compositions were used according to Colombo et al.^[20]:

	Artificial Lysosomal Fluid [g/L]	Gamble's solution [g/L]
magnesium chloride	0.050	0.095
sodium chloride	3.21	6.019
potassium chloride	-	0.298
disodium hydrogen phosphate	0.071	0.126
sodium sulfate	0.039	0.063
calcium chloride dihydrate	0.128	0.368
sodium acetate	-	0.574

sodium hydrogen carbonate	-	2.604
sodium citrate dihydrate	0.077	0.097
sodium hydroxide	6.00	-
citric acid	20.8	-
sodium tartrate dehydrate	0.090	-
sodium lactate	0.085	-
sodium pyruvate	0.086	-
glycine	0.059	-
pH	4.5	7.4

All of the excipients were dissolved in purified water in the listed order to avoid precipitation. In addition a 3 M sodium chloride solution was prepared. In each solution, 1 mg of bPEI-pCMV-SNP microrods, stabilized by 3.5 double-layers, were incubated for 7 days. The particles in the simulated lung fluids were incubated at 37 °C whereas the sodium chloride solution was heated to 80 °C. For visualization an aliquot of the suspension was applied to an agarose gel.

Agarose Gel Electrophoresis

The same electrophoresis method was used as in the section before to visualize the plasmid DNA. In addition a DNA ladder was applied covering the range from 1 to 10 kilo base pairs (kbp). According to the manufacturer, the applied plasmid DNA consists of 6233 base pairs and should be detected within the mid-range of the ladder.

II.3.2 Results and Discussion

In the last section, the successful incorporation of plasmid DNA and bPEI into the particulate carrier system was shown. The fabricated films provided stability for the micron architecture leading to the necessary integrity for the upcoming experiments. In the subsequent step of a successful delivery, the cargo has to be released from the carrier at the site of action exclusively. Therefore the release behavior of the microrods was tested *ex vivo* for a first approach preliminary to cell culture studies. Taking into account the pulmonary application, two different simulated lung fluids were prepared. Upon inhalation and pulmonary deposition, the particles can either reside on the alveolar epithelium for a restricted amount of time or be engulfed by phagocytes for natural clearance. Artificial lysosomal fluid (ALF) is an analogue to the conditions particles are exposed to after phagocytosis by alveolar macrophages whereas Gamble's solution is simulating the interstitial environment of the deep lung. According to literature, LbL-stabilized systems generally show high stability suggesting an extended incubation time, which was set to seven days.^[21-23] In a parallel experiment microrods were incubated at non-physiological conditions (3 M saline, 80 °C) to set a release benchmark expecting a more pronounced destructive effect. The sample suspensions were applied to EtBr loaded gels to visualize the plasmid DNA on the particles' surface or in the suspension water. In **Figure 13**, the evaluation of all incubation media after 7 days is shown. According to the expectations, the benchmark suspension showed DNA fluorescence signals both on the particles' surface within the pockets and free migrated plasmid in the gel. The bands of pCMV-luc appeared in the range of 6 kbp indicated by the DNA ladder in line II. For the simulated lung fluids no DNA release could be detected. However, signals from the rods' surface could be observed potentially due to the electrolytes interfering with the electrostatic environment of the PE layers. The disrupting effect of the salts may have been strong enough for EtBr to penetrate into the layers reaching the DNA bases, but the full release from the

electrostatic interactions with bPEI could not be provided. What can be concluded from this study is on the one hand the confirmation for the presented system to show high stability.



Figure 13: Agarose gel electrophoresis for the visualization of plasmid DNA extracted from microrods. Evaluation was carried out after 7 days of incubation. Bands: (1) DNA ladder as positive control: I – 1 kbp, II – 6 kbp, III – 10 kbp; (2) and (3) microrods in 3 M sodium chloride at 80 °C as benchmark; (4) and (5) microrods in Gamble’s solution at 37 °C; (6) and (7) microrods in ALF at 37 °C; (8) purified water as negative control.

Only benchmark conditions, which are not present in biological systems, led to a release of the cargo from the deposited films. On the other hand the design of the experiment did not include the enzymatic arsenal of phagocytes. While there is no high enzymatic activity in the interstitium of the lung, lysosomal enzymes of macrophages could trigger the cargo release highlighting the possibility of a targeted release. This could be in particular interesting for microrod systems featuring, in contrast to bPEI, a biodegradable transfection agent. To pursue this strategy, microrods were tested in presence of degrading hydrolases in the following chapter.

II.4 References

- [1] D. Kohler, M. Schneider, M. Kruger, C.M. Lehr, H. Mohwald, D.Y. Wang, *Adv. Mater.* **2011**, *23*, 1376-1379
- [2] L. R. Carr, S. Jiang, *Biomaterials* **2010**, *14*, 4186-93
- [3] M. A. Mateos-Timoneda, M. C. Hennink, J. Feijen, J. F. Engbersen, *ChemMedChem.* **2008**, *3*, 478-486
- [4] C. Lin, J. F. Engbersen, *J. Control. Release* **2008**, *132*, 267-272
- [5] A. Akinc, M. Thomas, A. Klibanoc, R. Langer, *J. Gene Med.* **2004**, *7*, 657-663
- [6] B. Schoeler, G. Kumaraswamy, F. Caruso, *Macromolecules* **2002**, *35*, 889-897
- [7] S. L. Clark, M. F. Montague, P. T. Hammond, *Macromolecules* **1997**, *30*, 7237-7244
- [8] M. Ferreira, M. F. Rubner, *Macromolecules* **1995**, *28*, 7107-7114
- [9] Y. Lvov, K. Ariga, I. Ichinose, T. Kunitake, *J. Am. Chem. Soc.* **1995**, *117*, 6117-6123
- [10] N. G. Balabushevitch, G. B. Sukhorukov, N.A. Moroz, D. V. Volodkin, N. I. Larionova, E. Donath, H. Mohwald, *Biotechnol. Bioeng.* **2001**, *76*, 207-213
- [11] Y. F. Fan, Y.N. Wang, Y.G. Fan, J.B. Ma, *Int. J. Pharm.* **2006**, *324*, 158-167
- [12] M. Pourasghar, Evaluations on infiltration efficiency of PLGA nanoparticles into PC template membranes, internal research documentation, Group of Prof. Marc Schneider, Saarland University
- [13] Z. H. Guo, T. Pereira, O. Choi, Y. Wang H. T. Hahn, *J. Mater. Chem.* **2006**, *16*, 2800-2808
- [14] N. Lu, S. Yang, S. Qiao, *Proc. SPIE Micro- and Nanotechnology Sensors, Systems and Applications* **2014**, *Conference Volume 9083*,
- [15] T. Yu, J. Lin, J. Xu, T. Chen, S. Lin, *Polymer* **2005**, *46*, 5695-5697
- [16] T. Lopez-Leon, E. L. S. Carvalho, B. Seijo, J. L. Ortega-Vinuesa, D. Bastos-Gonzalez, *J. Colloid Interface Sci.* **2005**, *283*, 344-351
- [17] D. Gan, L. A. Lyon, *J. Am. Chem. Soc.* **2001**, *123*, 7511-7517
- [18] O. Boussif, F. Lezoualc'h, M. A. Zanta, M. D. Mergny, D. Scherman, B. Demeneix, J. P. Behr, *PNAS* **1995**, *92*, 7297-7301
- [19] K. Ren, Y. Wang, J. Ji, Q. Lin, J. Shen, *Colloids Surf. B* **2005**, *46*, 63-69
- [20] C. Colombo, A. J. Monhemius, *Ecotox. Environ. Safe.* **2008**, *71*, 722-730
- [21] Z. Dai, L. Dähne, H. Möhwald, B. Tiersch, *Angew. Chem. Int. Ed.* **2002**, *41*, 4019-4022
- [22] J. Huang, Q. Shu, L. Wang, H. Wu, A.Y. Wang, H. Mao, *Biomaterials* **2015**, *39*, 105-113
- [23] Z. Feng, Z. Wang, C. Gao, J. Shen, *Adv. Materials* **2007**, *19*, 3687-3691

Chapter III

Microrods Featuring Biodegradability

III.1 Introduction: Stimuli-Responsive Drug Delivery Strategies

For the rational design of advanced drug delivery systems and therefore the optimization of pharmacotherapy, physiological and pathophysiological conditions of the human body can be exploited. Since decades, acidic non-steroidal anti-inflammatory drugs (NSAID) such as ibuprofen are used for pain relief showing a passive targeting to the actual site of action. Upon oral administration and resorption, NSAID show high accumulation in the inflamed tissue due to low extracellular pH. Here, the acidic drug molecules are present as free bases showing high permeability and a subsequent intracellular entrapment due to dissociation at higher pH within the cytosol.^[1] Promoted by recent progress in material sciences, novel carrier systems were created adapting the mechanism of pH-responsive targeting and also cargo release.^[2] Besides the utilization of pH, also enzymatic activity can be used to provide a controlled delivery of active agents. On the one side, extracellular enzymes can be used to reach an improved targeting of the carrier system. Noga et al. presented a study for the fabrication of nanoparticles decorated with hydroxyethyl starch (HES).^[3] Originally used as plasma expander, HES features high biocompatibility and biodegradability. Indented for intravenous administration within cancer therapy, they showed the HES decoration to be degraded by pancreatic amylase during circulation. Utilizing the enhanced permeability and retention effect (EPR) of solid tumors, particles accumulated in the malignant tissue as soon as a suitable particle size was reached.^[4] On the other side, enzymatic activity can be exploited to provide a controlled release of the cargo. Especially for the delivery of compounds with cytotoxic effects, a high beneficial impact for patients can be provided while restricting the pharmacological effects to a target area. Bernardos et al. presented a study for the controlled intracellular release of doxorubicin by polysaccharide crafted silica nanoparticles.^[5] They utilized lysosomal cleavage to reduce the chain length of the sugar polymers, which triggered the release of the cargo. The approach shows a specifically triggered release in a target

compartment with high potential to reduce side effects of the treatment where the necessary enzymatic activity is not present. Regarding the cargo release studies of the previous chapter, the utilization of new compounds for the microrod system was desired. Therefore, the introduction of enzyme-promoted degradability was in the focus to gain preliminary information about the release behavior of the particles for pDNA prior to cell culture studies. Taking into account the highly equipped enzymatic arsenal of macrophages as the target cells, applying stabilizing agents, which are substrates to lysosomal enzymes e.g. hydrolases, was a promising approach to trigger cargo release.^[6] For the selection process of suitable excipients the following important parameters had to be considered. The amino functionalization had to be maintained to provide both positive charges for the LbL coating procedure and high buffering capacity at the pH range from 4 to 7. A corresponding enzyme had to be present in macrophages to cleave the connecting structures to a high degree enabling chain length reduction and therefore facilitated pDNA release. Regarding polysaccharide materials, a broad range of dextran derivatives can be obtained including amino-functionalized species such as dextran amine or diethylaminoethyl-dextran (DEAE-D), which was preferred due to lower costs. Along with DEAE-D, chitosan was selected as a second amino-functionalized polysaccharide to carry out stabilization studies for the microrod system. The subsequent enzyme assays were performed in comparison to bPEI systems highlighting the introduction of sugar derivatives as a viable approach for the introduction of stimuli-responsive release behavior into the particle system.

III.2 Microrod Stabilization by Amino-Functionalized Sugar Polymers and DNA

III.2.1 Material and Methods

III.2.1.1 Material

For the production of microrods featuring biodegradability the same infiltration setup was used as in the chapter before. Nanoparticles made of silica were infiltrated into 3 μm pores of a PC template membrane. As amino-functionalized sugars DEAE-D 10 kDa was obtained from TdB (Uppsala, Sweden) and chitosan hydrochloride (CHT) 50-150 kDa (Protasan UP CL 113, degree of deacetylation > 85 %) was purchased from NovaMatrix (Sandvika, Norway). As DNA material the same plasmid pCMV-luc was used as in the previous experiments.

III.2.1.1 Methods

Layer-by-Layer Coating and Microrod Release

For the DEAE-D coating solution 200 mg were dissolved in 10 mL purified water for a 2 % (m/V) solution. The solution pH was adjusted to 7.0 and 100 mM sodium chloride was added. For chitosan the concentration was set to 1 % (m/V) considering the increase in viscosity caused by the distinct swelling in aqueous media. Using the hydrochloride salt of chitosan, it fully dissolved within 60 minutes without adding additional acid. The resulting solution appeared slightly yellow at a pH of 4.5 which was adjusted to 5.8 with additional 25 mM saline. Both PE⁺ were combined with pCMV-luc (PE⁻) using the same LbL cycle protocol as in the previous chapter. The release and purification was performed accordingly by template dissolution in THF and centrifugation.

III.2.2 Results and Discussion

DEAE-D as the amino-functionalized derivative of native dextran is a branched polysaccharide exclusively composed of glucose connected by α -1,6 or α -1,3 glycosidic bonds (**Figure 1**). It is widely used in biomedical applications such as protein stabilization, vaccine production or as transfection agent in gene therapy.^[7-9] Especially interesting for the utilization in LbL procedures Le Cerf et al. showed for DEAE-D that there is no significant increase in charge density by lowering pH even to its stability limit of 3.^[10] So a higher pH

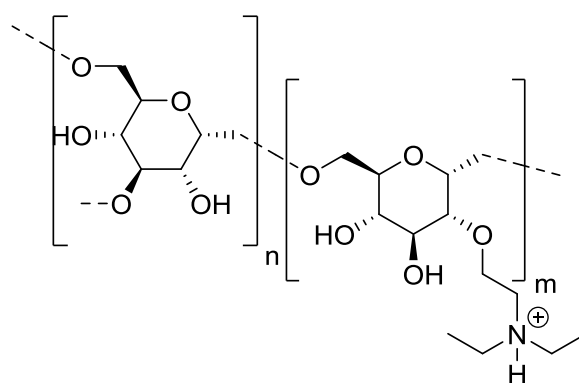


Figure 1: Chemical structure of DEAE-dextran featuring α -1,6 glycosidic bonds of glucose in the straight chains. Side chain branches start from α -1,3 linkages.

for the prepared solution was favored avoiding possible acidic hydrolysis of the plasmid DNA in the phosphate-sugar backbone. In the context of electrostatically driven LbL cycles, adjusting pH values always has to be regarded as a double-edged sword. On the one side, it can be possible to provide increased charge density for a promising excipient, but on the other side the amount of polymer deposition can be reduced by high acidity of the coating solution. This is due to the saturation of negative charges by protonation of the coating counterpart, especially when using strong PE-. For CHT this effect was studied in detail by Lundin and

colleagues.^[11] They investigated the deposition behavior of CHT from aqueous solutions onto negatively charged silica surfaces, which act as strong polyanion. Evaluated for two different pH values 4.2 and 5.8, they showed an increased deposition amount of CHT at higher pH due to an increased ratio of charged silanol groups at the template's surface. According to the authors for CHT this is in particular important since it interacts as a weak base and PE+. Their study found its way into the presented preparation of the CHT LbL solution as the amount of polymer deposition is crucial for the stabilization of the microrods. In addition, a reduced amount of saline was added to the solution at pH 5.8 since slight turbidity could be observed in preliminary studies for 100 mM. In contrast to bPEI and DEAD-D, CHT turned out to be a demanding excipient concerning the optimum coating conditions. Built up by randomly deacetylated D-glucosamine units (**Figure 2**) CHT is a highly investigated compound

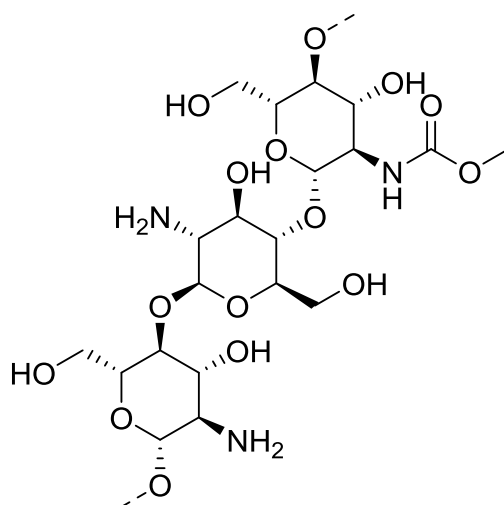


Figure 2: Chemical structure of chitosan built up by N-acetyl-D-glucosamine units with β -1,4 linkage. Monomers are randomly deacetylated due to hydrolytic treatment.

combining advantageous features for biomedical applications, such as tissue engineering or wound dressings due to its high biocompatibility, bacteriostatic effects and low toxicity.^[6, 7] Furthermore, it was shown to be a versatile carrier for biological macromolecules, including

genetic material for cell transfection, qualifying CHT for the stabilization and functionalization of microrods.^[12-14] For both excipients particle formation worked out leading to comparable yields in comparison to the bPEI systems (**Figure 3**). In contrast to the overview visualization of the bPEI batch, the sugar-stabilized batches were monitored in regular SEM mode under high vacuum. Therefore, the suspension is dried before measuring, which leads to the shown reversible agglomeration in the electron micrograph. The phenomenon is described as coffee ring effect caused by particle entrapment due to the collapse of the free surface after liquid evaporation.^[15] Within MilliQ water and organic solvents the particles remain well dispersed and do not show tendencies for agglomeration.

What can be concluded from the study is the confirmation for the engineering method to be robust for changes in excipients and layering conditions. By adjusting the coating solutions carefully regarding pH and saline, the deposition of PE of different charge densities can be provided adding new features such as enhanced biocompatibility or biodegradability to the carrier system. Substrate to glycoside glucosidases, DEAD-D and CHT stabilized microrods were expected to show a stimuli-responsive behavior enabling a triggered release of the plasmid DNA when applied to the right enzymatic conditions. Therefore, a protocol was established providing the prolonged enzymatic treatment of the rod formulations and a sensitive method for the measurement of the released plasmid, which will be presented in the following section.

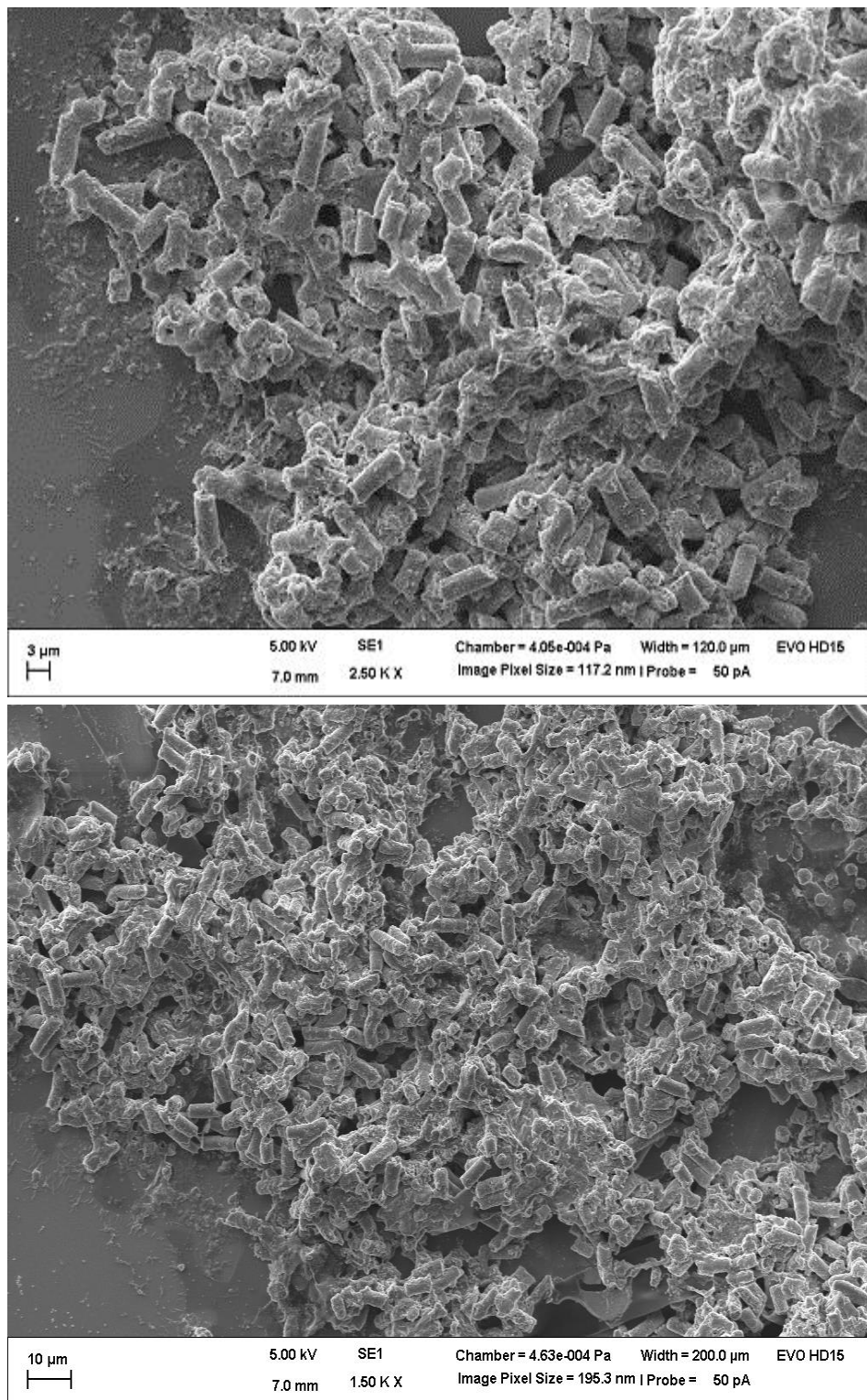


Figure 3: SEM visualization of microrods; A. Rods stabilized by 3.5 DL of DEAE-D and pCMV-luc; B. Rods stabilized by 3.5 DL of CHT and pCMV-luc.

III.3 Enzyme-Induced Release of DNA from Microrod Systems

III.3.1 Material and Methods

III.3.1.1 Material

For the enzymatic treatment of DEAE-D and CHT microrods lysosomal α -glucosidase from *saccharomyces cerevisiae* (300 units/mg) and lysozyme from chicken egg white (> 40.000 units/mg) were purchased from Sigma Aldrich (Taufkirchen, Germany). For fluorescence measurements a Tecan Reader Infinite 200 Pro (Tecan Group, Männedorf, Switzerland) was used. For confocal imaging particle suspensions were applied to 8 well μ -Slides from Ibidi (München, Germany).

III.3.1.1 Methods

Ethidium Bromide Assay for DNA Quantification

For the exact determination of the released plasmid DNA, a sensitive method allowing reproducible measurements down to 60 ng/mL was applied. Therefore, a protocol of Bonasera et al. was used who proposed an improved sensitivity by switching the excitation wavelength from the regularly used 270 nm to 250 nm while adding 0.5 μ g/mL ethidium bromide. The highest emission can be detected at 605 nm.^[16] This was in particular important since both enzymes also show fluorescence activity at an excitation wavelength of 280 nm due to tryptophan side chains featuring indole groups. Therefore, an increased separation of the excitation of the DNA and the enzymes could be combined with high detection sensitivity.

Enzymatic Treatment of Microrods

For both PE+, microrod batches were fabricated with a total polymer content of 3.5 DL. For the triggered release from the DEAE-D batch 1 mg microrods was incubated in an aqueous α -glucosidase solution. The concentration of glucosidase was set to 100 units equal to 340 μ g protein. After the addition of 50 mM sodium chloride, pH was adjusted to the activity maximum of the enzyme at 6.0 due to the manufacturer's specification. The suspension was stored in Eppendorf tubes at 37°C in an incubation chamber. The time points for the measurements were set to 0 h, 6 h, 12 h and 24 h to cover a burst release. After the first day, the measurement was performed once per day. Therefore, the suspension was centrifuged at 5000 g for 5 min using the resulting supernatant for analysis. For the CHT batches the same experimental setup was used, applying 100 units (2.5 μ g) lysozyme. pH was adjusted to the activity optimum of 6.2. In addition, DEAE-D and CHT microrods were stored in MilliQ water only to evaluate the unspecific influence of aqueous hydrolysis on the system. As a control microrods stabilized by bPEI were incubated with and without enzymes. All batches were evaluated in triplets.

Confocal Microscopy

For the visual evaluation of the degradation of the microrods the previous setting including bPEI controls were also incubated on 8 well microscopy plates. Utilizing the fluorescence label FluoBlue (Excitation 354 nm/Emission 450 nm) of the SNPs, microrods can be visualized for a qualitative evaluation of the degradation process.

III.3.2 Results and Discussion

In a preliminary study, fluorescence spectra of the applied enzymes were measured to verify strong signals at the expected wavelengths (**Figure 4**). Maximum fluorescence emission

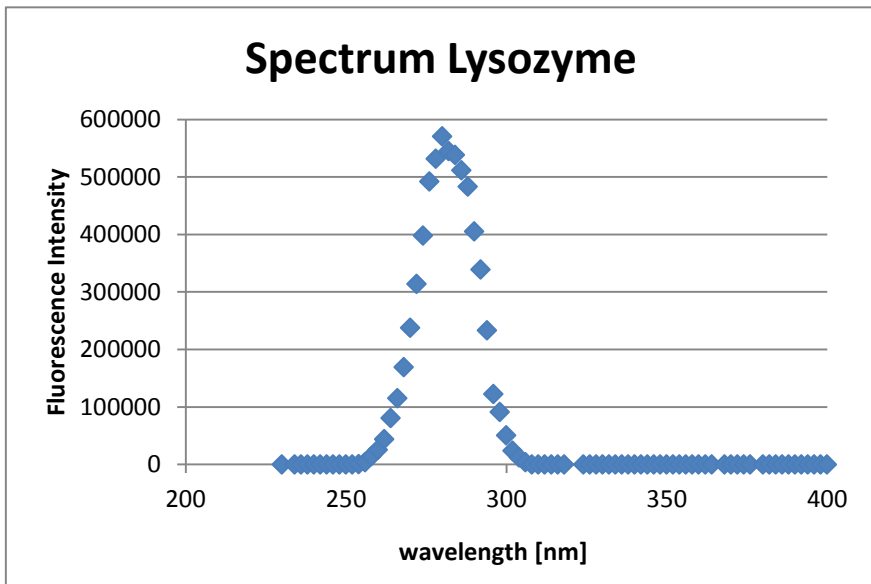
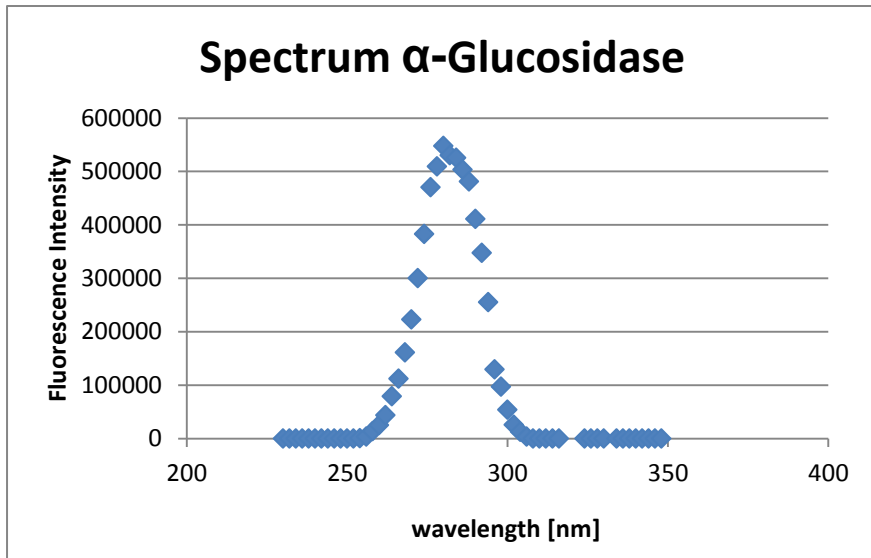


Figure 4: Fluorescence spectra of the applied enzymes α -glucosidase and lysozyme. Both proteins show maximum fluorescence emission for excitation wavelength $\lambda_{ex} = 280$ nm due to indole groups of the amino acid tryptophan.^[17, 18]

intensity was observed at an excitation wavelength of 280 nm for both α -glucosidase and lysozyme, which is linked to tryptophan residues in the amino acid sequence.^[17, 18] Upon excitation, aromatic indole groups in the side chains showed strong emission, which was measured at 305 nm. However, the decisive aspect about the spectra is the absence of signals for the excitation at 250 nm of the pDNA quantification assay where the results did not exceed the values of the base line. Therefore the measuring protocol was confirmed to selectively determine the amount of plasmid DNA in the supernatant without potential deviation by the degradation agents. In a consecutive step, a calibration of pCMV-luc with the addition of ethidium bromide was performed (**Figure 5**). Results indicated a suitable linear correlation down to a minimum of 60 ng/mL, which was regarded as the detection limit. Below this value no viable and reproducible results could be obtained from the measurement.

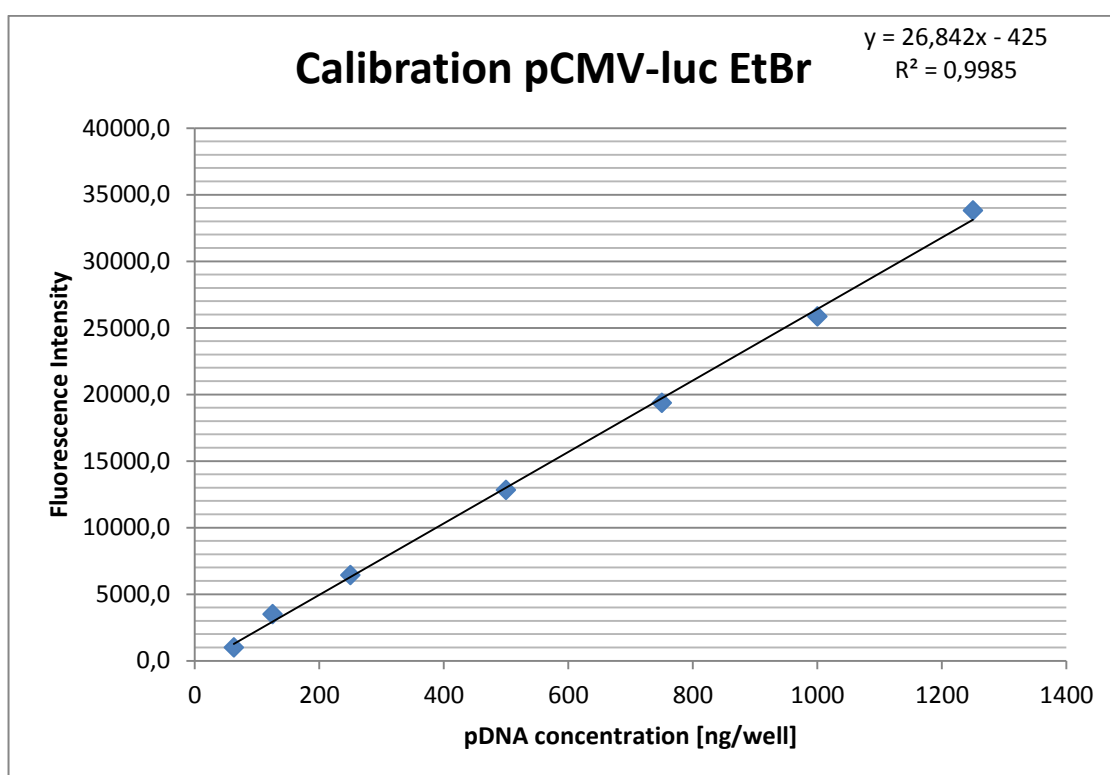


Figure 5: Calibration of pCMV-luc with the intercalating agent ethidium bromide at an excitation wavelength of 250 nm. A linear correlation could be obtained down to the concentration of 60 ng/mL. Corresponding error bars were too small to be displayed.

Applied to the incubated particle batches, the carried out measurements of the first day clarified that no burst release could be observed for the microrod systems (**Figure 6**). However, DEAD-D rods showed pDNA signals after 24 h and the highest overall release. Lysosomal α -glucosidase as a hydrolytic enzyme breaks down α -1,6 glycosidic bonds of DEAE-D disrupting the stabilizing matrix. As a consequence, the dissociation of the plasmid DNA from the carrier is facilitated leading to the highest release rates in the presented assay. But also CHT microrods showed a responsive behavior to the enzymatic treatment. Applied to lysozyme, which cleaves β -1,4 linkages from N-acetyl-D-glucosamines, CHT microrods started plasmid release at day 3 with a moderate increase within the studied time frame. Nevertheless, the dextran-glucosidase system performed at higher velocity and efficiency potentially caused by CHT, which is known to form hydrogels acting as a sustaining diffusion barrier.^[19, 20]

For bPEI no significant pDNA release could be measured according to the previous experiments. The same results were obtained for DEAE-D and CHT batches, which were only incubated in purified water. This observation indicated that the particles do not respond to unspecific aqueous hydrolysis, but are able to provide a controlled release, which can be triggered by the choice of the applied excipients for LbL coating. Furthermore, DEAE-D and CHT rods showed the tendency to reach a plateau for cargo release after 7 to 8 days. This could be a result of the completed degradation of the sugar derivatives with a maximum of free DNA or a loss in enzyme activity. Considering the enzymes to be exposed to repetitive mechanical stress during centrifugation and temperature variations, a decreased functionality of the enzymes was likely to occur during the study. In addition to that, it is also possible that diffusion as the driving force for release decreased to a level, where it was overcompensated by remaining attractive electrostatic forces within the polymer matrix. To further evaluate on the recent findings, the incubation and degradation process was monitored by confocal laser

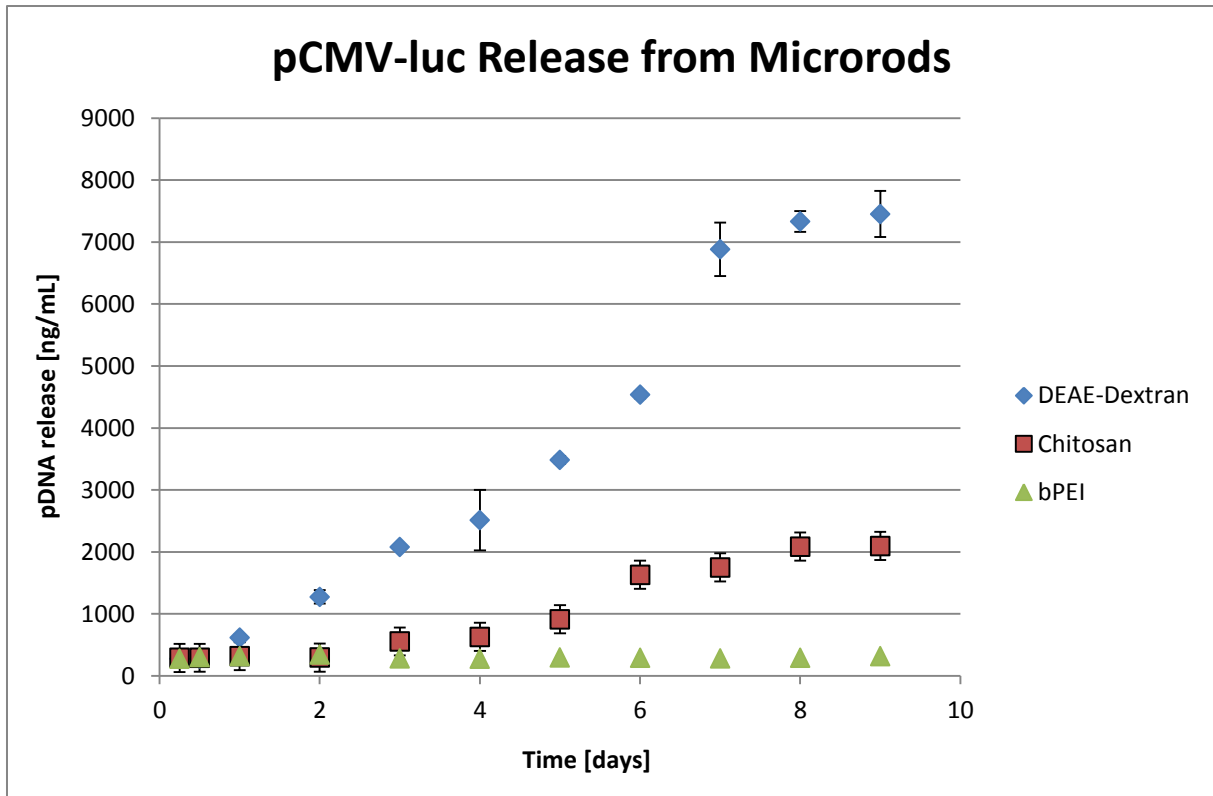


Figure 6: Evaluation of the enzyme-triggered pDNA released from DEAE-D, CHT and bPEI batches: For an observation time frame of 9 days bPEI did not show any pDNA release according to previous studies. For DEAE-D and CHT pDNA signals could be observed proving a stimuli-responsive behavior for the biodegradable excipients.

scanning microscopy. The whole setup was maintained, but transferred from Eppendorf tubes to 8-well microscope incubation chambers. Due to the FluoBlue fluorescence label of the SNPs, the micron structures could be easily monitored. As depicted in **Figure 7**, microrods show an increasing number of fragments during the observation time, but no complete disaggregation could be observed. The extent of fragmentation appeared higher for the DEAE-D batch, which would support the higher release rate and highlight a clear correlation between released plasmid DNA and enzymatic degradation of the carrier system.

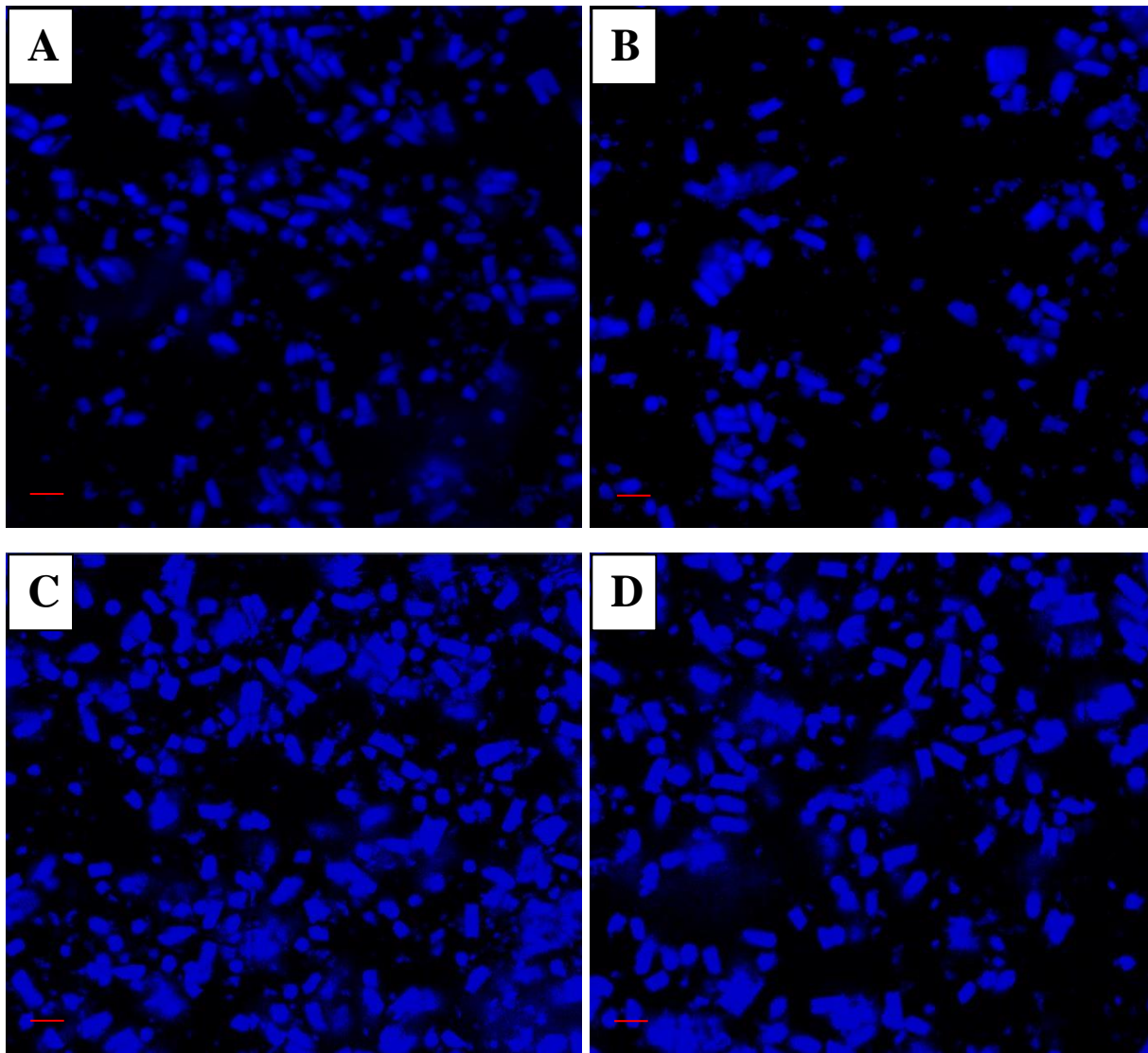


Figure 7: Confocal imaging of microrods incubated with degrading enzyme solution: a) and c) show DEAE-D stabilized rods right after incubation and after 9 days of treatment. b) and d) show CHT stabilized systems at the same time points. Scale bars refer to 10 μm .

Summarizing the study, the conducted experiments shed light on the pDNA release behavior of different microrod systems. By applying amino-functionalized sugars to the LbL coating, microrods could be stabilized to fabricate stimuli-responsive carrier systems. Plasmid DNA quantification was performed over a time period of 9 days indicating a triggered release when exposed to the appropriate enzymatic environment. A distinct increase in free DNA was measured in comparison to microrods featuring a non-biodegradable transfection agent. As substrates to enzymes present in alveolar macrophages, DEAE-D and CHT-based systems

qualify for the controlled delivery of nucleic acid based drugs. Whereas DNA release within phagolysosomes after engulfment can be expected, microrods were shown to remain stable in absence of high enzymatic activity. This can contribute to a targeted delivery of the transported genetic material to the cells of interest and at the same reduce unwanted side effects of free DNA in *in vitro* and *in vivo* environments.

III.4 References

- [1] K. Brune, P. Graf, *Biochem. Pharmacol.* **1978**, *27*, 525-530
- [2] T. Zhou, C. Xiao, J. Fan, S. Chen, J. Shen, W. Wu, S. Zhou, *Acta Biomater.* **2012**, *9*, 4546-4557
- [3] M. Noga, D. Edinger, R. Kläger, S. V. Wegner, J. P. Spatz, E. Wagner, G. Winter, A. Besheer, *Biomaterials* **2013**, *34*, 2530-2583
- [4] J. Fang, H. Nakamura, H. Maeda, *Adv. Drug. Deliv. Rev.* **2011**, *63*, 135-151
- [5] A. Bernardos, L. Mondragon, E. Aznar, M. D. Marcos, R. Martinez-Mañez, F. Sancenon, J. Soto, J. M. Barat, E. Perez-Paya, C. Guillem, P. Amoros, *ACS Nano* **2010**, *4*, 6353-6368
- [6] S. Gordon, *Fundamental Immunology*, Vol. 4 (Ed: W. Paul), Lippincott Raven, Philadelphia, PA, USA **1999**, Ch. 15
- [7] H. P. Erickson, D. W. Taylor, K. A. Taylor, D. Bramhill, *PNAS* **1998**, *93*, 519-523
- [8] D. Piedrafita, S. Preston, J. Kemp, M. de Veer, J. Sherrard, T. Kraska, M. Elhay, E. Meeusen, *PLOS ONE* **2013**, *8*, e78357
- [9] M. F. Carey, C. L. Peterson, S. T. Smale, *Cold Spring Harb. Protoc.* **2010**, *2*, 189-191
- [10] D. Le Cerf, A. S. Pepin, P.M. Niang, M. Cristea, C. Karakasyan-Dia, L. Picton, *Carbohydr. Polym.* **2014**, *113*, 217-224
- [11] Maria Lundin, F. Solaqa, E. Thormann, L. Macakova, E. Blomberg, *Langmuir* **2011**, *27*, 7537-7548
- [12] F. Croisier, C. Jérôme, *Eur. Polym. J.* **2013**, *49*, 780-792
- [13] S. Ahmed, S. Ikram, *J. ALS* **2016**, *10*, 27-37
- [14] Z.-X. Liao, S.-F. Peng, Y.-L. Chiu, C.-W. Hsiao, H.-Y. Liu, W.-H. Lim, H.-M. Lu, H.-W. Sung, *J. Con. Rel.* **2014**, *193*, 304-315
- [15] R. D. Deegan, O. Bakajin, T. F. Dupont, G. Huber, S. R. Nagel, T. A. Witten, *Nature* **1997**, *389*, 827-829
- [16] V. Bonasera, S. Alberti, A. Sacchetti, *BioTechniques* **2007**, *43*, 173-176
- [17] B. H. Neugebauer, R. Rudolph, *Biochemistry* **1991**, *30*, 11609-11614
- [18] T. Imoto, L. S. Forster, J. A. Rupley, F. Tanaka, *Proc. Nat. Acad. Sci.* **1971**, *69*, 1151-1155
- [19] K. Bowman, K. W. Leong, *Int. J. Nanomedicine* **2006**, *1*, 117-128
- [20] K. Oungbho, B. W. Müller, *Int. J. Pharm.* **1997**, *156*, 229-237

Chapter IV

Technological Characterization of Microrods

For section IV.1 the author of the thesis made the following contributions to the chapter:

Design, fabrication and sample preparation of defined masses of microrods, calculations and interpretation of all experimental data.

ICP-OES analysis was performed by Andrea Jung of the division Chemical Analysis at Leibniz Institute for New Materials (INM, Saarbrücken).

IV.1 Quantification of Microrod System Components

IV.1.1 Introduction to Layer-by-Layer Quantification

The introduction of Layer-by-Layer coating procedures to material and biomedical sciences prompted an increased demand of suitable analytical methods to study mechanisms and amounts of compound deposition. To answer this need, existing methods such as atomic force microscopy (AFM) were adapted allowing to measure layer thickness and showing polymers to be deposited in nanometer thin films.^[1] Szarpak and colleagues therefore studied the deposition of polyelectrolytes onto microparticles in dry state illuminating deposition patterns and also morphological changes of the films in dependence on the number of coated layers. Introducing isothermal titration calorimetry (ITC) to LbL coating evaluation, mechanistic studies could be performed at high sensitivity giving insights into binding affinities, dissociation constants and thus quantitative molecular interactions of excipients. Similar to the presented microrod system, Chiad et al. studied the interactions of colloidal silica particles with different polymers.^[2] For defined parameters such as temperature, solvents and polymer concentration, they were able to calculate binding constants giving detailed insights into adsorption mechanisms and therefore into film formation. By the introduction of quartz crystal microbalances (QCM) the monitoring of LbL films could be extended from structural properties and binding affinities to the determination of absolute amounts of deposited polymer. The technique is based on a quartz crystal showing the piezoelectric effect and therefore changes in resonant frequency upon film deposition. This made QCM a frequently used method for microgravimetry. Malmstöm et al. published a study on the evaluation of protein adsorption onto nanostructured surfaces utilizing QCM.^[3] They used laminin as a model protein quantifying the amount which was adsorbed to gold or silicon substrates. The substrates themselves were either present as homogenous films or as colloidal particles

immobilized onto the QCM electrodes. They were able to identify differences in deposition depending on the hydrophobicity and morphology of the substrates. Their results indicated high amounts of protein when coated onto hydrophobic gold substrates or onto nanostructured surfaces leading to a more detailed understanding of the deposition of large biomolecules onto colloidal substrates.

All the mentioned techniques contributed to gaining a general understanding for LbL principles, but they were not suitable to apply them as an in-process control during particle preparation. That is the reason why in many published works the layer quantification is spared out or performed by supernatant analysis after coating. Therefore polymer concentration is measured before and after coating assuming the difference to be present in the resulting films. When using a template-assisted approach for particle engineering, unspecific adsorption onto the template has to be taken into account, which will directly result in deviations for polymer quantification. To avoid these hurdles, a direct method for the final carrier system had to be introduced featuring high sensitivity for small amounts of compounds, high selectivity for specific excipients and low material consumption. In a publication by English et al. the quantification of DNA was performed by an element analysis for phosphorus showing high sensitivity and selectivity.^[4] For the microrod system this technique combined several advantages. On the one hand, selective cargo quantification in the range of one part per billion was possible and on the other hand a quantitative combustion ensuring to capture the whole phosphorus content present in the carrier. In addition to that, the low material consumption of the method allowed to reserve a small fraction for quantification whereas most of the batch could be used for further experiments such as cell culture studies.

IV.1.2 Material and Methods

IV.1.2.1 Material

For the quantification of the particle composition three batches of microrods were prepared. The particles were prepared according to the previous protocol stabilized by 2.5, 3.5 or 4.5 double-layers of bPEI and pCMV-luc using SNPs of 200 nm in size. ICP-OES measurements were carried out at a Jobin Yvon Ultima 2 (Horiba, Oberursel, Germany).

IV.1.2.2 Methods

Inductively Coupled Plasma – Optical Emission Spectroscopy (ICP-OES)

For the determination of the pCMV-luc and SNP content ICP-OES measurements were performed. By determining the amount of phosphorus and silicon, which are exclusively present in the DNA and nanoparticles respectively, the total amounts of the carrier system components can be calculated. Therefore 1 mg microrod samples of each batch were dissolved in a mixture of 0.5 mL hydrofluoric acid, 1.0 mL nitric acid and 5 mL deionized water. According to the operating principle displayed in **Figure 1**, the acid fusion was aerosolized using a nebulizer in combination with a high pressure (2.99 bar) argon stream.^[5] After the introduction into an argon plasma at 7,000 K, the sample gets atomized and excited for light emission. For quantification light emission intensity was measured at the specific wavelengths of phosphorus $\lambda = 214.914$ nm and silicon $\lambda = 252.611$ nm. The detected emission intensity is in direct proportion to the number of excited atoms in the sample solution. The results given by the device are calculated in mass percentages of the atom species with respect to the overall sample weight used for analysis.

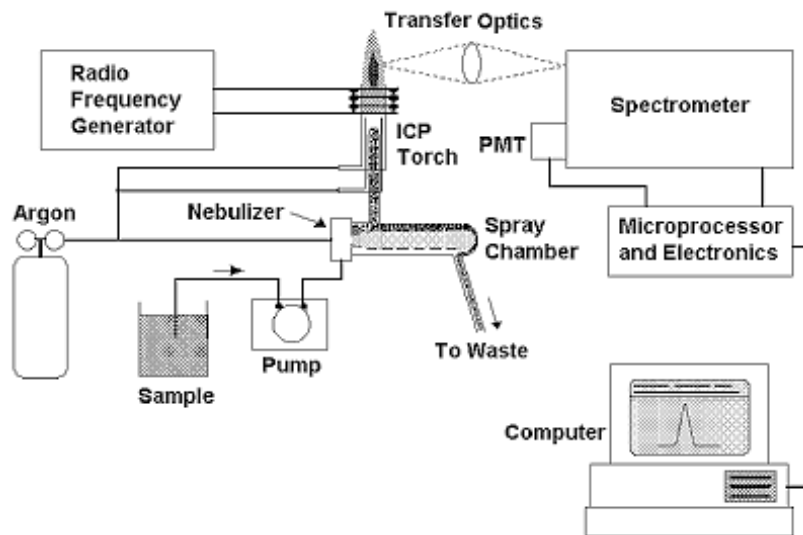


Figure 1: Operating principle ICP-OES: After acidic, aqueous dissolution, the sample gets nebulized and sprayed into an argon plasma. Resulting atomization and excitation allows quantification of elements by emission wavelengths and intensity.^[5]

Calculations for Mass Determination

After gaining mass percentage results for the determined atoms, the total amount of the molecules within the samples could be calculated. For the plasmid DNA the complete sequence was provided by the manufacturer allowing to calculate a mean value for the molecular weight of a nucleotide (M_{Nuc}) with respect to the ratio of bases present in the plasmid. Applying the molar mass of phosphor $M_{\text{P}} = 30.97 \text{ g/mol}$, the DNA amount was calculated as follows assuming one atom phosphor per nucleotide:

$$(1) \quad n_{\text{P}} = m_{\text{P}} / M_{\text{P}}$$

$$(2) \quad n_{\text{P}} = n_{\text{pCMV-luc}}$$

$$(3) \quad m_{\text{pCMV-luc}} = n_{\text{P}} \times M_{\text{Nuc}}$$

n_P – amount of substance phosphor [mol], m_P – mass phosphor [g], M_P – molar mass phosphor [g/mol], $n_{pCMV-luc}$ - amount of substance pCMV-luc, M_{Nuc} = median molecular mass of one nucleotide [g/mol]

For the determination of the silica content, the calculation was apparent from the simple chemical formula SiO_2 . For every mol of silicon detected by ICP-OES, two mol oxygen have to be added for the total amount of silica. The calculations were carried out according to the determination of the pCMV-luc with molar masses of silicon and silica $M_{Si} = 28.1$ g/mol $M_{SiO_2} = 60.1$ g/mol:

$$(1) n_{Si} = m_{Si} / M_{Si}$$

$$(2) m_{SiO_2} = n_{Si} \times M_{SiO_2}$$

n_{Si} – amount of silicon [mol], m_{Si} – mass silicon [g], M_{Si} – molar mass silicon [g/mol], M_{SiO_2} – molar mass silica [g/mol]

IV.1.3 Results and Discussion

For pCMV-luc with the size of 6233 base pairs a median molecular nucleotide mass $M_{Nuc} = 329.569$ g/mol was calculated. With the results from the phosphor determination summarized in **Table 1**, the total amount of the plasmid could be obtained for all three batches with increasing numbers of double layers. In the following, the exemplary calculations are depicted for a microrod test batch stabilized with 4.5 double-layers and a total sample weight of 1.21 mg:

$$(1) n_P = (2.3 \times 10^{-6} \text{ g}) / (30.97 \text{ g/mol}) = 7.43 \times 10^{-8} \text{ mol}$$

$$(2) n_{\text{pCMV-luc}} = 7.43 \times 10^{-8} \text{ mol}$$

$$(3) m_{\text{pCMV-luc}} = 7.43 \times 10^{-8} \text{ mol} \times 329.569 \text{ g/mol} = 2.45 \times 10^{-5} \text{ g} = 0.0245 \text{ mg}$$

According to the calculations 0.0245 mg plasmid DNA was incorporated into the particles with the deposition of 4.5 DL equal to 2.02 mass percentages of the whole sample. Here, the system behaved due to our expectations showing an increase in cargo loading with higher layer counts. At the same time the silica content was expected to decrease with an increasing ratio of polymer coating. With the results gained from the measurements the calculations are carried out for the same system as for the plasmid with a sample weight of 1.77 mg:

$$(1) n_{\text{Si}} = 6.759 \times 10^{-4} \text{ g} / 28.1 \text{ g/mol} = 2.4 \times 10^{-5} \text{ mol}$$

$$(2) m_{\text{SiO}_2} = 2.4 \times 10^{-5} \text{ mol} \times 60.1 \text{ g/mol} = 1.45 \times 10^{-3} \text{ g} = 1.45 \text{ mg}$$

	Batch 2.5	Batch 3.5	Batch 4.5
P [% m/m]	0.14 ± 0.04	0.16 ± 0.01	0.19 ± 0.01
pDNA	1.46	1.68	2.02
[% m/m]			
Si [% m/m]	44.30 ± 0,51	39.16 ± 0.11	38.20 ± 0.79
Silica	94.80	83.81	81.92
[% m/m]			

Table 1: Overview for the results gained from ICP-OES and subsequent calculations: For three batches of increasing LbL layer count phosphor and silicon content were measured. As a consequence pCMV-luc and silica content could be calculated.

With 1.45 mg silica in a sample of 1.77 mg in weight, SNPs represent 81.92 % of the microrod system. What can be concluded from the measurements and calculations is that the microrods are mainly composed of SNPs with nearly 95 % of total mass for the 2.5 DL batch. This additionally means that it is possible to stabilize the aspherical micron structure with only 5 % polymer content within the formulation. For the plasmid DNA only a slight increase of the content was observed by doubling up the layer count. However, the loading can be sufficient as the cargo features unique interactions within biological systems, which had to be evaluated in cell culture studies. By using ICP-OES, a fast and direct measurement method could be introduced for microrod characterization. The method shows high sensitivity with a sufficient amount of 1 mg sample. In addition to SEM visualization and EtBr-loaded agarose gels, ICP-OES is a viable tool for in-process monitoring during particle preparation.

As there is no element, which is exclusively present in bPEI, specific data was harder to obtain. By applying C-H-N (carbon, hydrogen, nitrogen) elemental analysis, the nitrogen content of the DNA had to be assessed with respect to different nitrogen contents of the four bases. One could also speculate that the amount of bPEI in the system is close to the mass needed to reach 100 % of the applied sample weight. This would lead to bPEI contents ranging from 3.7 to 15.63 % (m/m) for the three analyzed batches. However, concerning the quantification of the system components, the measurement of pDNA loading was supposed to be the most important parameter concerning the biological application, which was successfully managed. Therefore bPEI quantification was not evaluated into more detail.

IV.2 Aerodynamic Properties of Microrods

IV.2.1 Introduction to the Next Generation Impactor

Intended for pulmonary administration, the evaluation of aerodynamic properties of microrods is crucial to the full carrier characterization with respect to the application purpose. For the in-process monitoring of the engineering technique as well as for the specific design attributes of the particles, e.g. stimuli-responsive degradation, customized characterization methods had to be established and introduced to the lab routine. In contrast to that, globally harmonized procedures for the assessment of aerosolized particles are provided by regulatory bodies such as the American Food and Drug Administration (FDA) and the European Medicine Agency (EMA). In section 2.9.18 – “Preparations for inhalation” of the European Pharmacopoeia specific guidelines are given to ensure high quality of aerosolized formulations.^[6] Focusing on particle size distribution and fine particle dose, five different devices are listed allowing the reproducible determination of the parameters. Outlined as Apparatus E, the Next Generation Impactor (NGI, **Figure 1**) is a state-of-the-art cascade impactor based on a horizontal design. Cascade impactors are designed to divide a particle population into fractions of equal size ranges. Applying a vacuum pump at the airflow outlet, an air stream is created throughout the device from the induction port (IP) into the direction of the pump. Formulation samples can be applied by commercially available inhaler devices at the IP. Pulled into the device by the vacuum, particle sizing is realized by inertia impaction. Starting at the IP inlet, which is basically representing the pharynx region of the human upper respiratory tract, particles have to follow a 90° angle and a consecutive pre-separator, which are part of the design excluding larger agglomerates above 10 µm from entering the impactor. Smaller particles follow the air stream into the device passing 7 different nozzle stages. From stage 1 to 7 the diameter of the

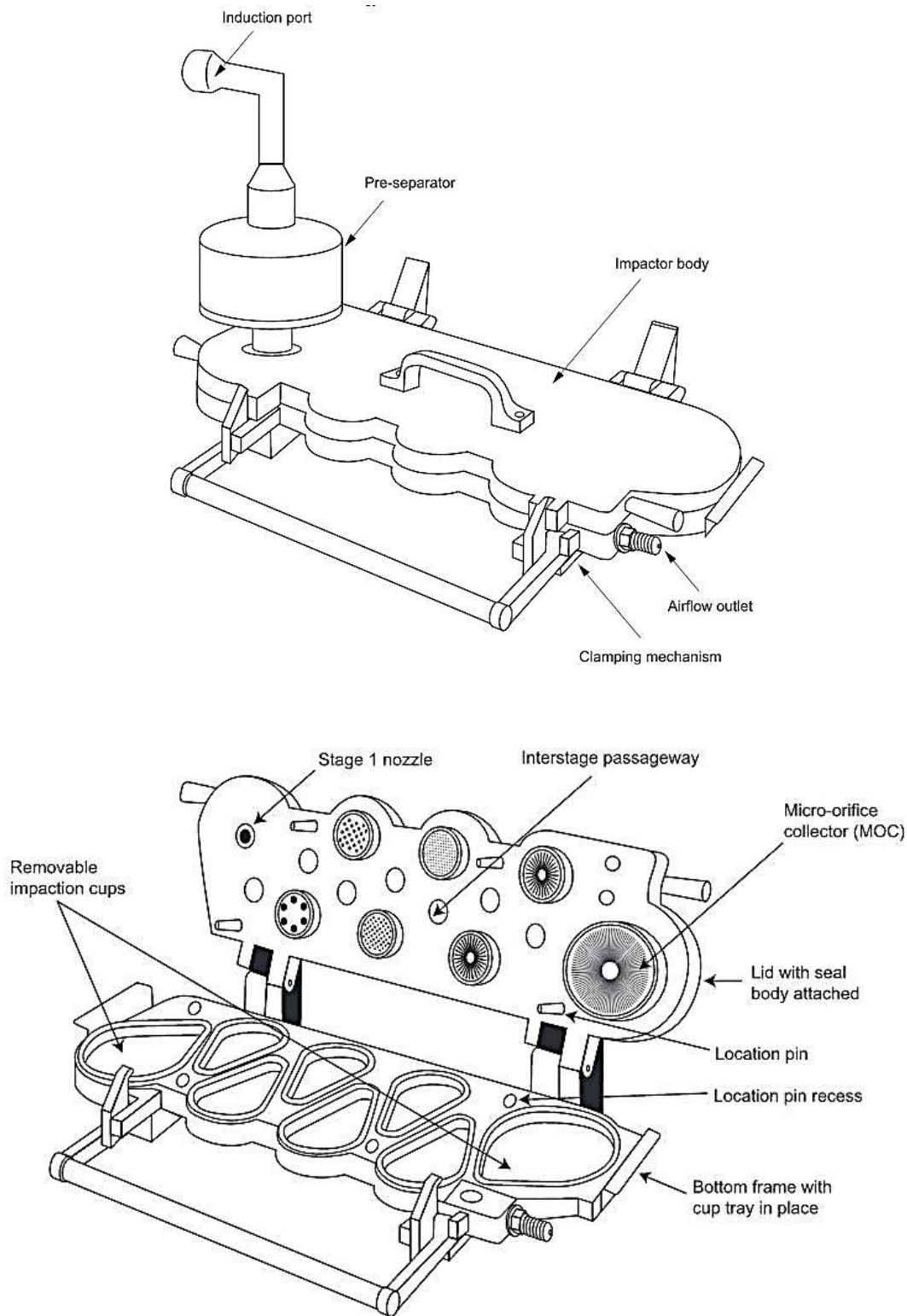


Figure 1: Illustration of the Next Generation Impactor: A) Closed setup of the impactor featuring the induction port and pre-separator. B) Interior of the NGI hosting 7 nozzle stations with corresponding cups for particle deposition and a micro-orifice collector (MOC) as the ending stage.^[6]

nozzles decreases and as a result the airstream velocity rises. Particles will deposit onto the collection cups whenever inertia exceeds the undertow provided by the vacuum pump, which is described as the volumetric air flow. Depending on this parameter, cut-off points for the nozzle stages can be created. Applying an air flow of e.g. 60 L/min will lead to cut-off diameters from 8.06 μm at stage 1 to 0.34 μm at stage 7 referring to the largest particle diameter, which is still deposited in the corresponding collection cup. Cut-off diameters will change by varying the undertow and therefore always have to be regarded as a function of the air flow inside of the device.

Regarding the metrics, which can be calculated from the particle mass distribution of an NGI run, the mass median aerodynamic diameter (MMAD) is frequently used to describe aerodynamic particle size distribution.^[7] The resulting information is used as an indicator for the deposition behavior of polydisperse airborne particles upon application. In addition to that, the fraction of particles below a critical aerodynamic diameter of 5 μm is particular in focus, since this particle population is expected to reach the lower respiratory tract to a high extend. Referred to as Fine Particle Dose (FPD) or Fine Particle Fraction (FPF) when expressed as a fraction to the overall dose which is applied to the inhaler, the gained results allow *in vitro* predictions, which are compliant to the regulatory guidelines.^[7] In order to improve the aforementioned deposition behavior, recent publications suggest that particle shape plays a significant role. In a theoretical approach conducted by Sturm et al., aspherical particles were highlighted to show a higher probability to reach the deep lung compared to spheres of comparable volume.^[8] This is due to their aerodynamic behavior mainly depending on their cylindrical diameter.^[9, 10] By this, the elongated rod geometry may provide the transport of higher volumes and therefore higher drug loads to the site of action. In the following section the determination of MMAD and FPF for nanostructured microrods are

depicted evaluating the suitability of the carrier for pulmonary application and therefore the ability to reach the cellular target.

IV.2.2 Materials and Methods

IV.2.2.1 Materials

For the NGI evaluation microrods were prepared using SNPs 200 nm and a template featuring 3 μm pores. Using bPEI and pCMV-luc for the stabilization, the LbL procedure was performed according to the previous sections. For impactor application the particles were transferred to hard gelatin capsules (size 3, transparent, WEPA Apothekenbedarf, Hillscheid, Germany), which were loaded into the single dose dry powder inhaler (DPI) HandiHaler[®] (Boehringer Ingelheim, Ingelheim, Germany). For sizing the particles, the DPI was applied to the Next Generation Impactor, which was obtained from Copley Scientific (Nottingham, UK). The collection cups were coated with a mixture of 40 % Brij[®]35 and 60 % glycerol. The evaluation of deposited particle masses was performed by fluorescence measurements using the Tecan Reader from the previous chapter.

IV.2.2.2 Methods

Calibration of Microrod Mass Using Fluorescence

For the determination of microrod masses, which deposit in the single compactor stages the fluorescence label of the particles was used. In contrast to microrod systems which are stabilized by sugar matrices the presented system was not intended to disaggregate readily when applied to aqueous media. As a consequence the fluorescence measurements were performed for the microparticles. Although particles showed fast sedimentation due to high masses and density, the measurement was not affected due to the bottom reading operating

principle of the Tecan Reader. For the calibration a serial dilution was prepared starting with a stock concentration of 0.5 mg/mL. Diluting the stock 1:1 up to ten times a minimum concentration of 490 ng/mL was prepared for measurement.

Determination of Aerodynamic Properties using the Next Generation Impactor

Prior to every NGI run the volumetric airflow was calibrated to 60 L/min suitable for the utilization of DPIs. To avoid bulging of the particles and therefore unwanted variations for the particle size distribution, the collections cups were coated with a mixture of glycerol and the surfactant Brij[®] 35. After closing the device, pre-separator and induction port were added to the setup. A mass of 15 mg microrods was used per NGI run. The particles were transferred into a hard capsule which was stored within an Eppendorf tube. To remove larger aggregates caused by the drying steps after engineering and to reach a sufficient flowability of the powder the tube hosting the capsule was applied to a Vortex for 30 mins. Showing an up-and-down movement the capsule was kept in motion until a free flowing powder was obtained. Applied to the HandiHaler (**Figure 2**) the capsule was pierced before aerosolization.^[11] The airflow was kept constant for 4 s before the collecting cups were flushed with water to recover the deposited particles. In addition to the 8 collection cups also the induction port, the pre-separator and the capsule were evaluated.



Figure 2: Single dose dry powder inhaler HandiHaler: Microrods are applied as a single dose within a hard capsule which gets pierced prior to aerosolization.^[11]

IV.2.3 Results and Discussion

For the calibration of microrods based on the fluorescence label of SNPs, a linear correlation was obtained within the tested concentration range (**Figure 3**). Therefore, a suitable read-out of the particle amounts impacted in the collection cups was available down to a detection limit of 490 ng/mL. For the consecutive NGI runs the particles had to be transferred to hard capsules for DPI application. After fabrication and purification microrods have to be dried from THF resulting in a dense particle pellet at the bottom of an Eppendorf tube. To regain a good flowability for capsule filling, but also capsule depletion during aerosolization, energy input was necessary for pellet disaggregation. Therefore, particles were treated by a vortex before and after capsule filling. Especially with the setup shown in **Figure 4**, a sufficient

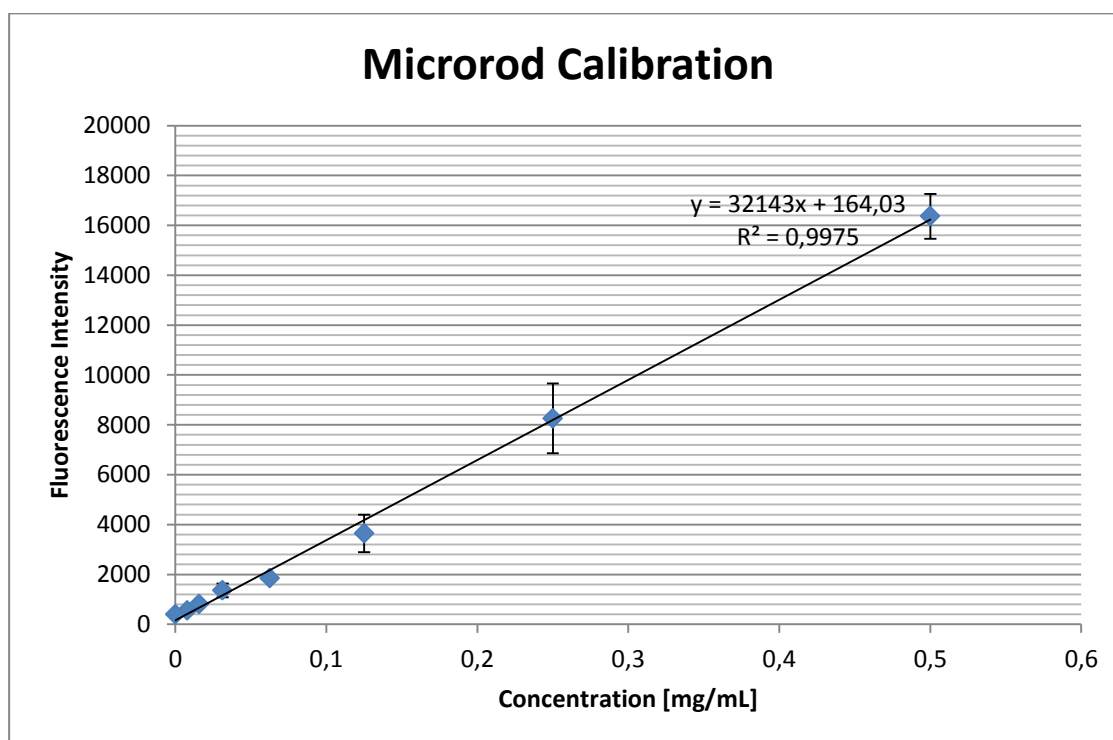


Figure 3: Linear correlation of fluorescence intensity and particle amount within the concentration range from 490 ng/mL to 0.5 mg/mL.

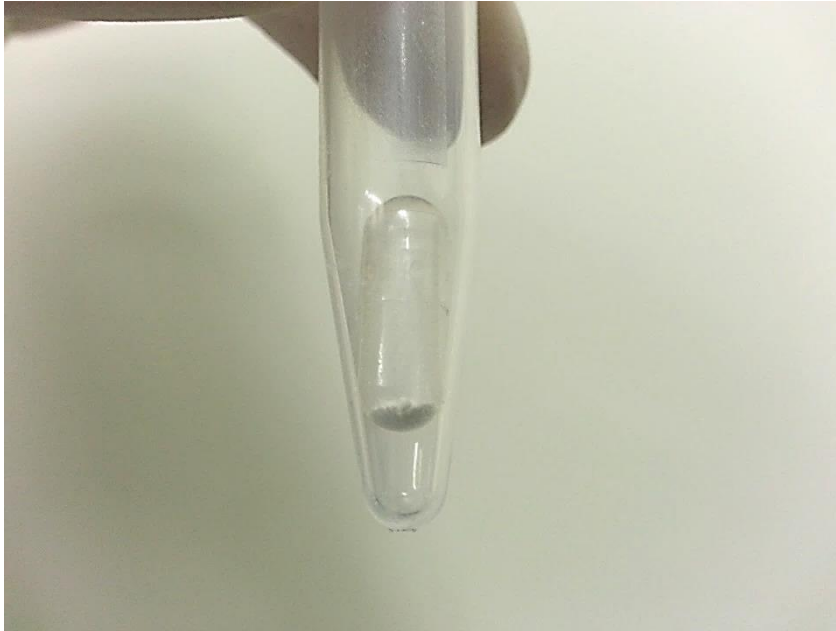


Figure 4: A hard capsule loaded with 15 mg microrods. Within an Eppendorf tube the capsule was kept in motion for the mechanical disaggregation of the particle pellet.

flowability of the particles could be reached. Inspired by the up-and-down motion of the capsule within the DPI, which contributes to dose depletion, the capsule was transferred to an Eppendorf tube. Whereas for the NGI the capsule is set in motion by the undertow of the vacuum, here the vortex movements provided the disaggregation of the pellet. The resulting mass distribution of an NGI run for the microrods can be seen in **Figure 5**. What can be concluded from **Figure 5 a**, which is including microrod residues of the capsule, induction port and pre-separator, is that the majority of the particles deposited within the preseparator. Here, particles deposit because of their aerodynamic diameter reaching 10 to 15 μm representing particle fractions not suitable to reach the lung. The results indicated that the particles still tended to show agglomeration when processed in dry state and the disaggregation procedure for the powder has to be optimized. It again has to be stated that the particles did not show tendencies for agglomeration when applied to aqueous media or organic solvents. Because of the high pronounced surface charge densities the powder also appeared to be very hydrophilic and hygroscopic. Therefore, exposure to air humidity also has to be regarded as problematic, which could be solved by blending the particles with a

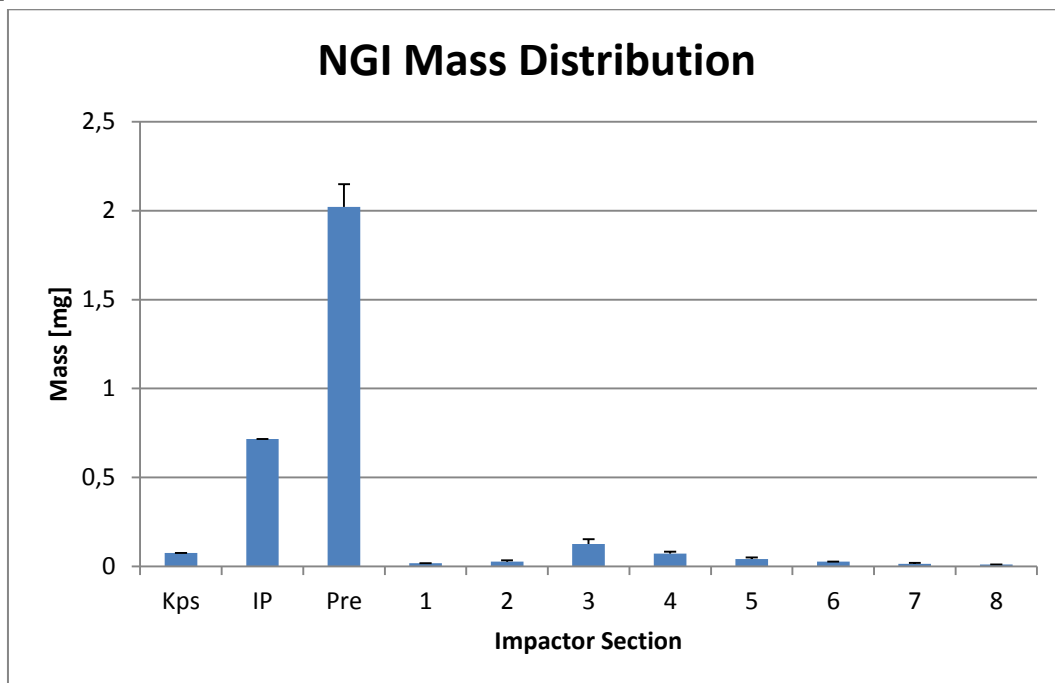
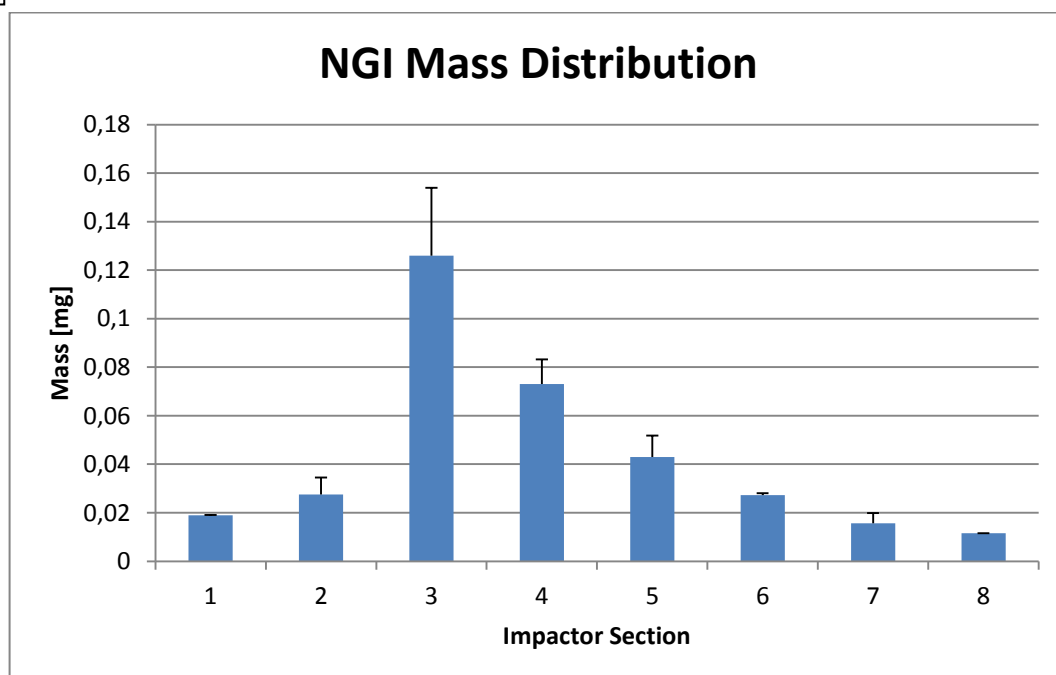
A**B**

Figure 5: Evaluation of the mass distribution of microrods after an NGI run: A) Evaluation including the capsule (Kps), the induction port (IP), the preseparator (Pre) and the 8 nozzle stages. B) Evaluation focusing on the nozzle stations as part of the batch actually able to reach the deep lung.

hydrophobic agent suitable for pulmonary applications such as the amino acid L-leucine. Focusing on the particle fractions, which were actually able to reach the nozzle stages of the impactor (**Figure 5 b**) the highest amount can be found in stage 3 featuring a cut-off aerodynamic diameter of 2.82 μm , whereas stage 2 and 4 show cut-offs at 4.46 and 1.66 μm respectively, indicating an aerodynamic diameter close to the geometric diameter of 3.0 μm . The evaluation and calculation of the MMAD and FPF was performed for three microrods batches (**Table 2**). What can be concluded from the results is that the microrods show an MMAD suitable for pulmonary delivery also indicating a deposition within the deep lung. The rather low fine particle fraction of 12.6 % (m/m) supports the assumption of aggregate formation leading to high impaction rates. Here, the introduction of new preparation methods such as blending, inert gas atmosphere to exclude air humidity or more sophisticated disaggregation techniques could improve FPF to further optimize the aerodynamic properties of the microrods.

	Batch 1	Batch 2	Batch 3	Mean Values
MMAD [μm]	2.89	2.36	2.46	2.57
FPF [% m/m]	14.59	9.87	13.34	12.60

Table 2: Aerodynamic parameters calculated from 3 NGI runs: Mass median aerodynamic diameter (MMAD) and fine particle fraction (FPF) were determined for microrods featuring a geometric diameter of 3.0 μm .

IV. 3 References

- [1] A. Szarpak, D. Cui, F. Dubreuil, B. G. De Geest, Liesbeth J. De Cock, C. Picart, R. Auzély-Velty, *Biomacromolecules* **2010**, *11*, 713–720
- [2] K. Chiad, S. H. Stelzig, R. Gropeanu, T. Weil, M. Klapper, K. Müllen, *Macromolecules*, **2009**, *42*, 7545–7552
- [3] J. Malmström, H. Agheli, P. Kingshott, D. S. Sutherland, *Langmuir* **2007**, *23*, 9760–9768
- [4] C. A. English, S. Merson, J. T. Keer, *Anal. Chem.* **2006**, *78*, 4630–4633
- [5] X. Hou, B. T. Jones, *Encyclopedia of Analytical Chemistry*, Wiley **2008**
- [6] Preparations for Inhalation: Aerodynamic Assessment of Fine Particles, European Pharmacopoeia 8th Edition, Supplement 8.7, 2016
- [7] D. Lewis, M. Copley, *Pharmaceutical Technology* 2011, November Issue
- [8] R. Sturm, W. Hofmann, *J. Hazard. Mater.* **2009**, *170*, 210–218
- [9] W.-C. Su, Y. S. Cheng, *J. Aero. Sci.* **2006**, *37*, 1429 – 1441
- [10] Stöber, W. (1972). Dynamic shape factors of nonspherical aerosol particles. in: T. Mercer et al. (Ed.), *Assessment of airborne particles* (pp. 249–289). Springfield, IL: Charles C. Thomas Publisher.
- [11] From the manufacturer's manual: <https://www.boehringer-ingenheim.de/verschreibungspflichtige-medikamente/spiriva/spiriva>

Chapter V

Transfection Studies on Murine Alveolar Macrophages

For Chapter V the author of the thesis made the following contributions to the chapter:

Design, fabrication and sample preparation of defined masses of microrods and interpretation of all experimental data.

MTT cytotoxicity, BCA and transfection assays were carried out by Shashank Reddy Pinnapireddy at the Institute of Pharmaceutical Technology and Biopharmaceutics, Philipps University Marburg.

V.1 Introduction: Macrophage Transfection

In chapter IV the presented microrod system was successfully shown to be cargo loaded with the plasmid pCMV-luc in order to evaluate the proficiency of the carrier to introduce external DNA into the nuclear core of a target cell line. According to the pulmonary application purpose, aerodynamic properties were determined showing the microparticles to be qualified to reach the deep lung and therefore the site of action. The following chapter is dedicated to the consecutive steps after deposition within a biological environment. In a first step the engulfment by phagocytes had to be shown, which is a crucial and rate limiting step for the intended cargo delivery. For cell culture studies the alveolar macrophage cell line MH-S was chosen, originally isolated from bronchoalveolar lavage of BALB/c mice showing adherent behavior and typical macrophage morphology.^[1] For the coating design the introduced transfection agents DEAE-D, CHT and bPEI were discussed prior to transfection experiments. Up to this point, the cargo release from bPEI microrod systems was not clarified. Whereas no release was shown within a simplified enzyme assay setup, literature showed similar systems to work efficiently under *in vitro* conditions.^[2-4] Furthermore, bPEI shows superior transfection efficiencies compared to other compounds throughout a very large number of publications, which is in particular interesting as macrophages are known as hard to transfect.^[5-7] DEAE-D and CHT could possibly lack the sufficient protection of the plasmid and buffering capacity, which is crucial when targeting macrophages with a highly disruptive, enzymatic arsenal. As a result, bPEI was chosen as lysosomal buffering agent for the transfection studies.

With the introduction of Layer-by-Layer technologies into gene delivery, numerous novel systems were presented for the controlled release of genetic material.^[8-10] Both the protection and targeted delivery of small and fragile RNA molecules, such as siRNA, or large plasmids can be provided.^[2, 11] But besides achieving a general protein expression it was in particular

interesting for us to evaluate the possibility to control luciferase expression patterns by the design choices for the LbL coating. This is in general not an easy task, taking into account that intracellular mechanisms such as the escape of the transported DNA from the phagolysosome and nuclear transport within the cytosol will influence the results of the experiments. The first parameter with a potential influence was cargo loading. Expecting a transient transfection of the macrophages, we hypothesized that higher pDNA loading could maintain the expression over a longer time frame. The second parameter was the position of the genetic material within the coating. Pavlov et al. published a work on LbL assembled microcapsules evaluating the position of a plasmid for the transfection of the human embryonic kidney epithelial cell line 293 T.^[12] They found the transfection to be more rapid and effective for pDNA in the outermost layer whereas no transfection was observed from layers which were located in inner positions of the LbL meshwork. For particles using PEI as the outermost layer they did not observe a difference in transfection from inner layers to those closer to the surrounding medium, which were indeed surprising results considering cargo release dependent on diffusion rates. In contrast to that, another study published by Reibetanz et al. showed a positive transfection from mid layers using the same cell line and protamine as a transfection agent.^[13] The examples from literature give first insights into LbL mediated gene delivery revealing a high dependence on applied excipients and LbL design. Up to now, there are no comparable studies carried out on macrophages revealing transfection kinetics or demonstrating how design changes within LbL coatings can be utilized to create optimized expression patterns. In the following, different microrod formulations were applied to MH-S cells introducing LbL design parameters into macrophage transfection.

V.2 Materials and Methods

V.2.1 Materials

For cell culture studies microrods were fabricated using SNPs 200 nm with a red fluorescence label (Excitation/Emission 569 nm/585 nm) and template membranes featuring 3 μm pores. For the stabilization and functionalization bPEI (25 kDa) and pCMV-luc were applied. As a substitute to the plasmid DNA dextran sulfate (10 kDa) was purchased from TdB (Uppsala, Sweden).

The studies were carried out on the murine alveolar macrophage cell line MH-S (CRL-2019™), which was obtained from the European Collection of Authenticated Cell Cultures/Public Health England (ATCC, Salisbury, UK). For cell culture RPMI-1640 medium (Capricorn Scientific, Ebsdorfergrund, Germany) was used, which was substituted with glutamin, 2-mercaptoethanol and fetal bovine serum purchased from Sigma Aldrich (Steinheim, Germany). For the evaluation of cytotoxicity, assays were performed using thiazolyl blue tetrazolium bromide (MTT, Sigma Aldrich). The positive control was carried out using Triton X-100 (Sigma Aldrich). Absorbance measurements were carried out using a BioDoc Analyse Ti5 trans-illuminator (Whatman Biometra, Göttingen, Germany)

Transfection studies were performed using jetPEI as a positive control (Polyplus transfection, Illkirch, France). The determination of bioluminescence was performed by applying the Luciferase Assay Kit and Cell Lysis Buffer provided by Promega (Mannheim, Germany). For the quantification of protein amounts Pierce Protein BCA assay kits were used (ThermoFisher Scientific, Darmstadt, Germany). The visualization by confocal microscopy was enabled by Concanavalin A:Alexa Fluor 488 Conjugate and DAPI staining (Fisher Scientific, Schwerte, Germany). Therefore cells were seeded onto 8-well tissue culture-treated slides (Ibidi,

Martinsried, Germany). Fluorescence micrographs were taken by the confocal laser scanning microscope LSM 710 (Carl Zeiss Microscopy GmbH, Jena, Germany).

V.2.2 Methods

LbL Coating Design

To evaluate the influence of the LbL coating design on cellular protein expression, different particle batches were fabricated. In the first experiment the influence of cargo loading was addressed, adjusting the double-layer amount to 2.5, 3.5 or 4.5 to create three batches of increasing cargo loading. For both the first and last layer of the coating bPEI was used since the provided amino groups are required to coat negatively charged silica as well as for the intraphagolysosomal buffering capacity upon engulfment by the cells. For the second study the overall polymer content was adjusted to 3.5 DL for all the fabricated batches. The same amount of plasmid DNA was applied incorporating only one layer and shifting its position within the coating. As a substitute to the genetic material dextran sulfate (**Figure 1**) was used providing negative charges and stable films for the system in combination with bPEI. As a result three particle batches containing pCMV-luc in the innermost, mid or outermost layer were produced. The influence of the parameters cargo loading and position on protein expression was evaluated within identical experimental setups.

Cell Culture

According to the supplier's recommendations, macrophages were cultured in RPMI-1640 medium based on glucose, saline, amino acids and vitamins with the addition of 2 mM

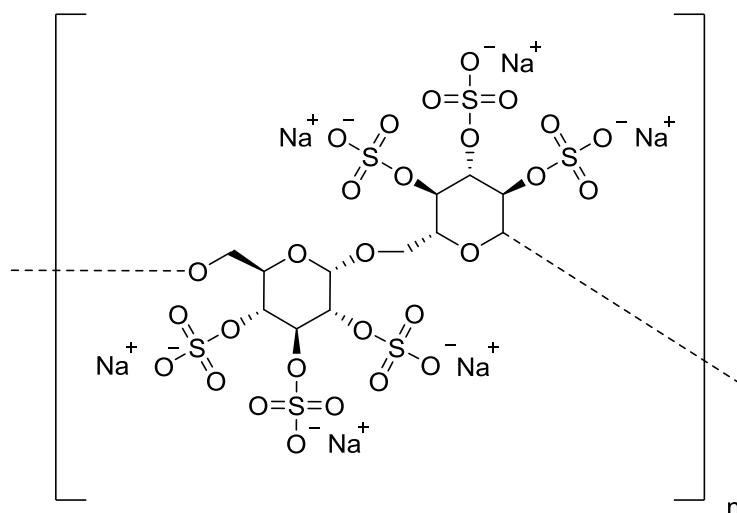


Figure 1: Chemical structure of dextran sulfate featuring negative charges as a substitute to plasmid DNA within LbL coatings.

glutamine, 0.05 mM 2-mercaptoethanol and 10 % (V/V) fetal bovine serum. Incubation conditions were maintained at 37 °C and 5 % carbon dioxide in humid atmosphere. The cells were grown in monolayers and passaged as soon as 70-80 % of confluence was reached.

Uptake Visualization by Confocal Microscopy

MH-S cells were seeded into 8-well plates at a concentration of 2×10^5 cells per milliliter medium and incubated at 37 °C/5 % carbon dioxide. After 24 hours fresh medium containing 1×10^7 microrods per milliliter was added per well and again the plates were stored in the incubator. After defined time points of 0.5, 1, 2 and 4 hours of incubation cells were fixed with cooled methanol for 30 minutes. After two times washing with PBS buffer (pH 7.4) the cells were incubated with the lectin Concanavalin A (ConA), which was conjugated to the green fluorescent dye Alexa Fluor 488 (**Figure 2**). ConA selectively binds to terminal α -D-mannosyl and α -D-glucosyl groups, which are present in MH-S actin filaments leading to a green fluorescence labeling (Excitation/Emission 495 nm/519 nm). For counterstaining of the nuclear core 4',6-diamidino-2-phenylindole (DAPI) was used. DAPI as a small molecule can diffuse into the cytosol of any cell strongly binding to DNA in the nuclear region especially

when it is rich in adenine and thymine content. Upon binding, DAPI shows high absorption at wavelength 358 nm and emission at 461 nm within the blue spectrum. The fluorescence setup is completed by the red labeling of the microrods enabling the visualization of the uptake of the particles into the macrophages by phagocytosis.

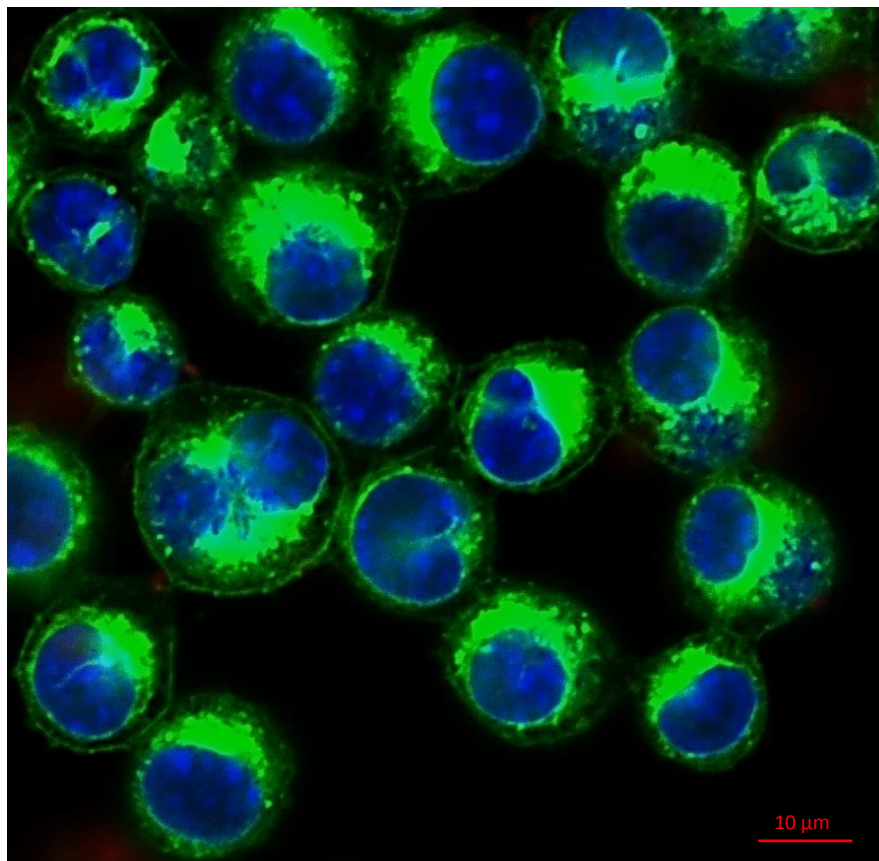


Figure 2: MH-S cells with DAPI staining (blue) of the nuclear core and Alexa Fluor 488 staining (green) of actin filaments provided by ConA.

MTT Cytotoxicity Studies

In order to prove the microrods to be well tolerated by the cells, MTT cytotoxicity assay was performed. Within a defined concentration range from 1.05 mg/mL to 16.4 µg/mL, macrophages were incubated with the particles for 48 hours. After two times washing with PBS buffer containing calcium and magnesium, medium containing MTT assay reagent was added to each well. Cells were incubated for another four hours giving viable MH-S time to metabolize MTT within their mitochondria leading to a reduction to formazan (**Figure 3**).^[14] Formazan appears as insoluble, purple crystals, which can be transferred into a colored solution by the addition of 300 µL dimethyl sulfoxide (DMSO). Cell viability can be determined as a function of formazan absorbance at wavelength 570 nm.

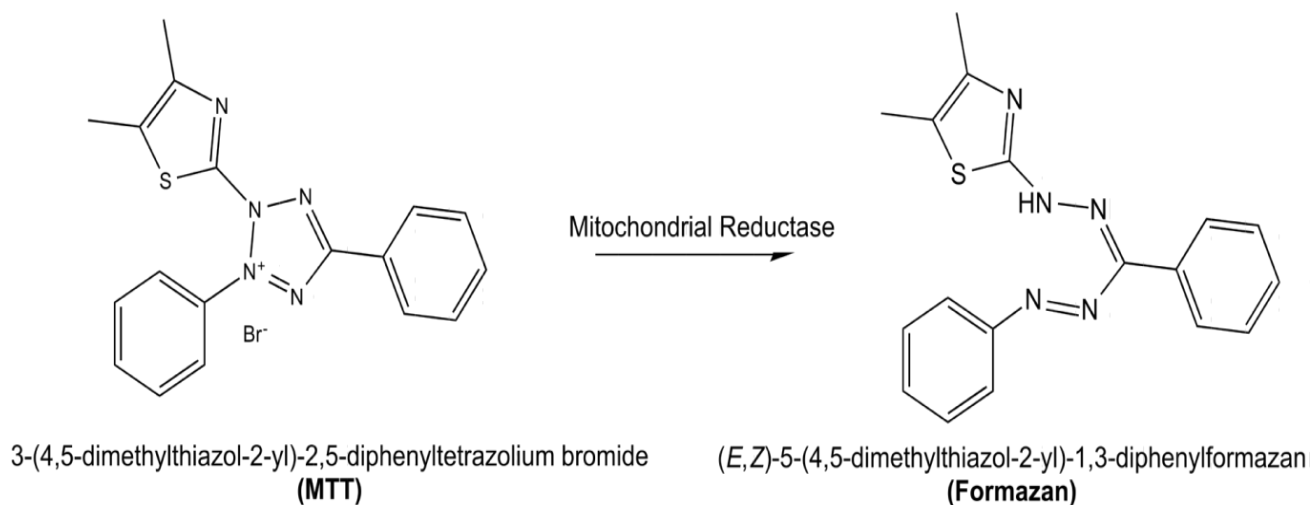


Figure 3: MTT assay read-out: Viable MH-S cells reduce MTT enzymatically, which will lead to the precipitation of formazan crystals. The concentration of formazan can be measured by a spectrophotometer giving information about the viability of the incubated cells.^[14]

Transfection Assays

Macrophages were seeded onto 24-well plates at a density of 10,000 cells per well. The following day, 50 µg microrods per batch, diluted to a final volume of 100 µL with serum free RPMI-1640 medium, were added dropwise into wells containing 900 µL of RPMI-1640. In addition to that, the same amount of microrods was applied to MH-S, which were pretreated with chloroquine (RPMI-1640 medium with 10% FBS and 100 µM chloroquine), a known inhibitor of endocytosis, to exclude alternative uptake mechanisms to phagocytosis.^[15] The commercially available transfection system jetPEI was used as positive control for the experiments. After particle addition all plates were swirled and returned to the incubator. All the transfection experiments were performed in triplicates and each experiment was repeated thrice.

Luciferase Assay and Protein Analysis

To determine the introduction of the transported plasmid DNA into the nuclear core of MH-S, the luciferase reporter gene was utilized. Upon successful implementation the enzyme luciferase is expressed by the cells. When applying its natural substrate D-luciferin, luciferase provides the oxidation to oxyluciferin under the emission of bioluminescence, which can be measured as a read-out (**Figure 4**).^[16] Using luciferase as reporter gene combines several advantages. On the one hand, luciferase is not naturally expressed in mammalian cells so there is no background regarding the measurement and detected bioluminescence can be exclusively associated with the successful transfection. On the other hand, the method is extremely sensitive and highly reproducible with standardized protocols. For the measurement the transfected cells were lysed after defined time points of 2, 4, 7 and 9 days. Therefore, cells were washed twice with PBS buffer before the lysis agent was added. Lysate aliquots of 20 µl

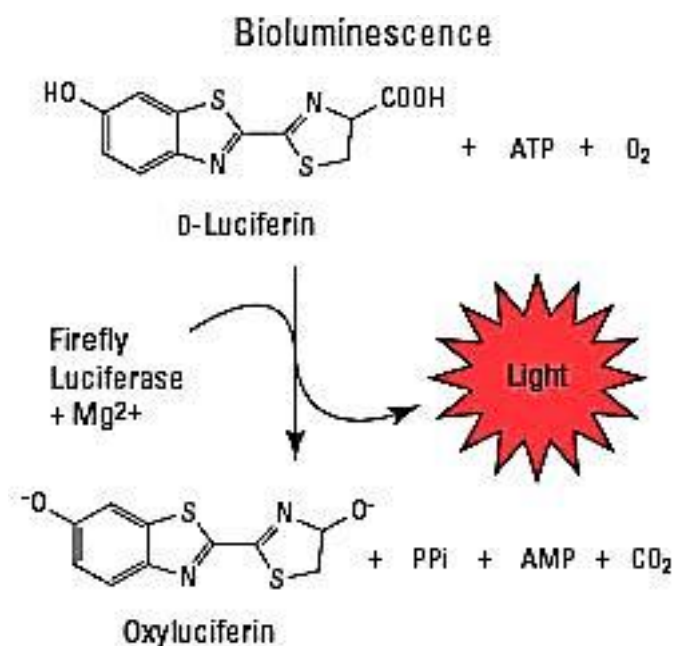


Figure 4: Luciferase read-out: Luciferase oxidizes D-luciferin to oxyluciferin in presence of the cofactors ATP and magnesium. The enzymatic reaction occurs under the emission of bioluminescence and hydrolysis of ATP into AMP and pyrophosphate (PPi).^[16]

were added to white opaque microtiter plates or clear transparent bottom microtiter plates for the luciferase assay or BCA protein analysis respectively. For luciferase assays, the opaque plate containing lysate was measured within a plate reader equipped with an autoinjector. The device pumps the luciferase assay mixture containing D-luciferin and the cofactors adenosine triphosphate (ATP) and magnesium. Therefore aliquots of luciferase assay reagent (ATP, Mg) and the luciferin substrate were freshly thawed, mixed and primed into the pump. A protocol was used with a 10 seconds integration time for luminescence detection. The instrument automatically pumped the luciferase assay mixture into each well and measured before proceeding to the next. Protein quantification was performed using a Pierce Protein BCA assay kit according to the manufacturer's protocol. Based on a colorimetric assay, copper(II) gets reduced to copper(I) by peptide bonds within an alkaline environment. Here, the reduced amount of copper is proportional to the full amount of protein in the sample. In a second step

copper(I) chelates two molecules of bicinchoninic acid resulting in a purple complex which was quantified at wavelength 570 nm. By determining the amount of protein in combination with the bioluminescence the overall results of the transfection are expressed in relative luminescence units (RLU) per milligram protein.

V.3 Results and Discussion

For every successful gene delivery approach the first and important step is the full invagination of the carrier into the target cells. Regarding the size of the presented microparticle system featuring 10 μm in length, phagocytosis is the only possible pathway for cellular uptake of objects that large.^[17] Upon pulmonary application, epithelial cells are generally not able to engulf the microrod system indicating a targeted delivery to phagocytes according to the intended delivery approach. Professional phagocytes such as neutrophils and monocytes/macrophages are the only cell populations capable of actin-driven uptake of particles exceeding a size of 0.5 μm . The confocal laser scanning microscopy visualization shown in **Figure 5** indicated an active uptake process of the rods into alveolar macrophages. Particle batches were also applied to MH-S, which were treated with chloroquine, an inhibitor of endocytosis, which did not affect luciferase expression excluding endocytosis as a relevant uptake mechanism. To achieve high uptake rates, two studies were taken into regard focusing on particles' geometry. Champion and Mitragotri published a work evaluating the influence of the particle diameter on uptake efficiency by alveolar macrophages. Illustrated in **Figure 6**, they clearly showed a peak in uptake for two particle species when adjusting the diameter to 3 microns.^[18] In a second study their group showed that also aspect ratio plays a significant role for the uptake rate. Here, they found that aspect ratios round about 3 showed even higher internalization rates than spherical particles of comparable diameters.^[19]

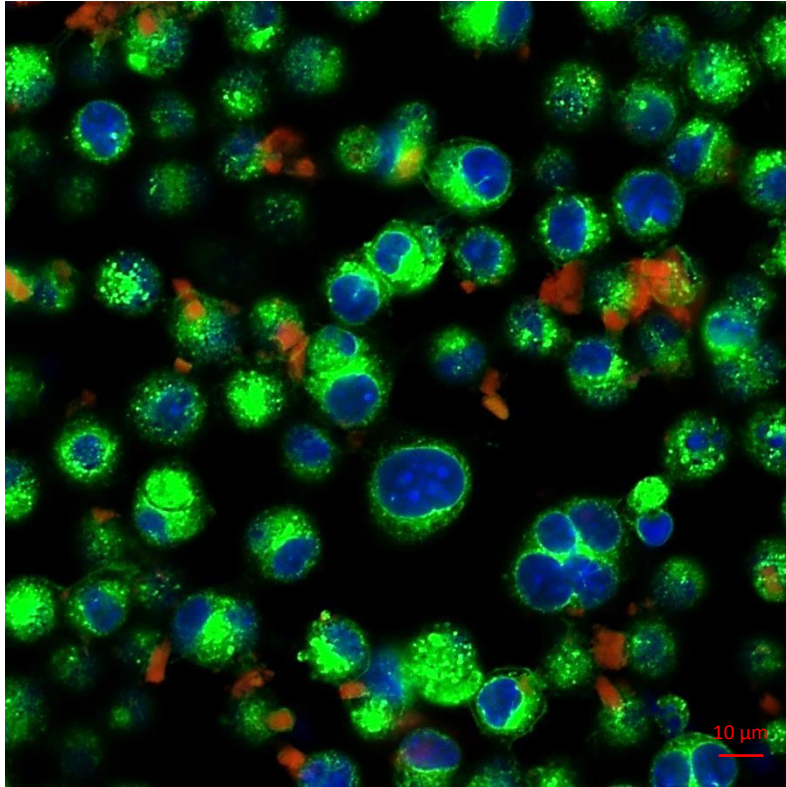


Figure 5: Fluorescence micrograph depicting MH-S alveolar macrophages during uptake of microrods (red) after 1 hour of incubation.

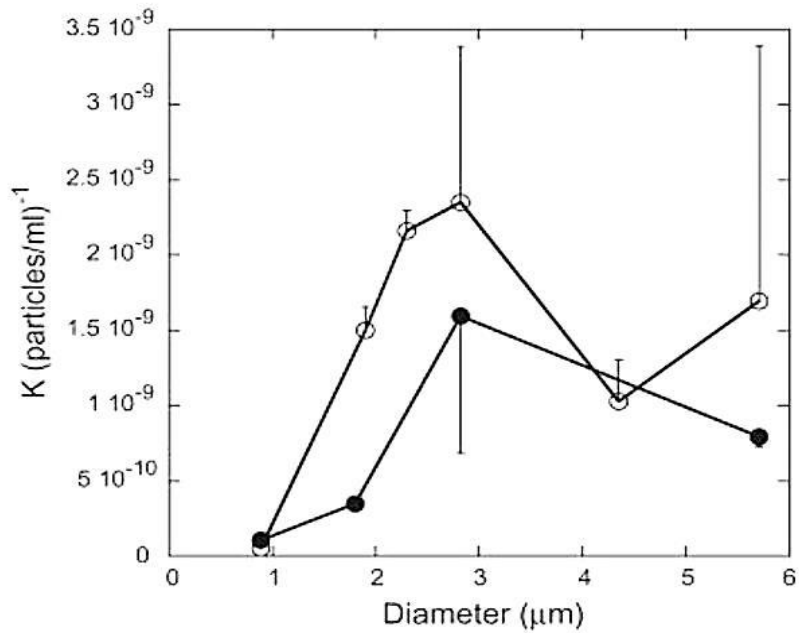


Figure 6: Evaluation of uptake efficiency by rat alveolar macrophages in dependency of particle diameter for two particle species.^[18] Figure was displayed with permission from the journal.

Both parameters were taken into account and due to the template-assisted engineering technique they could be easily introduced to the carrier system. After imaging the uptake into the target cells, particles had to be shown to be well tolerated. Therefore MTT cytotoxicity assay was performed, testing three particle batches of increasing polymer content stabilized by 2.5, 3.5 or 4.5 DL of bPEI and pCMV-luc (**Figure 7**). The tested microrod concentrations showed high cell viability especially below a concentration of 1.05 mg/mL. For the consecutive transfection studies a concentration of 50 µg/mL was chosen to yield high macrophage viability of 90 % and above for all three formulations. Two different design parameters of the LbL coating were in the focus for evaluation. On the one side increasing amounts of cargo loading were tested and on the other side we were curious about the

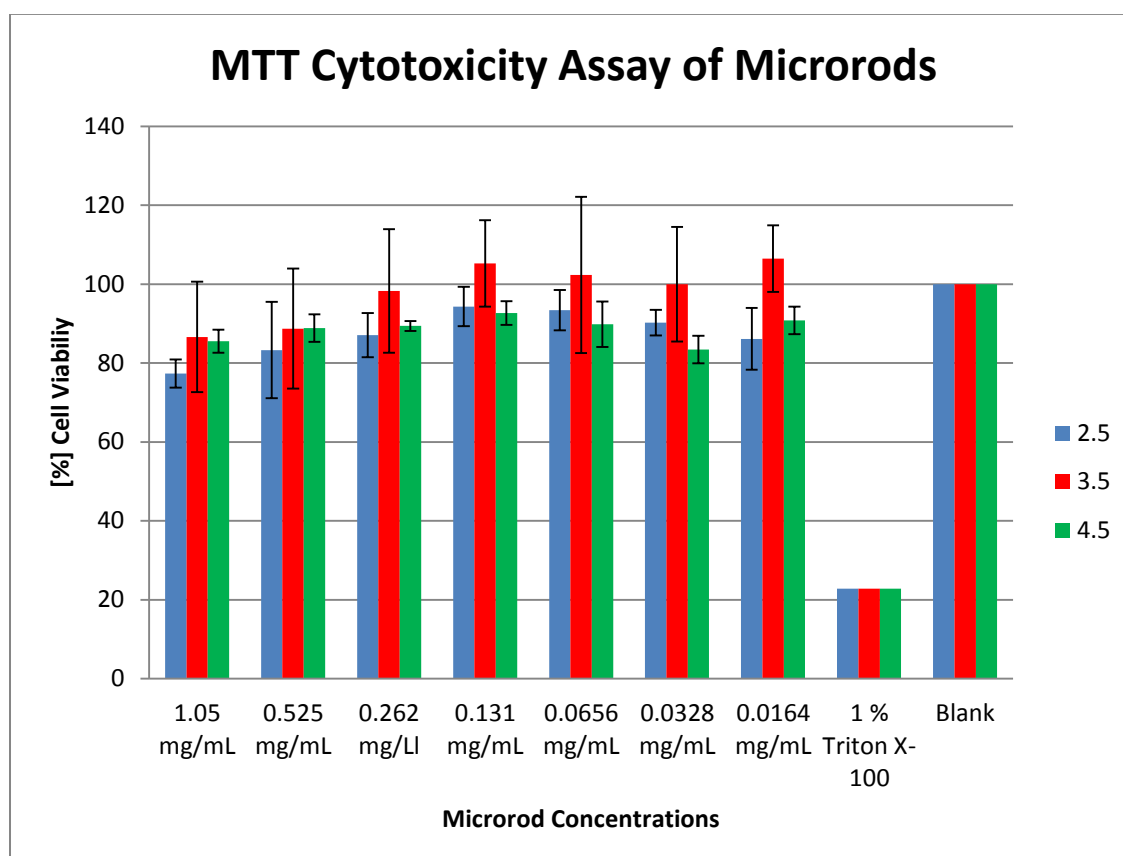


Figure 7: MTT cytotoxicity assay for three microrod batches of increasing polymer content. MH-S cells were incubated at a concentration range from 1.05 – 0.0164 mg/mL. Triton-X on MH-S was used as a negative control whereas untreated cells were used as a positive

influence of the position of the pDNA within the LbL coating on protein expression. Starting with increasing pDNA amounts, the microrod batches from the MTT evaluation were applied to MH-S for defined time frames of 2 to 9 days. Within the particle system the plasmid DNA acts both as a stabilizer component for the microrod architecture and as the active agent, so its delivered amount most likely influences the extent of protein expression, but also the integrity of the carrier system itself. In this regard, for the first *in vitro* study the initial assumption was that every additional layer of DNA can increase protein expression in the target cells, but will sustain its own release at the same time due to higher attracting electrostatic interactions. Results from the performed luciferase assays indicated a successful luciferase expression by MH-S for the prepared batches depending on the LbL coating design (**Figure 8**).

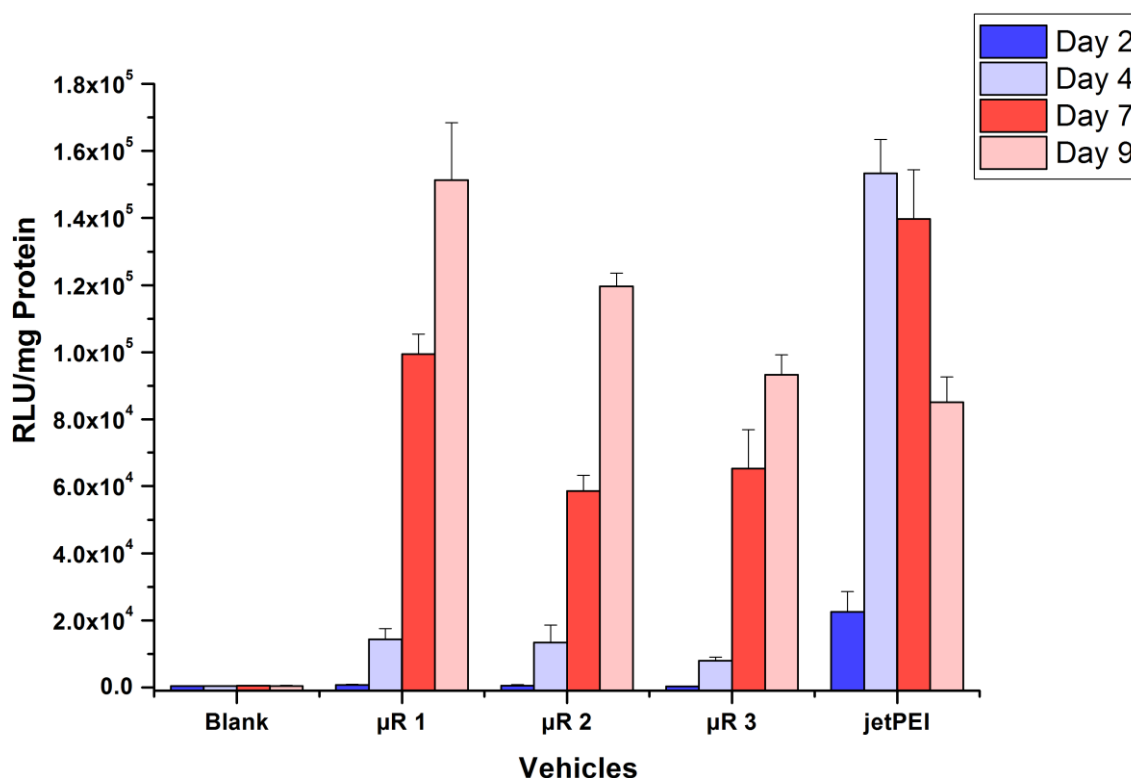


Figure 8: Luciferase assay for three particle batches $\mu\text{R } 1 - \mu\text{R } 3$ of increasing cargo loading. Luciferase activity was measured 2, 4, 7 and 9 days after transfection. jetPEI was used as a positive control, untreated cells as a negative control. Bioluminescence is depicted in relative light units (RLU) per milligram protein including SD for $n = 6$.

Protein expression was associated with time and a steady increase in luciferase activity has been detected for every batch up to day 9 of the experiment. For the commercial transfection reagent jetPEI, we already observed a decline after the 4th day of transfection. For all three formulations, the same pattern in luciferase expression over time was observed showing differences in the total protein amount. The results supported our hypothesis that for every time point measured, particles even though loaded with higher DNA amounts provided lower amounts of protein.

Regarding cargo release, it has to be stated that faster kinetics do not automatically lead to improved delivery efficiencies. Specific pharmacokinetic hurdles have to be respected especially when applied to challenging biological environments. For the applied particle system featuring bPEI as a non-biodegradable transfection agent, cargo release is most likely driven by diffusion. Provided by the saturation of negatively charged phosphate groups by phagolysosomal protons, the genetic material forfeits the electrostatic attraction to bPEI, which enables the diffusion out of the LbL meshwork and into the lumen of the phagolysosome. As a consequence, the amount of released pDNA available for nuclear transport depends on the diffusion of protons into the polymer layers and the consecutive diffusion of the DNA into the opposite direction. In addition to that, the acidic environment can also lead to a higher degree of protonation of bPEI resulting in high repulsive forces for the polymer chains and therefore spaces of facilitated diffusion of the plasmid. It is obvious to expect faster release rates from pCMV-luc layers, which are closer to the surrounding acidic medium, but this does not necessarily result in higher protein expression. Therefore, the transfection agent has to provide the phagolysosomal escape, which is a time-dependent step during gene delivery. For the presented particle system the highest luciferase expression can be expected from pDNA layers which show the best match of release and bPEI promoted escape from the degrading environment. To evaluate on this, again three batches of microrods

were fabricated and the polymer content was kept constant at 3.5 DL. For the positive charges bPEI was maintained, for the negative charges one layer pCMV-luc and two layers dextran sulfate were used. Thereby, the single DNA layer was shifted in its position within the coating to produce three different batches of microrods, whereas the dextran derivative acted as a fill-in. The rest of the experimental setup was kept identical to the previous transfection. Again, studied for defined time frames of 2 to 9 days after application, successful transfection of MH-S could be repeated (**Figure 9**).

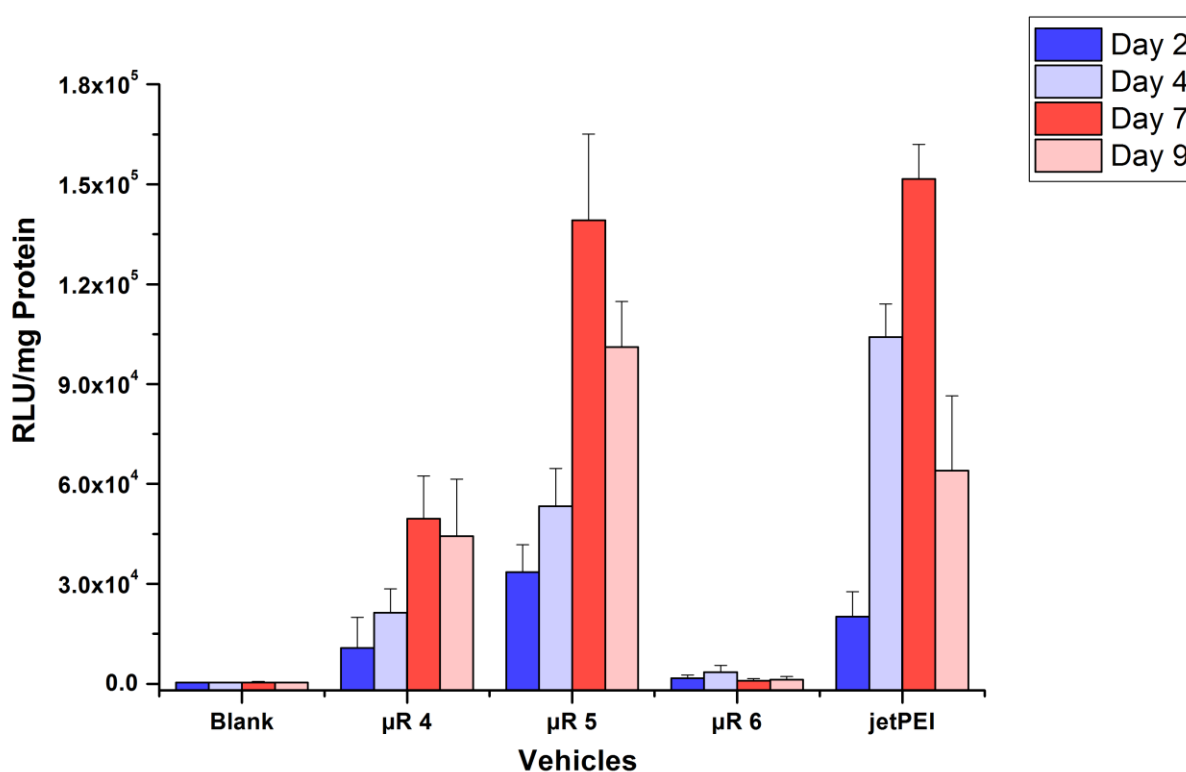


Figure 9: Luciferase assay for three particle batches $\mu\text{R } 4 - \mu\text{R } 6$ stabilized by 3.5 DL using bPEI, pCMV-luc and dextran sulfate. The position of the single pDNA layer within LbL coating was shifted from the innermost layer ($\mu\text{R } 4$) to the outermost layer ($\mu\text{R } 6$) to create three different microrod formulations. Time frame and controls were maintained from the previous assay. Bioluminescence is depicted in relative light units (RLU) per milligram protein including SD for $n = 6$.

Highest luciferase activity was observed for batch $\mu\text{R } 5$ featuring pCMV-luc in the mid position and showing RLU/mg values comparable to the first assay (**Figure 8**). For batch $\mu\text{R } 4$ featuring pDNA in the innermost layer, lower signals were measured according to

longer diffusion tracks and therefore sustained release behavior. For the batch with the plasmid in the outermost layer (μ R 6) the lowest signals were measured. According to the previous remarks, the reduced luciferase activity can be associated to high enzymatic degradation of the genetic material. For all three batches μ R 6 most likely made the DNA available at the highest velocity before the integrity of the surrounding vesicle could be reduced by the transfection agent. Whereas in the first transfection study multiple DNA layers could compensate the degradation of the outer layer, the reduced loading yielded in low signals. Additionally, the reduced loading led to a decrease of luciferase activity after day 7 indicating a transient character of the transfection.

What can be concluded from the *in vitro* studies on alveolar macrophages is an active uptake process of aspherical microparticles by phagocytosis. The formulations were able to provide a successful and transient introduction of genetic material into the nuclear core. Microrods were also shown to be superior to the commercially available transfection system jetPEI for prolonged DNA delivery. Therefore two parameters loading and position were shown to influence protein expression giving insights into Layer-by-Layer-promoted transfection kinetics of MH-S cells. Showing high enzymatic degradation, the incorporation of the DNA cargo into the outermost layer is not suitable for efficient delivery indicating the highest protein expression from inner layers. A single application of microrods provided protein expression over a period of at least 9 days qualifying the system as a continual genetic engineering system for alveolar macrophages.

V.4 References

- [1] I. N. Mbawuiké, H. B. Herscowitz, *J Leukoc Biol.* **1989**, *46*, 119-27
- [2] S. Kakade, D. S. Manickam, H. Handa, G. Mao, D. Oupický, *Int. J. Pharm.* **2009**, *365*, 44–52
- [3] K. Itaka, A. Harada, Y. Yamasaki, K. Nakamura, H. Kawaguchi, K. Kataoka, *J. Gene Med.* **2004**, *6*, 76–84
- [4] Z. Dai, C. Wu, *Macromolecules* **2012**, *45*, 4346–4353
- [5] A. Schallon, V. Jérôme, A. Walther, C. V. Synatschke, A. H.E. Müller, R. Freitag, *React Funct Polym.* **2010**, *70*, 1-10
- [6] S.-G. Ding , L.Yu, L.-H. Wang, L.-D. Wang, Z.-Q. Yu, Y.-Z. You, *J. Mater. Chem. B* **2016**, *4*, 6462-6467
- [7] X. Zhang, J. P. Edwards, D. M. Mosser, *Methods Mol. Biol.* **2009**; *531*, 123
- [8] B. M.Wohl, J. F.J.Engbersen, *J. Control. Release* 2012, *158*, 2-14
- [9] P. T. Hammond, *Mater. Today* **2012**, *15*, 196-206
- [10] D. Ibraheem, A. Elaissari, H. Fess, *Int. J. Pharm.* **2014**, *459*, 70-83
- [11] A. Elbakry, A.Zaky, R. Liebl, R. Rachel, A. Goepferich, M. Breunig, *Nano Lett.* **2009**, *9*, 2059–2064
- [12] A. M. Pavlov, G. B. Sukhorukov, D. J. Gould, *J. Control. Release* **2013**, *172*, 22-29
- [13] U. Reibetanz, C. Claus, E. Typlt, J. Hofmann, E. Donath, *Macromol. Biosci.* **2006**, *6*,153–160
- [14] T. Mosmann, *J. Immunol. Methods* **1983**, *65*, 55-63
- [15] C.-L. Chen,W.-H. Hou, I.-H. Liu, G. Hsiao, S. Shian Huang, J. S. Huang, *J. Cell Sci.* **2009**, *122*, 1863-1871
- [16] Firefly Luciferase Assays & Vectors, Consumer Guide, ThermoFisher Scientific
- [17] A. Aderem, D. M. Underhill, *Annu. Rev. Immunol.* **1999**, *17*, 593-623
- [18] J. A. Champion, A. Walker, S. Mitragotri, *Pharm. Res.* **2008**, *25*, 1815-1821
- [19] S. Barua, J.-W Yoo, P. Kolhar. A. Wakankar, Y. R. Gokarn, S. Mitragotri, *PNAS* **2013**, *110*, 3270– 3275

Chapter VI

Transfection Studies on BALB/c Mice

For Chapter VI the author of the thesis made the following contributions to the chapter:

Draft and submission of the animal proposal 16/2016 to the local government (Landesamt für Verbraucherschutz Saarland, Saarbrücken); design, fabrication and sample preparation of defined masses of microrods and interpretation of all experimental data.

Microrod application to BALB/c mice, macrophage collection and the preparation of tissue cross-sections were performed by Bodo Wonnenberg and Andrea Rabung at the Institute of Anatomy and Cell Biology, Medical Faculty, Saarland University.

Transfection assays were carried out by Shashank Reddy Pinnapireddy at the Institute of Pharmaceutics and Biopharmaceutics, Philipps University Marburg.

V.1 Introduction: Mouse Lung Models

In biomedical research the mouse is the most frequently used animal model.^[1] This is due to the advanced knowledge of the murine genome featuring high synteny with those of humans.^[2] As a consequence many murine disease models were developed in order to identify corresponding human genes, which are responsible for the studied disease phenotype.^[2] Especially in the fields of oncology and immunology, murine physiological and pathophysiological cascades have been analyzed in high detail offering basic research, but also pharmaceutical companies a broad range of *in vivo* models.^[3]

For alveolar macrophages as the target cells of the presented gene delivery approach, participation in inflammatory conditions of the lung, such as pulmonary fibrosis or chronic obstructive pulmonary disease, was shown.^[4, 5] To further study the role of macrophages for these diseases, mouse lung models were established. Harvey and colleagues published a work on the stimulation of the phagocytic activity of alveolar macrophages by a natural compound.^[6] They could successfully show an enhanced clearance of harmful bacteria, such as *Haemophilus influenza* and *Pseudomonas aeruginosa*, and a reduced inflammation in the murine lung revealing the importance of a specific pathway, which is vital for antibacterial defense. On this basis, they were able to translate their findings into a clinical trial for COPD patients who correspondingly suffer from decreased phagocytic activity of alveolar macrophages and persistent bacterial infections. Regarding pulmonary fibrosis, various models were introduced applying different methods to induce the known scar-like changes within the murine lung. One of the most frequently used methods utilizes the side effect of an active agent called bleomycin.^[7] Commonly used in cancer treatment, the drug causes the typical histologic patterns in mice lungs, which are known from human patients. Macrophages have been shown to be involved in the development of bleomycin-induced fibrosis offering an *in vivo* system for the detailed study of their role within this ultimately fatal disease.^[8] In

addition to inflammatory conditions, also murine lung models for the evaluation of malignant diseases are available. Herein, alveolar macrophages were shown to promote neoplastic growth dependent on their polarization to different subsets and therefore mediator secretion patterns.^[9]

For both inflammatory and malignant diseases, murine lung models are available to study the role of alveolar macrophages both for the onset of the disorder and the progression. As outlined in chapter I, gene therapy is a viable approach to address macrophages in order to find new treatments for such serious conditions mentioned before. Therefore, aspherical microrods can act as a potential delivery system. In a first step, the successful transfection had to be translated from *in vitro* to *in vivo* conditions within a proof-of-concept study. The uptake of the rods into the target cells had to be shown within a more complex biological environment as well as the implementation and transcription of the encoded gene. In addition, the carrier must be well tolerated and non-toxic to the animals to reach the planned end points of the experiment. In the following chapter, the *in vivo* evaluation of the transfection proficiency of aspherical microrods is presented applying the carrier system to a BALB/c mouse lung model.

VI.2 Material and Methods

VI.2.1 Material

Microrods were fabricated using SNPs 200 nm with a green fluorescence label (Excitation/Emission 485 nm / 510 nm) and template membranes featuring 3 µm pores. For the Layer-by-Layer coating bPEI (25 kDa) and pCMV-luc were applied. The placebo formulation was stabilized by bPEI in combination with dextran sulfate (10 kDa).

The studies were carried out on female BALB/c mice obtained from Charles River Laboratories (Sulzfeld, Germany). For the collection of alveolar macrophages Cytospins (ThermoFisher Scientific, Darmstadt, Germany) were used. The subsequent transfection studies were performed according to the procedure as presented in chapter V using transfection and cell culture lysis reagent purchased from Promega (Mannheim, Germany). The bioluminescence was measured using a BioDoc Analyse Ti5 trans-illuminator (Whatman Biometra, Göttingen, Germany)

VI.2.2 Methods

Layer-by-Layer Coating Design

For the transfection studies *in vivo*, the polymer content of the microrods was set to 3.5 double-layers. The intermediate amount of the *in vitro* setting was chosen to compromise transfection efficiency within the planned time frame and rod stability giving respect to the more challenging application before reaching the site of action and therefore the target cells. In addition to that, for all tested concentrations microrods featuring 3.5 DL showed the highest MH-S viability in the performed MTT assay. To minimize differences in rod properties the placebo formulation was also set to 3.5 DL with dextran sulfate used as a substitute to the plasmid DNA in every double-layer.

BALB/c Keeping, Anesthesia and Microrod Application

50 female BALB/c mice were caged in a controlled and pathogen-free environment. They were granted unlimited excess to water and chow for the whole duration of the study. After reaching an age of 8 to 10 weeks (**Figure 1 A**), the application of the microrods was performed. Therefore mice were divided into 5 groups of 10 animals. The first two groups were used as control without any microrod application or using the placebo formulation. To study transfection proficiency of the pCMV-luc loaded particles, three time points were evaluated in correspondence to the *in vitro* setup. After 4, 7 and 9 days animals were analyzed, sparing out the evaluation after 2 days. This was due to very low luciferase signals in the cell culture studies, which were expected to be even lower after application to a demanding biological environment. At the day of microrod application, mice were anaesthetized one at a time using isoflurane within an inhalation chamber shown in **Figure 1 B - D**. The consecutive particle application was performed by nasal instillation of microrods dispersed in isotonic water containing 0.9 % (m/V) sodium chloride. Placed on their back, aliquots of 10 μ L were applied to the nostrils of the mouse in an alternating manner up to a maximum of 60 μ L and therefore 100 μ g of particles (**Figure 1 D**). After application mice were returned to the cage for recovery. During observation time, the animals were regularly checked for signs of sickness such as loss of fur, weight reduction or breathing difficulties and apathetic behavior as a result to pneumonia. According to the guidelines of the local government animals suffering from these conditions would have been removed from the study.

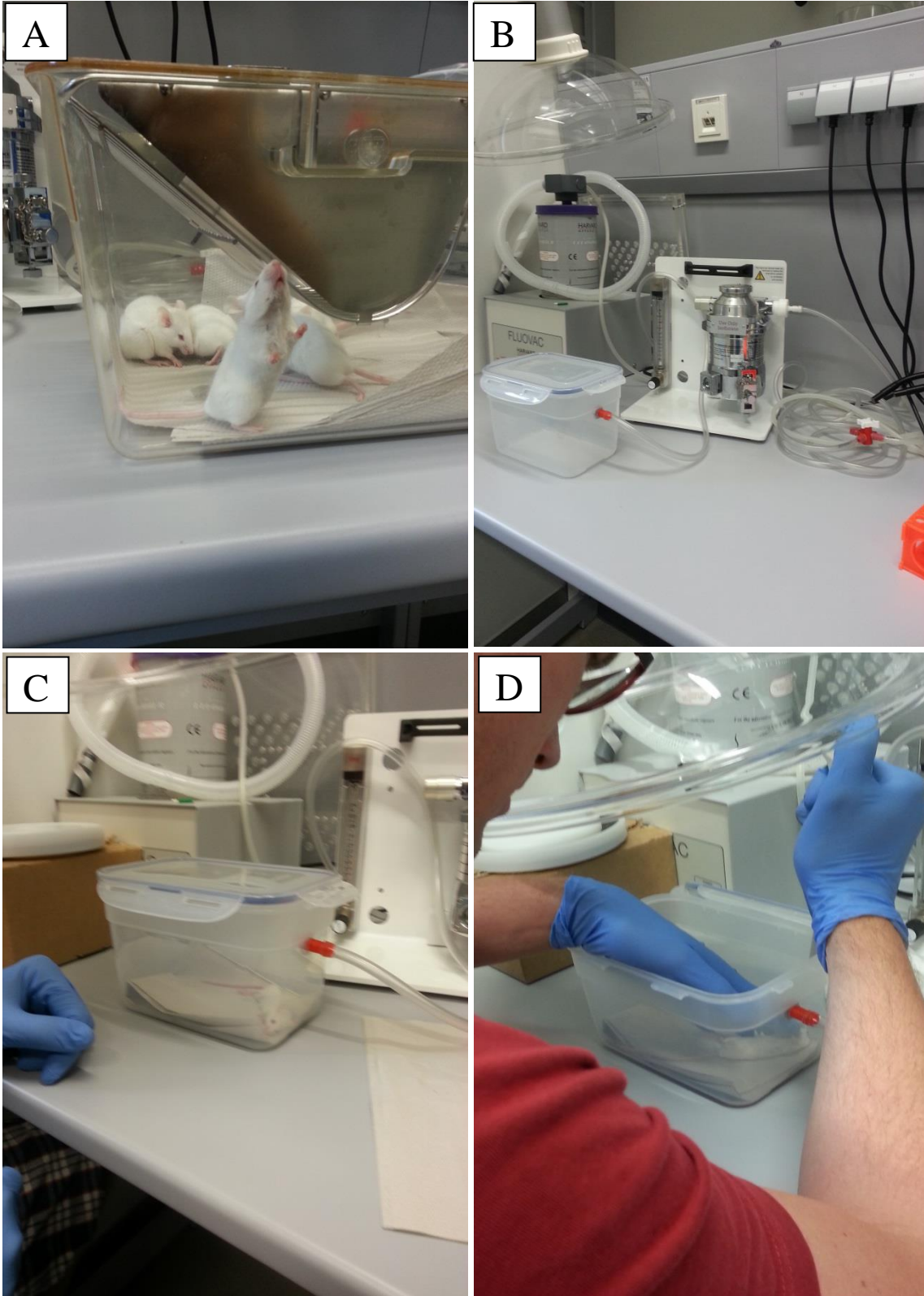


Figure 1: BALB/c mice during caging (A) and microrod application. Placed into an inhalation chamber (B) mice were treated with isoflurane (C) to facilitate microrod application (D).

Transfection Studies

For analysis the same protocol was applied to all the tested groups. Alveolar macrophages from the mouse lung were collected performing a bronchoalveolar lavage. Therefore the lung was flushed three times with 800 μ L PBS buffer (pH 7.4) using a tracheal cannula. As a single washing step the obtained cell suspension was centrifuged at 300 g and 4 °C with a consecutive redispersion in PBS buffer after supernatant disposal. To isolate macrophages the centrifugation at 300 g was repeated using a Cytospin, which allows cell separation due to size and density. The following steps of cell lysis and luciferase determination were carried out according to the protocol described in the previous chapter.

Histology

In addition to the collection of alveolar macrophages by bronchoalveolar lavage, lung tissue cross-sections were evaluated. Therefore, after lavage the mouse lungs were filled with gel and snap frozen. Kryostat sections were prepared with haematoxilin and eosin staining to determine inflammatory changes of the epithelium. In case of inflammation, the alveolar septa and epithelium would be thickened due to inflammatory infiltrate in combination with an apparent hyperplasia of neutrophils and alveolar macrophages. Haematoxylin is applied for nuclear staining and binds to DNA and RNA molecules due to electrostatic interactions. As a result the cellular core appears in a dark blue colour, which can be observed in dark spots. The counterstaining was performed by eosin, which binds to positively charged arginine and lysine residues of proteins resulting in a red to pink color. Non-stained sections were applied to a fluorescence microscope for the visualization of microrods ingested by residential macrophages.

VI.3 Results and Discussion

The first important aspect about the animal studies, which had to be discussed, was the way of particle administration. The most suitable way for the carrier system intended for pulmonary application is the aerosolization of the dry powder. The main drawback of this approach is the missing information about the dose, which is taken up by the mice depending on the respiratory rate of the individual animal. In order to get more information about the delivered dose actually reaching the site of action to correlate with the experimental read-out, nasal instillation was preferred for microrod administration. Instillation is a very simple and therefore the most widely used technique for the pneumatic introduction of material into the lungs of mice managing delivery without expensive equipment and devices.^[10] In addition, during the procedure the risk of injury for the animals is very low in comparison to intubation methods.^[10] Eyles et al. presented a study evaluating the efficiency of microsphere deposition by nasal instillation. Depending on parameters such as the choice of the anesthetic agent, suspension media and especially dose volume they observed an average pulmonary deposition rate of 50 %.^[11] Using isoflurane for anesthesia and PBS buffer for particle suspension, they applied a maximum of 50 μ L to BALB/c mice to reach highest deposition efficiency in comparison to lower dose volumes. This was also in accordance with the experience of our cooperation partners at the university hospital in Homburg allowing us to adjust the dose of microrods reaching the lung to the same amount, which was used in the previous cell culture studies. The animals were observed for a maximum time period of 9 days showing no negative reactions to the carrier. No signs of sickness were observed for any mouse, so the experiment could be carried out to the planned ending points with all the animals. The observation for the rods to be well tolerated was supported by histology samples

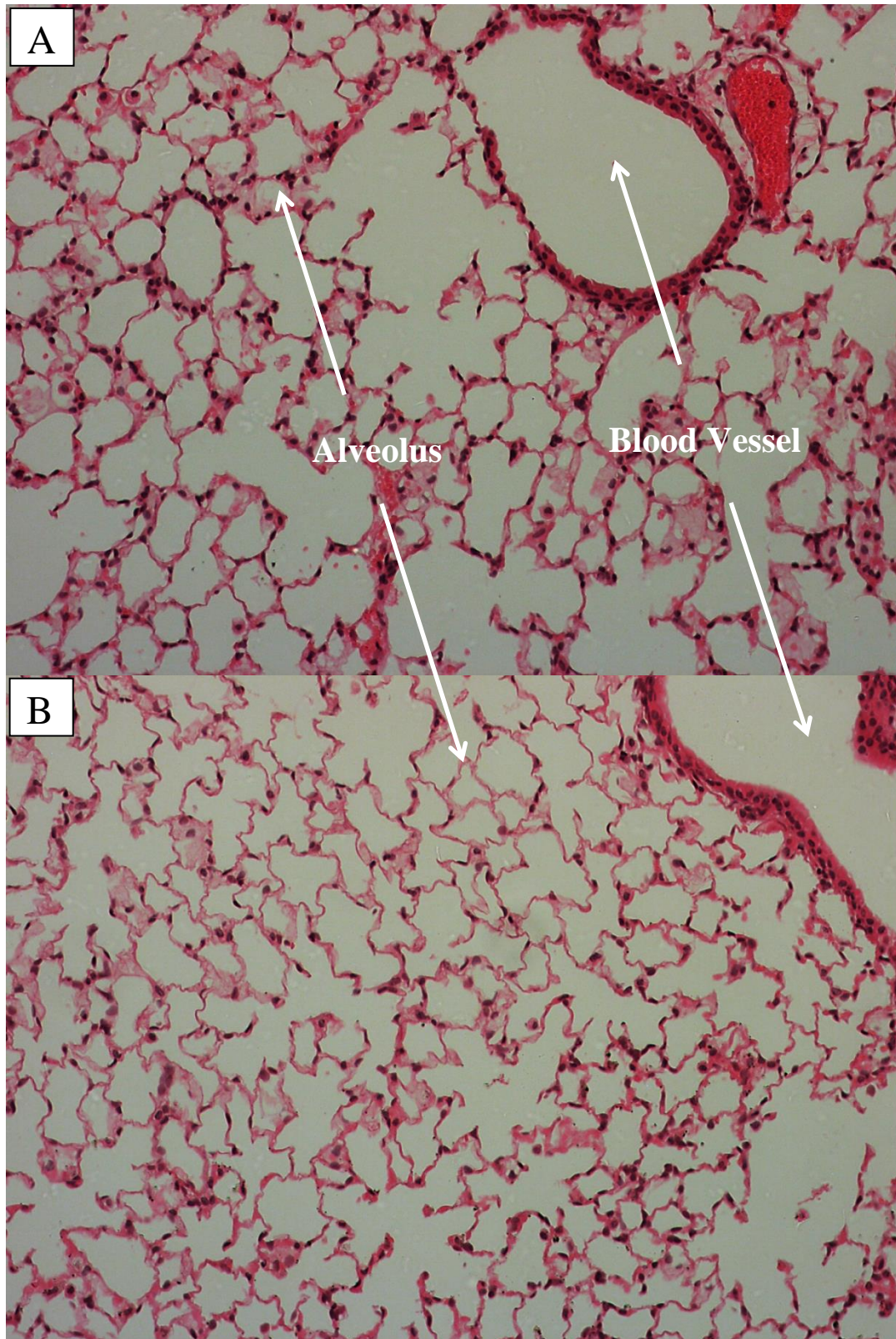


Figure 2: Cross-sections of the alveolar region from BALB/c mice. Sections were stained with haematoxylin and eosin showing tissue after 4 (**A**) and 7 (**B**) days after microrod application. The absence of inflamed sections indicated to particles to be well tolerated.

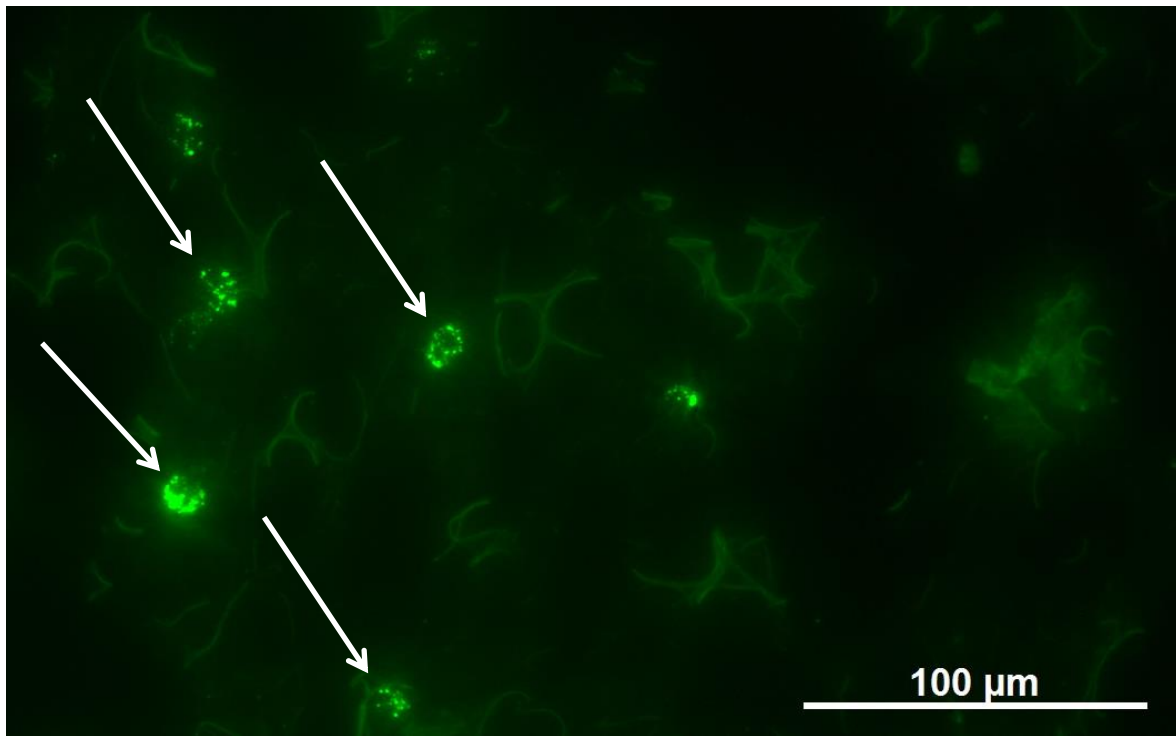


Figure 3: Fluorescence microscopy visualization of microrods after engulfment into alveolar macrophages within the alveolar tissue. By excitation of the green fluorescence label of the particles, they can be shown to be exclusively associated to the cells (example white arrows).

from the mouse lung displayed in **Figure 2**. The alveolar tissue can be observed in its typical morphology after cutting the bubble-like structured alveoli. It appears in a normal, healthy state throughout the study without an increased infiltration of immune cells such as neutrophils as sign of acute inflammation. Additional information, which could be gained from the cross-section, was the visualization of the microrods within the interstitium. Therefore, the green fluorescence label of the SNPs was excited revealing the rods to be exclusively associated to alveolar macrophages in an ingested state. In **Figure 3** (white arrows) particles were visualized 4 days after instillation. This observation was highly important for us as it indicated a successful targeted delivery of the carrier and therefore the cargo to the cells of interest under *in vivo* conditions. After the set time frames of observation animals were analyzed. Alveolar macrophages were extracted from the mouse lung by bronchoalveolar lavage and treated due to the luciferase assay protocol. Results from the

assay are shown in **Figure 4** indicating a successful implementation and transcription of the delivered model gene. For the placebo rods (P1-P10), which were applied as a negative control, no luciferase activity was found. For the plasmid DNA-loaded particles bioluminescence was measured for 50 % of the animals after 4 days of transfection at very low values. After 7 days a more pronounced signal pattern could be observed for 90 % of the mice showing bioluminescence values within a quite narrow range. For the results after 9 days again a higher fluctuation was obtained with very high maximum values, but also 40 % of the animals showing no luciferase activity.

What can be concluded from the study is a correspondence to the expression patterns gained from the *in vitro* studies on MH-S cells. An increase in luciferase activity over time can also be observed for *in vivo* conditions. The *in vivo* situation expands the biological evaluation of the microrod system from an isolated to an open and dynamic system. As a consequence the natural clearance mechanism of the lung had to be taken into account. Upon particle engulfment macrophages can migrate from the respiratory tract into the direction of the pharynx in order to get swallowed for host protection.^[12] So before the study it was not predictable if enough macrophages would reside within the lungs for a time frame of up to 9 days to actually allow us to measure luciferase activity. This point was in particular important since in the *in vitro* setting higher luciferase expression was observed for a longer residence time of the rods in the cells. But in contrast to the preliminary thoughts, residential macrophages were present in the lungs at every evaluated time point, carrying particles and expressing luciferase. This observation was vital for the initial working hypothesis to design a carrier for the engineering of alveolar macrophages, which stay in the respiratory system influencing their microenvironment due to the genetic modifications provided by the particles. Therefore the particles were successfully shown to be an efficient delivery vehicle for the

implementation of genetic material, which can be easily translated from cell culture to *in vivo* environments.

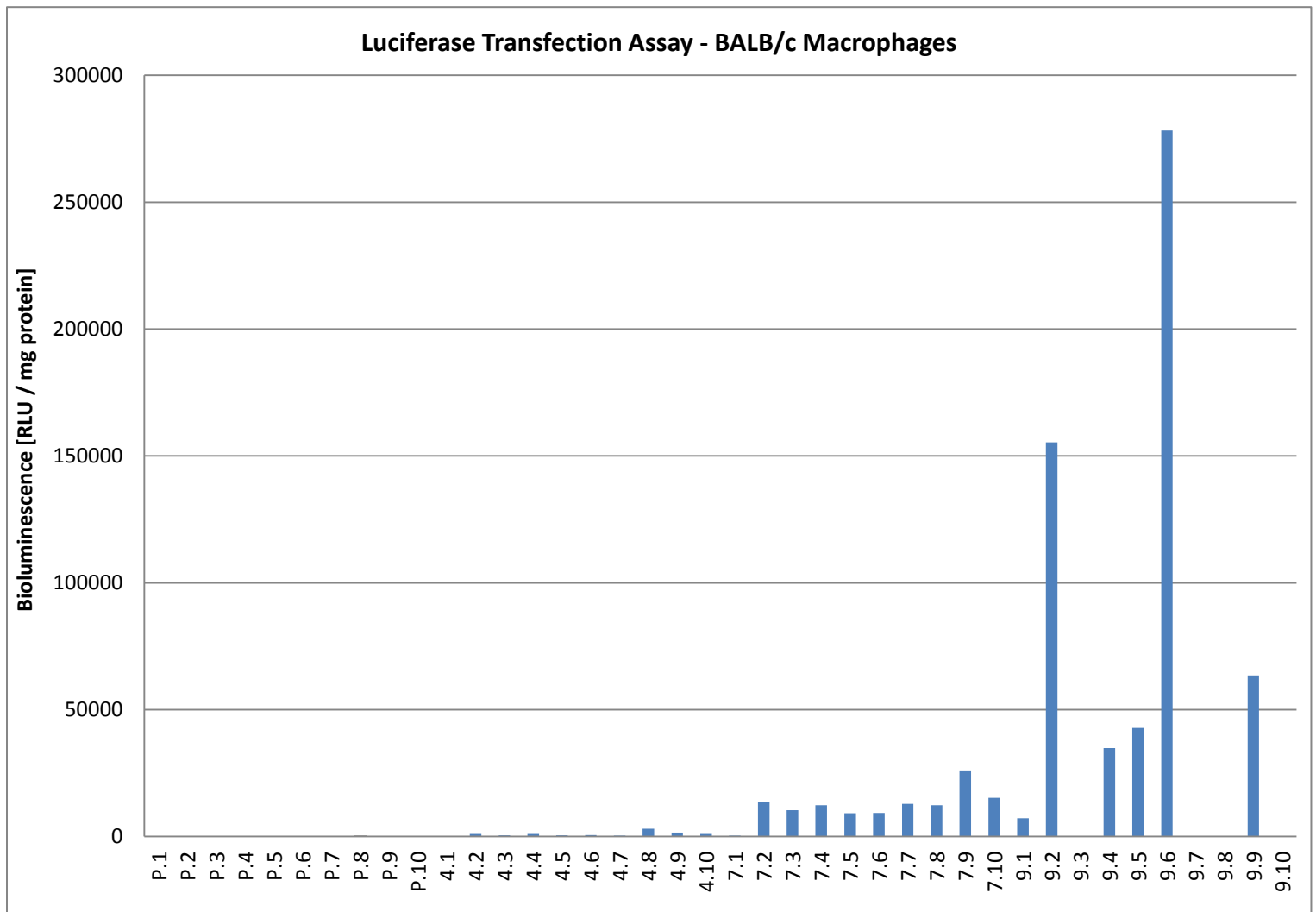


Figure 4: Results of the luciferase assay for alveolar macrophages from BALB/c mice. Values of the x-axis are given in double digits referring to the evaluated time point in days for the first digit. For every time point 10 individual animals are depicted with the second digit. In addition placebo particles (P) were also evaluated for 10 animals.

VI. 4 References

- [1] Official Annual Report „Tierschutz in der Forschung 2015“, Bundesministerium für Ernährung und Landwirtschaft, Berlin, Germany
- [2] A. Braun, H. Ernst, H. G. Hoymann, S. Rettinghausen, in *The Laboratory Mouse*, Vol. 4 (Ed: H. Hedrich), Elsevier, London, UK, **2010**
- [3] L. Zitvogel, J. M. Pitt, R. Dailière, M. J. Smyth, G. Kroemer, *Nat. Rev. Cancer* **2016**, *16*, 759–773
- [4] Y. Zhang, T. C. Lee, B. Guillemin, M. C. Yu, and W. N. Rom, *J. Immunol.* **1993**, *150*, 4188–4196
- [5] R. Shaykhiev, A. Krause, J. Salit et al., *J. Immunol.* **2009**, *183*, 2867–2883
- [6] C. J. Harvey, R. h. K. Thimmulappa, S. Sethi, X. Kong, L. Yarmus, R. H. Brown, D. Feller-Kopman, R. Wise, S. Biswa, *Sci. Transl. Med.* **2011**, *78*, 78
- [7] A. Moeller, K. Ask, D. Warburton, J. Gauldie, M. Kolb, *Int. J. Biochem. Cell, Biol.* **2008**, *40*, 362–382
- [8] A. L. Degryse, W. E. Lawson, *Am. J. Med. Sci.* **2011**, *341*, 444-449
- [9] E. F. Redente, L. D. Dwyer-Nield, D. T. Merrick, K. Raina, R. Agarwal, W. Pao, P. L. Rice, K. R. Shroyer, A. M. Malkinson, *Am. J. Pathol.* **2010**, *176*, 2972–2985
- [10] M. A. Miller, J. M. Stabenow, J. Parvathareddy, A.J. Wodowski, T. P. Fabrizio, X. R. Bina, L. Zalduondo, J. E. Bina, *PLoS One* **2012**, *7*, e31359
- [11] J. E. Eyles, I. D. Spiers, E. D. Williamson, H. O. Alpar, *J. Pharm. Pharmacol.* **2001**, *53*, 601-7
- [12] A. C. Kirby, M. C. Coles, P. M. Kaye, *J. Immunol.* **2009**, *183*, 1983–1989

Summary and Outlook

Since decades gene therapy is one of the greatest promises held by biomedical research. Potentially adaptable to a wide range of individual conditions and clinical pictures of patients, it offers, in theory, a nearly unlimited toolbox to treat diseases at its origin. Although there are only few market products available, gene therapy is still regarded as a powerful tool, which needs further improvement to exploit its full potential.

In order to contribute to this development, a novel pulmonary delivery system for genetic material was presented in this work. Therefore, the objective of the thesis was the adaptation of a previously introduced particle preparation technique to the needs of successful transport of genes into a target cell of therapeutic relevance. Based on a bottom-up engineering approach, nanoparticles were connected with each other within the pores of a shape-defining template membrane. According to the aspherical, cylindrical shape of the pores, the resulting nanostructured microparticles were successfully formed into a rod-like geometry. The micron architecture was stabilized by a Layer-by-Layer coating procedure, which turned out to be very flexible and robust to changes in excipients allowing the use of different polyelectrolytes. Both non-biodegradable and biodegradable excipients were applied for stabilization offering the freedom to choose the most suitable agents depending on the desired target cell line.

Two analytical methods were identified, which could be applied as in-process controls during fabrication. Ethidium bromide-loaded agarose gels were a viable tool to visualize the progress of the stabilization also giving information about the efficient condensation of the DNA onto the surface of the particles as well as for the protection by the buffering agent. Applying ICP-OES as a cargo quantification tool provides the fast determination of excipients consuming only low amounts of particles. Therefore, the method can be used as a standard analytical tool for every particle batch prior to application. The particle dimensions were chosen according to the pulmonary application route showing an MMAD of 2.57 μm . This indicates the particles

to be able to reach the deep lung. The fine particle fraction of 12 % is quite low in comparison to market products highlighting a need for further optimization. This could potentially be achieved by an efficient method to reduce residual moisture in the foremost hygroscopic formulation.

In terms of the functionality of the microrod system, it was shown to be efficient in implementing the transported model gene into alveolar macrophages for *in vitro* and *in vivo* environments. In both cases, the particles were well tolerated and no toxic effects could be observed. Overall, it can be stated that all main hurdles during the development of the presented system could be overcome. Starting with the first DNA-stabilized microrods and the application of suitable physicochemical and administration-related characterization methods, the project was advanced to a successful application in the target cells. Here, we could show our particles to be superior to a commercial transfection agent in terms of prolonged gene expression. Building on this data, an animal study was conducted showing the microrods to be easy to translate from cell culture to *in vivo* environments.

Furthermore, for the first time the dependency of gene expression in murine alveolar macrophages on the LbL design could be shown. As presented in the first transfection experiment, microrods stabilized by the least number of double-layers showed higher luciferase expression within the observed time frame of the study. A clear trend was observed in comparison to higher layer numbers due to the increasing electrostatically driven stability of the carrier system, which sustained plasmid-DNA release. In addition to cargo loading, also the position of the plasmid was found to have a strong impact on transfection. Whereas pCMV-luc in the outermost layer got degraded under harsh acidic and enzymatic conditions in phagolysosomes, a successful gene delivery from inner layers was demonstrated. These new insights into macrophage transfection can contribute to the controlled and prolonged expression of transported genes for therapeutic purposes.

Regarded as a platform technology, the introduced methods have the potential to pave the way for more specialized and therefore therapeutically relevant applications. Especially by addressing altered gene expression of macrophages, which is assumed to promote diseases within the respiratory tract, microrods are a promising tool to evaluate the impact of therapeutic nucleic acid-based drugs, including RNAs, such as siRNAs or miRNAs.

Furthermore, the applied nanoparticulates can be exploited to not only provide a moldable material. Drug-loaded nanoparticles enable combination therapies potentially improving the therapeutic performance of the microrod system. In this context, a switch from silica to biodegradable compounds, such as calcium phosphate, could be viable, but also organic polymers, e.g. PLGA can be used. For future experiments including extended *in vitro* and *in vivo* setups large amounts of rods are needed indicating a need of scalability of the method. A cost-efficient yield optimization to the gram scale is desired and also currently under investigation.

Abbreviations

AFM	Atomic Force Microscopy
ALF	Artificial Lysosomal Fluid
AR	Aspect Ratio
ATP	Adenosine triphosphate
BCA	Bicinchoninic acid
bPEI	branched Polyethyleneimine
C	Carbon
CHT	Chitosan
ConA	Conavalin A
DANN	Desoxyribonucleic acid
DAPI	(4',6-diamidino-2-phenylindole)
DCM	Dichloromethane
DEAE-Dex	Diethylaminoethyl Dextran
DexS	Dextran sulfate
DL	Double-Layer
DMSO	Dimethyl sulfoxide
DPI	Dry Powder Inhaler
EDTA	Ethylenediaminetetraacetic acid
EMA	European Medicine Agency
EPR	Enhanced Permeability and Retention
EtBr	Ethidium bromide
FDA	Food and Drug Administration
FPF	Fine Particle Fraction
GFP	Green Fluorescent Protein
H	Hydrogen
HES	Hydroxyethyl starch
ICP-OES	Inductively Coupled Plasma – Optical Emission Spectroscopy
IFN	Interferon gamma
IL	Interleukine
ITC	Isothermal Titration Calorimetry
LbL	Layer-by-Layer
MDI	Metered Dose Inhaler
Mg	Magnesium
MMAD	Mass Median Aerodynamic Diameter
MTT	3-(4,5-dimethylthiazol-2-yl)-2,5-diphenyltetrazolium bromide
N	Nitrogen
NSAID	Non-steroidal, Anti-inflammatory Drug
pCMV-luc	Plasmid DNA, CMV-Promotor, encoding for Luciferase
PE-	Polyanion
PE+	Polycation
SEM	Scanning Electron Microscopy
SNP	Silica Nanoparticles
TAM	Tumor-associated Macrophage
TEM	Transmission Electron Microscopy
THF	Tetrahydrofuran
TNF	Tumor Necrosis Factor
TRIS	Tris(hydroxymethyl)aminomethane

Acknowledgements

First and foremost, I want to express my deepest gratitude to my doctoral father Prof. Dr. Marc Schneider for making me a member of his research group. I would like to thank him for creating a working environment based on trust and appreciation, which made the last years a real joy. His continuous support and inspirational scientific contributions were substantial factors to advance a fascinating field of research.

I want to thank Prof. Dr. Claus-Michael Lehr for his expert opinion on the thesis and many fruitful discussions during joint meetings with his drug delivery division at the HIPS. In this regard I want to highlight Remi and her positive attitude as a kind gift from the Netherlands.

As my first scientific supervisor always said, it's all about people. In this regard I want to thank all my cooperation partners. Prof. Dr. Udo Bakowsky and Shashank Reddy Pinnapireddy from the Institute of Pharmaceutical Technology and Biopharmaceutics at Marburg University made essential contributions to the thesis carrying out all *in vitro* assays. Thank you, Shashank for your tremendous work and constant efforts to make this thing work. I always appreciated your relaxed and positive attitude as well as your operational skills at the bench.

Animal studies would have not been possible without the help of Prof. Dr. Thomas Tschernig and Bodo Wonnenberg from the Medical Faculty of Saarland University. Thank you, Thomas and Bodo for the interesting discussions and insights into lung physiology and medical research.

I want to thank all my colleagues from Marburg and Saarbrücken for a great time. Here, I especially want to address Matthias and Boris, which are outstanding personalities and it was a blast for me spending a year with you in Marburg. I want to thank my colleagues Clemens, Saeed, Chen, Agnes, Afra, Joschi, Caro, Sarah, Nesma and Baseer for so many social events

making Schneider Lab a second family. In this context I want to highlight Marcel and Daniel. Thank you Marciboy for your clever ideas and design skills, burger sessions and trash talk. Stay the kind and helpful swaggy teddy bear that you are. Thank you Daniel for your analytical, political and nerdy mind, which led to so many hilarious discussions; simply an essential part of my PhD time.

I would also like to thank the staff from Schneider Lab Isabelle, Peter and especially Marijas, who spent many hours in the dark caves of the cell culture for my project.

I want to address my interns Johannes Büscher, Alexander König and Felicia Hartmann, who did a great job during their time in my lab. Thank you Feli for your ambition and appreciative support, for your constant encouragement and your love.

I deeply thank my siblings and parents Daniela, Alexander, Dorothea and Jürgen for all your support for the path I chose.

Curriculum Vitae

Personal Information

Michael Möhwald

Date of Birth: September 26th, 1986 in Heidelberg

Nationality: German

Contact: michael.moehwald@gmx.de

Doctoral Thesis

04/14 – 03/17

Institute of Biopharmaceutics and Pharmaceutical Technology,
Department of Pharmacy, Saarland University, Saarbrücken

Group of Prof. Dr. Marc Schneider

Professional Training

05/13 – 10/13

Pharmaceutical Training in the Division Formulation Sciences – New
Biological Entities at AbbVie Germany, Ludwigshafen

11/12 – 04/13

Pharmaceutical Training at St. Ulrich Apotheke, Östringen

03/11 – 05/11 Assistant Scientist, Pharmaceutical Technology and Biopharmaceutics, Group of Prof. Dr. Gerhard Winter, LMU München

02/08 – 09/08 Assistant Scientist, Pharmaceutical Biology-Biotechnology, Group of Prof. Dr. Ernst Wagner, LMU München

Vocational

Training

04/14 – 03/17 Advanced Curriculum in Pharmaceutical Technology
“Fachapotheker für Pharmazeutische Technologie”

Educational

Background

01/14 Licensed Pharmacist (Approbation)

10/07 – 10/12 Pharmaceutical Studies at Ludwig-Maximilians-Universität
München

10/06 – 09/07 Medical Studies at Ruprecht-Karls-Universität Heidelberg

07/97 – 07/06 Abitur at Leibniz-Gymnasium Östringen